Impact of Genetic Variation during Cross-Species Transmission on Lentiviral Capsid-Host Protein Interactions

Brigitte Ella Lawhorn

A dissertation

submitted to the Faculty of

the department of Biology

in partial fulfillment

of the requirements for the degree of

Doctor of Philosophy

Boston College
Morrissey College of Arts and Sciences
Graduate School

November 2020

Impact of Genetic Variation during Cross-Species Transmission on Lentiviral Capsid-Host Protein Interactions

Author: Brigitte Ella Lawhorn

Advisor: Welkin E. Johnson

For lentiviruses such as HIV-1, the viral capsid protein (CA) plays a crucial role in replication by facilitating active transport across nuclear pore complexes (NPCs). Nucleoporin Nup358/RanBP2 – a large, multidomain protein that comprises the main component of cytoplasmic NPC filaments – was previously identified as a potential cofactor for HIV-1 nuclear entry, and its C-terminal cyclophilin-like domain ($Nup358_{Cyp}$) is able to interact with the CA of both HIV-1 and HIV-2. The importance of this interaction to viral replication is unclear though as certain cell-culture experiments suggest CA interaction with $Nup358_{Cyp}$ is dispensable for viral replication, and the CA of several other lentiviruses like SIVmac do not appear to interact with the $Nup358_{Cyp}$ domain. However, we have found that CA interaction with Nup358 is widely conserved among primate lentiviruses and is maintained by natural selection. The exception, SIVmac, likely reflects an evolutionary trade-off allowing escape from rhesus macaque $TRIM5^{Cyp}$. Together, our observations are strong evidence that the interaction between viral CA and the $Nup358_{Cyp}$ domain must be biologically relevant *in vivo*.

Specifically, by comparing interactions between multiple SIVsm/HIV-2 lineage CAs and several primate orthologs of Nup358, we identified interspecies differences in the $Nup358_{Cyp}$ domain that affect the CA interaction, but only when assayed in conjunction with the preceding Ran-binding domain 4 ($Nup358_{R4}$). We next found that selection preserves the interaction during cross-species transmission, resulting in

adaptation to differences between the $Nup358_{Cyp}$ homologs of the reservoir and spillover hosts. For example, SIVsm CA does not interact with human $Nup358_{R4\text{-}Cyp}$, while HIV-2 CA interacts with both the human and sooty mangabey orthologs. We confirmed these distinct interaction phenotypes in an extended set of SIVsm/HIV-2 CAs, and mapped the difference to a single position – residue 3173 – in the $Nup358_{Cyp}$ domain. The differing ability to interact with human $Nup358_{R4\text{-}Cyp}$ is due to residue 85 in the CA 4-5 loops; most SIVsm strains encode a glutamine at position 85, whereas most HIV-2 strains encode an isoleucine. Reciprocal swaps reverse the interaction phenotypes, such that the SIVsm Q85I CA mutant strongly interacts with human $Nup358_{R4\text{-}Cyp}$, while HIV-2 I85Q CA mutant does not. This difference also correlates with differences in single- and multi-cycle infectivity on human cell lines and levels of nuclear import in HeLa cells. Together, these results indicate that HIV-2 adapted to human Nup358 during emergence in humans.

We also examined the ability of our CA panel to interact with Cyclophilin A. While all HIV-2 CA interact with CypA, the ability to interact varied among the other SIVsm CA tested, and was absent for SIVpbj. Thus, conservation of CA interaction with $Nup358_{Cyp}$ does not correlate to the ability to interact with CypA, and is not simply a consequence of maintaining the CA-CypA interaction.

TABLE OF CONTENTS

LIST OF TABLES

LIST OF FIGURES

LIST OF ABBREVIATIONS

°C	Degree Celsius
A	Alanine
A3F	Apolipoprotein B MRNA Editing Enzyme Catalytic Subunit 3F protein
AIDS	Acquired immunodeficiency syndrome
AZT	Zidovudine
BIV	Bovine immunodeficiency virus
C	Cysteine
CA	Capsid protein
CAEV	caprine arthritis-encephalitis virus
CCR5	C-C chemokine receptor type 5 protein
CD4	Cluster of differentiation 4 protein
cDNA	Complementary deoxyribonucleic acid
CLD	Cyclophilin-like domain
CO_2	Carbon dioxide
CPSF6	Cleavage and polyadenylation specificity factor subunit 6 protein
CRFK	Crandell-Rees Feline Kidney cells
CsA	Cyclosporin A
CTD	C-terminal domain
CXCR4	C-X-C chemokine receptor 4 protein
CypA	Cyclophilin A protein
D	Aspartic acid
DMEM	Dulbecco's modified Eagle Media
DNA	Deoxyribonucleic acid
dNTP	Deoxynucleotide triphosphate
E	Glutamic acid
EGFP	Enhanced green fluorescent protein
EIAV	Equine infectious anemia virus
ELVgv	Colugo endogenous lentivirus
Env	Envelope glycoprotein
env	Envelope gene
EURIPRED	European Research Infrastructures for Poverty Related Diseases
F	Phenylalanine
FBS	Fetal bovine serum
FIV	Feline immunodeficiency virus

G	Glycine
gag	Group specific antigen gene
Gag	Group specific antigen protein
H	Histidine
HA	Influenza hemagglutinin
HEK293T/17	Human Embryonic Kidney 293T/17 cells
HIV	Human immunodeficiency virus
HIV-1	Human immunodeficiency virus type 1
HIV-2	Human immunodeficiency virus type 2
HIV-2 EHO	Human immunodeficiency virus type 2 isolate EHO
HIV-2 GH-1	Human immunodeficiency virus type 2 isolate GH-1
HIV-2 ROD	Human immunodeficiency virus type 2 isolate ROD
HIV-2 UC1	Human immunodeficiency virus type 2 isolate UC1
hu	Human
I	Isoleucine
IL-2	Interleukin-2
IN	Integrase protein
ITC	Isothermal titration calorimetry
JDV	Jembrana disease virus
K	Lysine
KBD	Kinesin-binding domain
Kd	Equilibrium dissociation constant
kDa	Kilodalton
L	Leucine
L-glut	L-glutamine
LB	Luria-Bertani
LRR	Leucine-rich region
LTR	Long terminal repeat
M	Methionine
MA	Matrix protein
MELVmpf	*Mustelidae* endogenous lentivirus of domestic ferret genome
ml	Milliliter
MLV	Murine leukemia virus
mRNA	Messenger ribonucleic acid
MVV	Maedi-Visna virus
Mx2	Myxovirus resistance 2 protein
N	Asparagine
NC	Nucleocapsid protein
nef	Negative regulatory factor gene

Nef	Negative regulatory factor protein
NEPRC	New England Primate Research Center
NIAID	National Institute of Allergy and Infectious Diseases
NIBSC	National Institute for Biological Standards and Control
NIH	National Institutes of Health
NL4-3 HIV-1	Human immunodeficiency virus type 1 isolate NL4-3
NPC	Nuclear Pore Complex
NTD	N-terminal domain
Nup153	Nucleoporin 153 protein
Nup358	Nucleoporin 358 protein
$Nup358_{Cyp}$	C-terminal cyclophilin domain of Nup358 protein
$Nup358_{R4}$	Ran-binding domain 4 of Nup358 protein
$Nup358_{R4\text{-}Cyp}$	The supradomain formed by $Nup358_{R4}$ and $Nup358_{Cyp}$
P	Proline
PCR	Polymerase chain reaction
Pen-Strep	Penicillin-Streptomycin
PIC	Pre-integration complex
pol	Polymerase gene
Pol	Polymerase protein
PR	Protease protein
pSIV	Prosimian immunodeficiency virus
ptm	Pig-tailed macaque
Q	Glutamine
R	Arginine
RanBP2	Ran-binding protein 2 protein
RANBP2	Ran-binding protein 2 gene
RBCC	Ring, B-Box, and Coiled-coil domains of TRIM5 protein
RELIK	Rabbit endogenous lentivirus K
Rev	Regulator of expression of viral proteins protein
rev	Regulator of expression of viral proteins gene
rh	Rhesus macaque
RING	Really Interesting New Gene
RNA	Ribonucleic acid
RPMI	Roswell Park Memorial Institute
RSV	Rous sarcoma virus
RT	Reverse Transcriptase
RTC	Reverse transcription complex
S	Serine
SEAP	Secreted alkaline phosphatase

SEC	Size-exclusion chromatography
SIV	Simian immunodeficiency virus
SIVagm	Simian immunodeficiency virus of African green monkey
SIVcol	Simian immunodeficiency virus of guereza colobus
SIVcpz	Simian immunodeficiency virus of chimpanzee
SIVgor	Simian immunodeficiency virus of gorilla
SIVgsn	Simian immunodeficiency virus of greater spot-nosed monkey
SIVmac	Simian immunodeficiency virus of rhesus macaque
SIVmac239	Simian immunodeficiency virus of rhesus macaque isolate 293
SIVmnd	Simian immunodeficiency virus of mandrill
SIVmon	Simian immunodeficiency virus of mona monkey
SIVmus	Simian immunodeficiency virus of mustached monkey
SIVpbj	Simian immunodeficiency virus of pig-tailed macaque
SIVpbj1.5	Simian immunodeficiency virus of pig-tailed macaque isolate 1.5
SIVpbj1.9	Simian immunodeficiency virus of pig-tailed macaque isolate 1.9
SIVrcm	Simian immunodeficiency virus of red-capped mangabey
SIVsm	Simian immunodeficiency virus of sooty mangabey
SIVsmD215	Simian immunodeficiency virus of sooty mangabey isolate D215
SIVsmE041	Simian immunodeficiency virus of sooty mangabey isolate E041
SIVsmE543	Simian immunodeficiency virus of sooty mangabey isolate E543
SIVsmE660	Simian immunodeficiency virus of sooty mangabey isolate E660
SIVsmG932	Simian immunodeficiency virus of sooty mangabey isolate G932
SIVstm	Simian immunodeficiency virus of stump-tailed macaque
SIVstm37.16	Simian immunodeficiency virus of stump-tailed macaque isolate 37.16
sm	Sooty mangabey
SP1	Spacer peptide 1 protein
SP2	Spacer peptide 2 protein
SU	Surface unit of envelope glycoprotein
T	Threonine
tat	Trans-activator of transcription gene
Tat	Trans-activator of transcription protein
TF	TRIM-Fusion
TM	Transmembrane subunit of envelope glycoprotein
TRIM5α	Tripartite motif-containing protein 5 alpha isoform protein
V	Valine
Vif	Viral infectivity factor protein
vif	Viral infectivity factor gene
Vpr	Viral protein R protein
vpr	Viral protein R gene

Vpu	Viral protein U protein
vpu	Viral protein U gene
W	Tryptophan
WT	Wild-type
Y	Tyrosine
YFP	Yellow fluorescent protein
ZnF	Zinc-finger region
µl	Microliter
µM	Micromolar

ACKNOWLEDGEMENTS

To everyone who made the pursuit of my PhD and completion of this thesis possible: thank you.

Alla mia anima gemella: Mi piacciono gli scoiattoli grassi.

CHAPTER 1: INTRODUCTION

1.1 Primate Lentiviruses

1.1.1 Taxonomy

Lentiviruses are viruses that belong to the *Lentivirus* genus within the retrovirus or *Retroviridae* family [1]. Retroviruses include a vast and diverse array of enveloped, single-stranded positive-sense RNA viruses that infect vertebrate animals and are defined by the conversion of the RNA viral genome into DNA and the subsequent insertion of the viral DNA into the host chromatin during viral replication. This family is subdivided into two subfamilies: *Spumaretrovirinae* and *Orthoretrovirinae*. The *Spumaretrovirinae* contains five genera: *Bovispumavirus*, *Equispumavirus*, *Felispumavirus*, *Prosimiispumavirus*, and *Simiispumavirus* [2]. The *Orthoretrovirinae* contain six genera: *Alpharetrovirus*, *Betaretrovirus*, *Gammaretrovirus*, *Deltaretrovirus*, *Epsilonretrovirus*, and *Lentivirus*. Viruses in the *Lentivirus* genus can be further organized into seven distinct monophyletic lineages based on the host species infected: primate (simian/prosimian), cologo, carnivoran (feline), bovine, ovine/caprine (small ruminant), equine, and lagomorph (Figure 1.1) [3–7]. The primate lentiviruses consist of the human immunodeficiency virus type-1 (HIV-1), human immunodeficiency virus type-2 (HIV-2) and over 40 different strains of simian immunodeficiency viruses (SIVs) [8]. Each non-human primate species is typically infected by its own unique SIV virus [9]. HIV-1 is the most well-known among these viruses due to it being the cause of acquired immunodeficiency syndrome (AIDS).

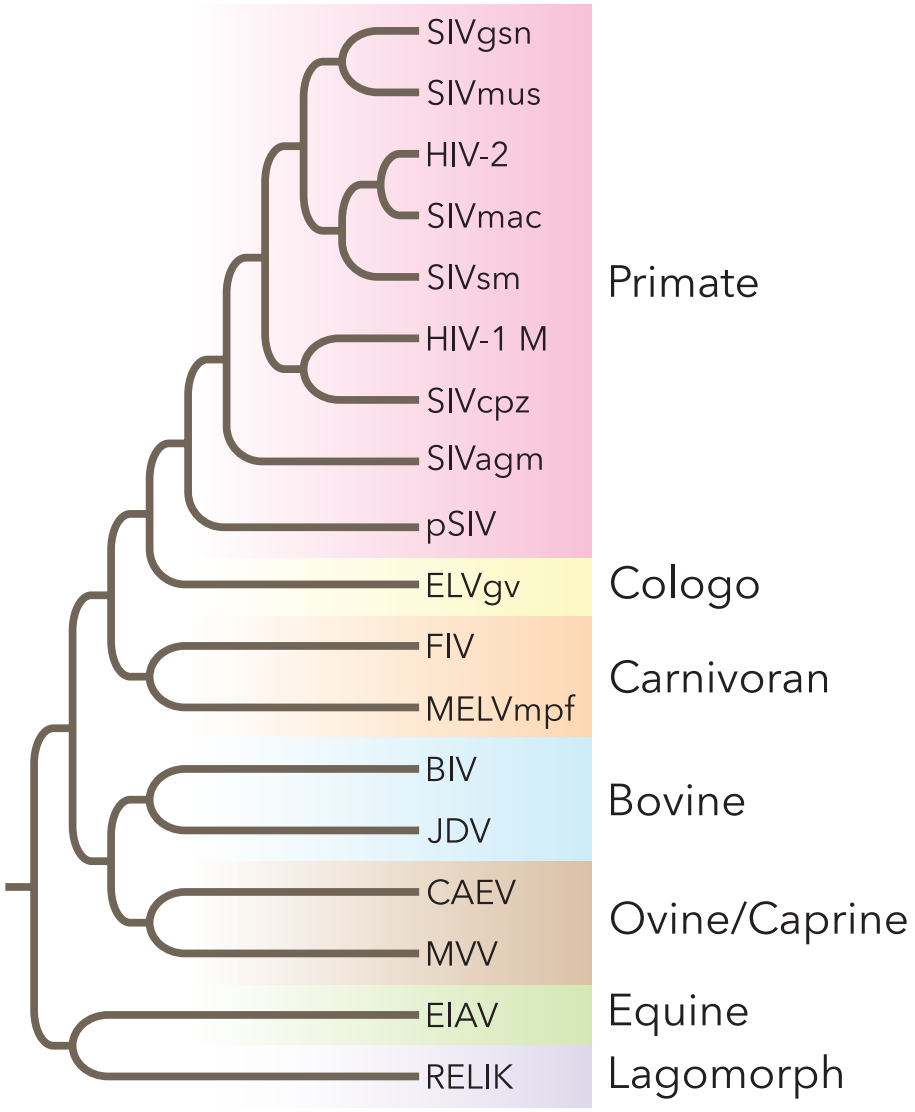

Figure 1.1. Lentivirus Phylogeny
Phylogenetic tree showing select viruses from the different lineages within the Lentivirus genus and their evolutionary relationship to one another based on phylogenies published in [3,7,10]. Listed on the left is the host species group infected by the viral lineage. Figure not drawn to scale. SIVgsn, SIV of greater spot-nosed monkey; SIVmus, SIV of mustached monkey; SIVmac, SIV of rhesus macaque; SIVsm, SIV of sooty mangabey; SIVcpz, SIV of chimpanzees; SIVagm, SIV of African green monkey; pSIV, prosimian immunodeficiency virus; ELVgv, colugo endogenous lentivirus; FIV, feline immunodeficiency virus; MELVmpf, Mustelidae endogenous lentivirus of domestic ferret genome; BIV, bovine immunodeficiency virus; JDV, Jembrana disease virus; CAEV, caprine arthritis-encephalitis virus; MVV, Maedi-Visna virus; EIAV, equine infectious anemia virus; RELIK, rabbit endogenous lentivirus K.

1.1.2 Genomic Structure

Like all retroviruses, the lentiviral genome encodes for *gag*, *pol*, and *env* genes (Figure 1.2A). The *gag* gene encodes for the group specific antigen (Gag) polyprotein, which is eventually cleaved into the viral structural proteins matrix (MA), capsid (CA), and Nucleocapsid (NC) as well as p6 and two spacer peptides SP1 and SP2. Within the extracellular, mature virion, MA is found associated with the lipid bilayer, CA assembles into a protein shell (capsid core) encasing the viral genome, and NC associates with the viral RNA (Figure 1.2B) [1]. The *pol* gene encodes for the viral enzymatic proteins: protease (PR), reverse transcriptase (RT), and integrase (IN) (Figure 1.2A). These proteins are expressed as a Gag-Pol polyprotein due to a programmed ribosomal frameshifting event during Gag translation. During what is known as the maturation step, PR in the newly budded virion cleaves the Gag and Gag-Pol polyproteins which leads to formation of the conical capsid core [11]. The *env* gene encodes for envelope glycoprotein (Env) that is cleaved into the surface subunit (SU) and transmembrane subunit (TM). Env is found on the exterior of the virion and is arranged as a trimer (Figure 1.2B) [1].

Lentiviruses are considered complex retroviruses as their genomes possess an additional inventory of genes alongside the standard *gag*, *pol*, and *env* (Figure 1.2A). Primate lentiviral genomes encode for the regulatory genes *tat* and *rev* as well as several accessory genes that can vary among these viruses (Figure 1.2A) [1]. For HIV-1, these accessory genes are *vif, vpr, vpu, and nef* and the encoded proteins perform a variety of functions throughout viral replication including counteracting host antiviral proteins [12].

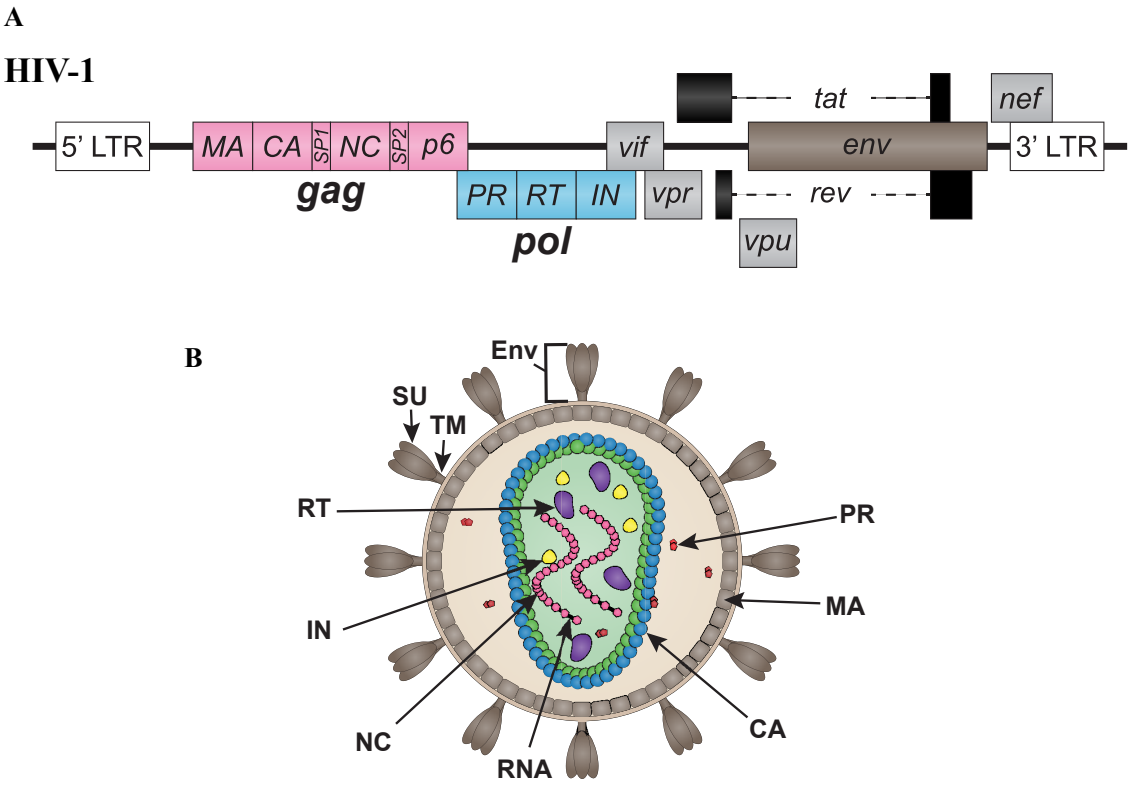

Figure 1.2. HIV-1 genome and virion
(A) Schematic of the HIV-1 provirus genomic organization. The gag gene (pink) encodes for the viral matrix (MA), capsid (CA), spacer peptide 1 (SP1), nucleocapsid (NC), spacer peptide 2 (SP2), and p6 proteins. The pol gene (blue) encodes for the viral protease (PR), reverse transcriptase (RT), and integrase (IN). The env gene (brown) encodes for the viral envelope glycoprotein (Env). The genes which encode for the various HIV-1 accessory proteins and regulatory proteins are shown in grey and black, respectively. A long terminal repeat (LTR) region (white box) is found at both ends of the proviral sequence and has regulatory functions.
(B) Schematic of the mature HIV-1 virion. Following PR (red) cleavage, the CA protein (green/blue protein) forms a conical protein shell around the two copies of the viral RNA genome (black curvy lines), and the RT (purple) and IN (yellow) proteins. NC (pink) protein coats the viral RNA. The MA (lighter brown) protein is located right below the host-derived lipid bilayer (tan). The Env protein is found as a trimer on the exterior of the virion, embedded in the lipid bilayer.

1.1.3 Replication

Interaction between the Env protein on the virion's surface and the host receptor protein on the target cell initiates retroviral entry (Figure 1.3). Primate lentiviruses utilize the host protein CD4 as a primary receptor, and a host chemokine receptor as a co-receptor for entry. The two chemokine co-receptors frequently associated with primate lentiviruses are C-C chemokine receptor 5 (CCR5) and C-X-C chemokine receptor 4 (CXCR4) [13–20]. The binding of Env to CD4 and then CCR5 or CXCR4 triggers a series of protein conformational changes and fusion between the viral and target cell membranes, releasing the viral capsid core into the cytoplasm (Figure 1.3) [1]. Encased in the deposited viral complex are the two copies of the viral RNA genome, RT, and IN, among other host and viral proteins [21–24].

Once in the target cell cytoplasm, RT begins to convert the viral single-stranded RNA genome into double-stranded DNA [25]. At this point, the viral genome and associated proteins are known as the reverse transcription complex (RTC), which traffics towards the nucleus (Figure 1.3). Once reverse transcription is complete and the viral DNA ends are processed by IN, the viral genome and associated proteins are known as the pre-integration complex (PIC) [26,27]. While reverse transcription was typically thought to be completed prior to nuclear import of the viral genome, recent evident indicates that HIV-1 completes reverse transcription within the host cell nucleus [28,29]. Upon gaining access to the host chromatin and completion of reverse transcription, IN catalyzes the insertion of the viral DNA into the host cell genome (Figure 1.3). Lentiviruses are unique from other members of the *Retroviridae* family in that these viruses can productively infect non-dividing cells, undergoing active transport through

the nuclear pore complexes (NPCs) which stud the host cell nuclear envelope. This distinct ability enables lentiviruses to replicate within cells like macrophages and resting CD4+ T cells, which are considered crucial cell types in HIV-1 persistence and pathogenesis [30–32]. Once inserted into the host genomic material, the viral genomic DNA is known as the provirus (Figure 1.3).

Proviral expression is regulated by the LTR sequences and enhanced by the trans-activator of transcription (Tat) viral protein [1]. The regulator of expression of viral proteins (Rev) viral protein facilitates nuclear export of intron-containing viral mRNA. Unspliced viral mRNA functions as both genetic material for new primate lentiviral progeny and the template for Gag and Gag-Pol expression. New primate lentiviral progeny assemble at the host cell plasma membrane and particle maturation occurs during or immediately following virion release [11].

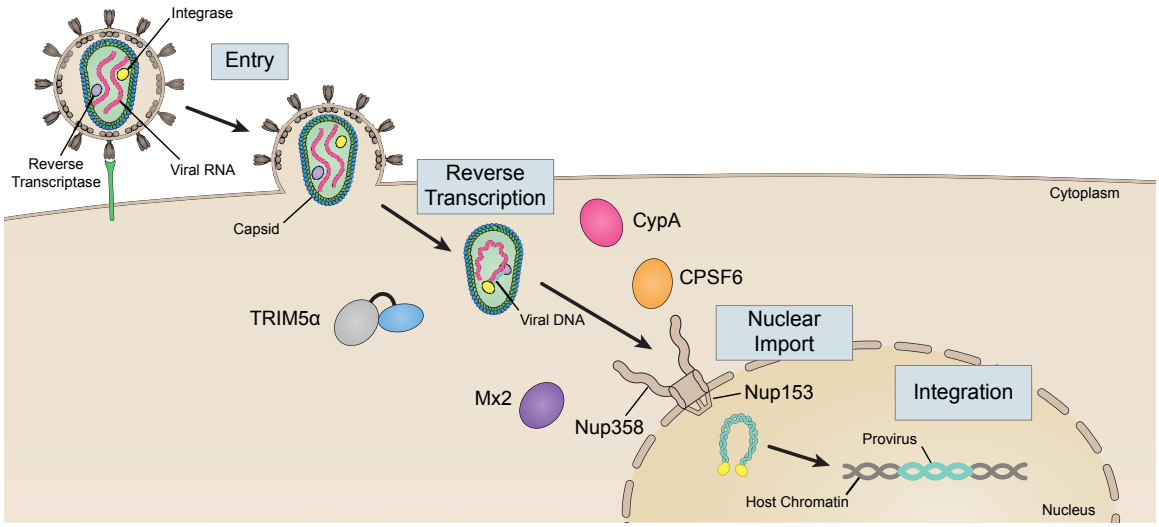

Figure 1.3. Early HIV-1 replication
HIV-1 entry is facilitated by the binding of the viral glycoprotein to the CD4 receptor and chemokine co-receptor on the cell surface. This interaction results in fusion between the viral cellular membranes and releases the viral capsid core into the cytoplasm. This core then traffics towards the nucleus. Along the way, reverse transcriptase begins to convert the RNA genome into DNA. Following arrival at the nucleus, the viral genome and associated proteins translocate through the nuclear pore complex (NPC) and then integrase inserts the viral DNA into the host chromatin, at which point it is referred to as the provirus. CypA, Nup358, CPSF6, and Nup153 are HIV-1 co-factors that interact with CA to facilitate post-entry steps of early replication. TRIM5α and Mx2 are restriction factors that target the CA and block replication prior to integration. CypA, cyclophilin A; Nup358, nucleoporin 358; CPSF6, cleavage and polyadenylation specificity factor subunit 6; Nup153, nucleoporin 153; TRIM5α, tripartite motif-containing protein 5 alpha isoform; Mx2, myxovirus resistance 2.

1.1.4 Cross-Species Transmission

SIVs are genetically very diverse and infect a wide range of old-world monkeys [33,34]. The nomenclature of primate lentiviruses can be misleading from an evolutionary perspective because, in stark contrast, the distinction between HIV-1 and SIV of chimpanzees (SIVcpz) is based on their respective hosts, while the two species actually share deep homologies [33–36]. Comparison of primate host species and primate lentivirus phylogenies show that these viruses have a long history of cross-species transmissions [35,37]. Multiple, independent events of SIV spillover into humans have occurred over time, giving rise to the four main HIV-1 groups (M, N, O, and P) and nine HIV-2 subtypes (A-I) [33–36,38]. HIV-1 group M alone is responsible for more than 95% of all documented infections [34]. Viruses belonging to the M and N groups of HIV-1 are thought to have originated from two separate and independent cross-species transmission events of SIVcpz [8]. SIVcpz also separately and independently gave rise to SIV of gorilla (SIVgor) [39,40]. SIVgor also gave rise to HIV-1 O and P groups from independent zoonotic transmission events from gorillas to humans [41].

Another source of multiple cross-species transmissions is SIV of sooty mangabeys (SIVsm; Figure 1.4). HIV-2 subtypes A through I arose from separate, independent cross-over events of SIVsm into humans [35,38,42–45] and the emergence of SIVsm in rhesus macaques (*Macaca mulatta*) gave rise to SIV of rhesus macaques (SIVmac) [42,46,47]. SIVsm has additionally jumped into two other macaque species, stump-tailed macaques (*Macaca arctoides*) and pig-tailed macaques (*Macaca nemestrina*), giving rise to SIVstm and SIVpbj, respectively (Figure 1.4) [42,48–53]. Pig-tailed macaques are also associated with infection by another SIV, SIVmne [54];

however, SIVmne did not originate from a SIVsm spill-over event [55,56]. Each species presented a unique set of genetic barriers that placed selective pressure on the virus during SIVsm emergence. As such, SIVsm offers a rare opportunity to examine how genetic differences between emergent hosts species drive the viral cross-species transmission process.

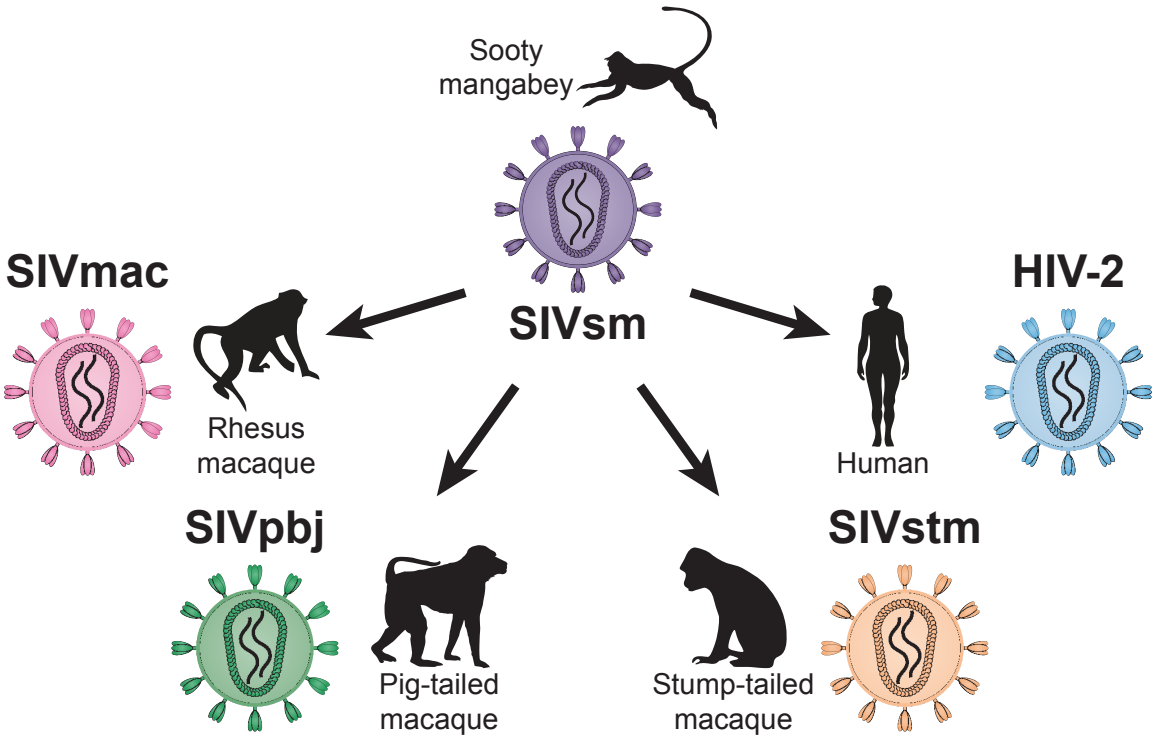

Figure 1.4. SIVsm has undergone multiple cross-species transmission events
SIVsm (purple) which infects sooty mangabeys has given rise to multiple primate lentiviruses following its emergence into several primate species, including: HIV-2 (blue) in humans; SIVstm (orange) in stump-tailed macaques; SIVpbj (green) in pig-tailed macaques; and SIVmac (pink) in rhesus macaques.

1.2 Lentiviral Capsid

1.2.1 Structure

In mature virions, the lentiviral capsid core exhibits a fullerene-like cone morphology and is composed of the viral CA protein assembled into pentamers and hexamers (Figures 1.5A and 1.5B). The CA monomer is a 24 kDa protein that is comprised of two independently folding domains: a N-terminal domain (NTD; Figure 1.5C) and a C-terminal domain (CTD) separated by a small flexible linker [57–59]. The CA NTD forms the surface of the intact capsid core and consists of a β-hairpin at the N-terminus followed by seven α-helices. Between CA α-helix 4 and α-helix 5, there is an proline-rich loop that extends from the surface of the assembled CA core and is known as the 4-5 loop or CypA-binding loop (Figure 1.5C, highlighted in pink) [60–62]. Despite a lack of amino acid sequence homology, the lentiviral CA structures exhibit remarkable structural homology (Figure 1.6) [21,63–67]. As with HIV-1, the role of capsid in mediating proper reverse-transcription and nuclear import has been established for multiple, diverse lentiviruses – highlighting the conservation of capsid functionality across this genus [68–71].

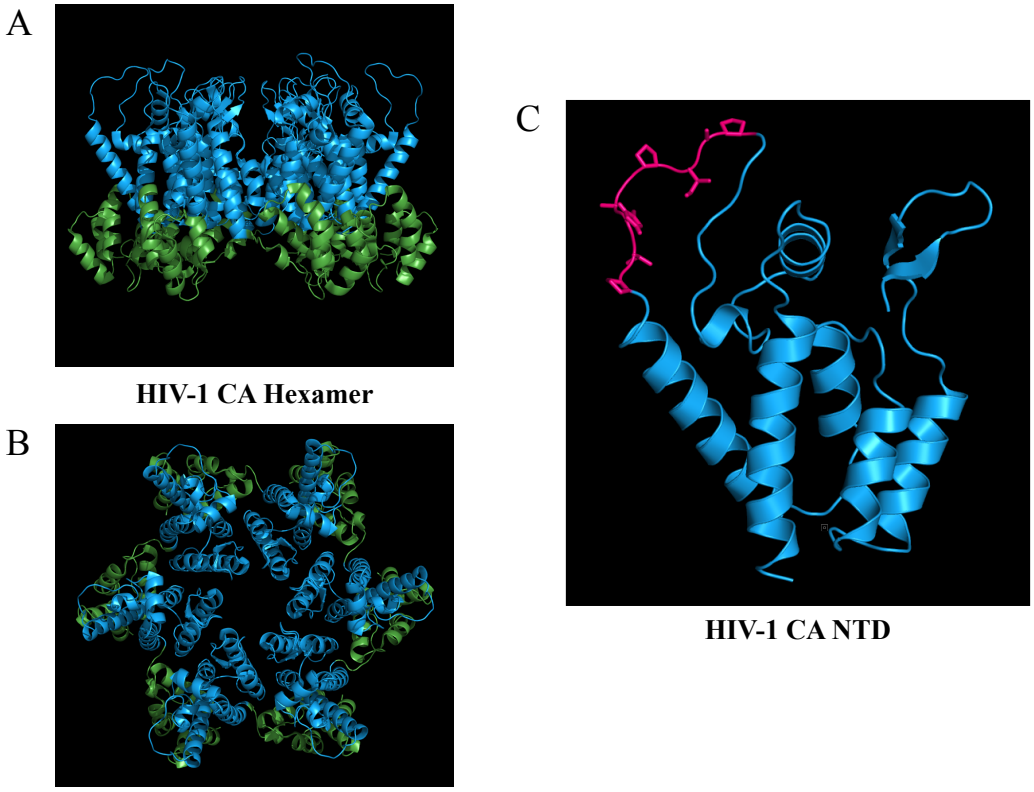

Figure 1.5. HIV-1 CA Structure
(A-B) Crystal structure of a single HIV-1 hexamer (pdb: 3GV2) as viewed from the side (A) or from the top (B). The CA NTD is colored in blue while the CA CTD is colored in green.
(C) Crystal structure of the HIV-1 CA NTD (pdb: 4LQW). The 4-5 loop is highlighted in pink.

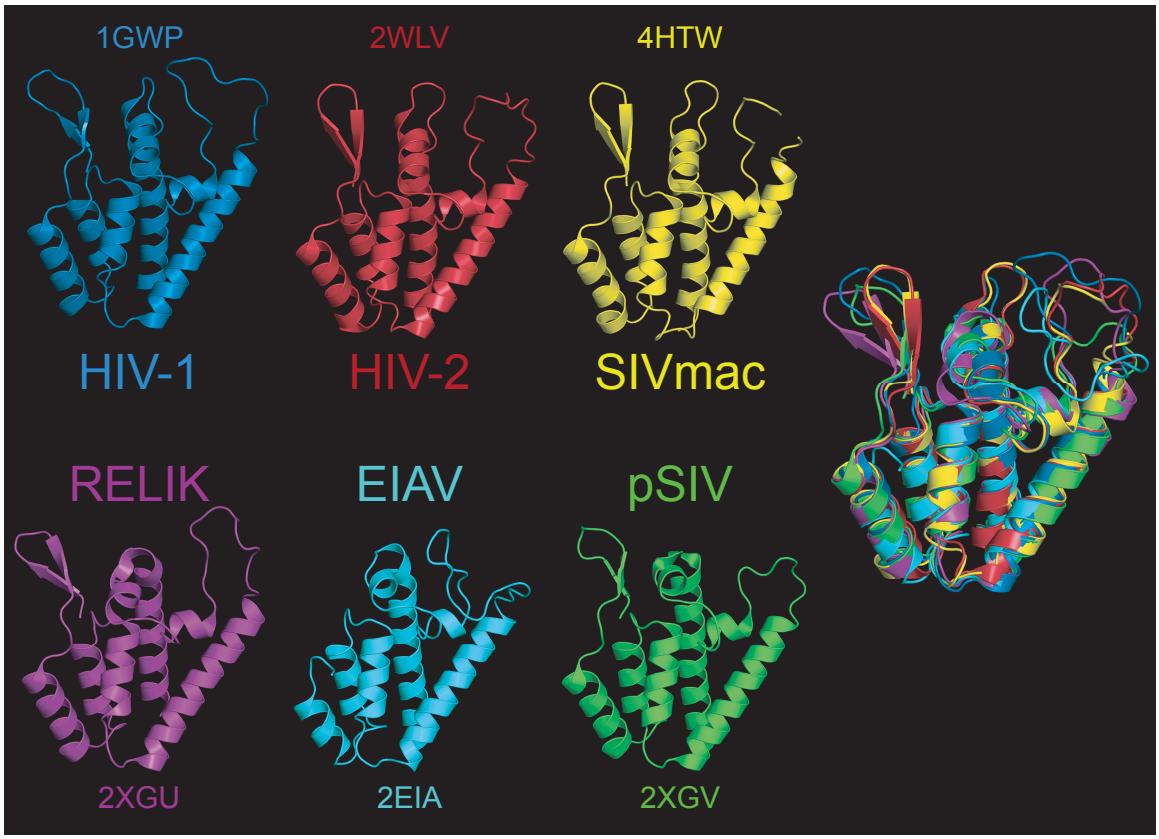

Figure 1.6. Crystal structures of Lentiviral CA NTD
Crystal structures of multiple lentiviral CA NTDs and a structural overlay of all the CA NTDs. The pdb number is shown above the crystal structure.

1.2.2 Function

Prior to integration into the host chromatin, HIV-1 must reverse transcribe the viral RNA to DNA. This process is dependent on proper capsid disassembly or uncoating as mutations in the CA CTD that either increase or decrease the intrinsic stability of the core result in defective reverse transcription [72].

While the precise mechanism is unclear, interactions with CPSF6 and CypA appear to stabilize the HIV-1 capsid and regulate the timing/kinetics of reverse transcription [73–77]. These capsid-cofactor interactions are critical as they enable the capsid to shield the viral genome from host antiviral proteins capable of sensing cytosolic DNA. Within non-immune cell lines, interactions with CPSF6 and CypA appear to be dispensable for replication [72,78,79]. Prior to integration into the host chromatin, HIV-1 must reverse transcribe the viral RNA to DNA. This process is dependent on proper capsid disassembly or uncoating as mutations in the CA CTD that either increase or decrease the intrinsic stability of the core result in defective reverse transcription [72]. The HIV-1 capsid facilitates proper uncoating through interactions with the peptidyl-prolyl-cis-trans-isomerase (PPIase) enzyme cyclophilin A (CypA), and the cellular protein cleavage and polyadenylation specificity factor 6 (CPSF6).

1.2.3 Interactions

Table 1.1. Summary of previous human Nup358-CA interaction studies
TRIM-Fusion (TF) assay utilizes the capsid binding-dependent restrictive ability of TRIM5α to detect CA-host protein interactions and is described in more detail later on. ITC, isothermal titration calorimetry; SEC, size-exclusion chromatography; SIVgor, SIV of gorilla; SIVcpz, SIV of chimpanzee; FIV, feline immunodeficiency virus; SIVmac, SIV of rhesus macaque; SIVmnd, SIV of mandrill; SIVcol, SIV of guereza colobus; SIVgsn, SIV of greater spot-nosed monkey; SIVmus, SIV of mustached monkey; SIVmon, SIV of mona monkey; EIAV, equine infectious anemia virus; MLV, murine leukaemia virus.

Viral CA	Interacts with human Nup358Cyp?	Method(s) used to detect interaction
HIV-1 Group M	Yes	TF assay [62,80–83]; ITC[1] [60,62,84]; Co-sedimentation assay[2] [85]; SEC[1] [84]; Co-crystal structure [60]
HIV-1 Group P[3]	Yes	TF assay [83]
SIVgor[3]	Yes	TF assay [83]
SIVcpz[3]	Yes	TF assay [83]
HIV-2	Yes	TF assay [80,82]
FIV	Yes	TF assay [81,83]; ITC[1] [60]
SIVmac	No	TF assay [80,82,83]; ITC[1] [62]
SIVmnd	No	TF assay [80]
SIVcol	No	
SIVgsn	No	
SIVmus	No	
SIVmon	No	
MLV	No	TF assay [81,83]

[1]Performed using purified human $Nup358_{Cyp}$ and purified, monomeric N-terminal domain (NTD) of CA. [2]Performed using *in-vitro* assembled CA-like complexes and Human Embryonic Kidney 293T/17 (HEK293T/17) cell lysates containing GFP-tagged full-length human Nup358 or Nup358ΔR4-Cyp deletion mutant. [3]Performed using the 4-5 loop in an HIV-1 Group M CA background

1.3 Nup358

1.3.1 Structure and Cellular Functions

Nucleoporin 358 (Nup358; also known as RanBP2) is the largest component of the NPC (358 kDa in size) and has a multimodular structure [86,87]. Nup358 plays an important role in nucleocytoplasmic trafficking by providing key interaction sites for the various components of the transport machinery [88–91]. Nup358 has multiple other functions, though, which are facilitated by distinct domains within its structure – including a cyclophilin-like domain at its C-terminus ($Nup358_{Cyp}$) [60,62,80–82,84]. Similar to CypA, $Nup358_{Cyp}$ has peptidyl-prolyl-cis-trans-isomerase (PPIase) activity; these enzymes are generally thought to facilitate proper protein folding through their catalytic activities [60,84,92–94]. Unlike CypA, which is comprised of a single domain, $Nup358_{Cyp}$ and the preceding Ran-binding domain 4 ($Nup358_{R4}$) act in concert as a chaperone and these contiguous domains form the R4-Cyp supradomain of Nup358 ($Nup358_{R4\text{-}Cyp}$) [95–97]. Furthermore, $Nup358_{R4}$ appears to influence the access/release of substrates to/from $Nup358_{Cyp}$ [97]. In other words, proteins that interact with $Nup358_{Cyp}$ by itself may not always interact with $Nup358_{Cyp}$ in the context of the $Nup358_{R4\text{-}Cyp}$ supradomain (which is the biologically-relevant form).

1.3.2 Role in HIV replication

Previous studies found that depletion of Nup358 (the entire protein) in human cell lines reduced HIV-1 infectivity [60,62,81,85,98,99], and appeared to inhibit replication at the point of nuclear import [62,85,98]. These results suggest that HIV-1 utilizes Nup358 to cross the nuclear pore complex (NPC) prior to integration. However, these findings do not necessarily point to a functional role $Nup358_{Cyp}$ in HIV-1 replication. Knockdown

(KD) of Nup358 can be cytotoxic in cell lines [81,99–102] and knockout (KO) of Nup358 in mice is embryonic lethal [100,101,103]. Meehan et al. found that deletion of Nup358Cyp in mouse embryonic fibroblast cells (MEFs) had little effect on HIV-1 infectivity [81]. Cre-lox mediated KO of murine Nup358 in MEFs reduced HIV-1 infectivity (although this defect was found to occur at the point of integration and not nuclear import). Deletion of the 1,884 C-terminal amino acids of Nup358, however, had no effect on HIV-1 infectivity. It is important to consider though that MEFs are neither host-species relevant or cell-type relevant for studies of HIV/AIDS. It is possible that nuclear import pathways differ between human and mice cells. HIV-1's dependency on several host proteins during nuclear import appears to be dictated by capsid-interactions with upstream factors including CPSF6 [62,73–76,99,104–109] and while HIV-1 CA is able to interact with murine CPSF6, there is evidence that suggests a functional difference between murine CPSF6 and human CPSF6 in HIV-1 replication [106]. It is also possible that nuclear import pathways may differ between cell types. HIV/SIV infect CD4+ T cells and macrophages *in vivo* thus it is possible that nuclear import requirements differ between fibroblasts and either of these cell types. In support of this possibility is the observation that NPC have been shown to vary in nucleoporin composition between different cell types [110–115]. Furthermore, it is possible that this interaction is important, but at another step of replication that is cell-type specific (i.e., innate immune evasion). This statement is true of other CA-interacting factors with roles in early infection like CypA and CPSF6 as either KD of CPSF6 or CypA results in a defect to HIV-1 replication which appears to be cell-type specific [99,106].

1.4 TRIM5α

TRIM5α (tripartite motif-containing protein 5 alpha isoform) is a cytoplasmic host restriction factor that is capable of blocking retroviral replication prior to integration [116–118]. This protein belongs to the tripartite motif (TRIM) protein family, whose members all contain a Really Interesting New Gene (RING) domain, one or two B-box domains and a coiled-coil domain [119]. The presence of these three protein domains in this particular order is known as a "RBCC" motif and the term is RBCC is used to collectively refer to the RING, B-Box, and coiled-coil domains of TRIM proteins. Some TRIM proteins have one or more C-terminal domains subsequent to the RBCC domains. In TRIM5α, the RBCC domains are followed by a C-terminal B30.2 or PRYSPRY domain that is absent from other TRIM5 isoforms [120].

TRIM5α acts to restrict retroviral replication by targeting the capsid core deposited into the target cell cytoplasm post entry [116–118]. The B30.2/PRYSPRY domain mediates CA core recognition through direct interaction with CA and thus dictates TRIM5α restriction specificity, whereas the RBCC domains generate the TRIM5α restrictive activity [116,121–133]. The self-association properties of both the B-box 2 and coiled-coil domains impart on TRIM5α the strong proclivity for high-order assembly required for retroviral restriction [134]. These assemblies activate the E3 ubiquitin ligase activity of the RING domain, which promotes further higher-order assembly [134]. Precisely how the B30.2/PRYSPRY domain binds CA is unclear but recognition appears to be driven through a series of high-avidity but low-affinity interactions [121,122,135–137].

In several species, including rhesus macaques, the B30.2/PRYSPRY domain of TRIM5α has been replaced with a CypA-derived domain (TRIM5Cyp) [138–144]. Like CypA, the C-terminal Cyp domain of TRIM5Cyp proteins binds the lentiviral CA 4-5 loop; however, the sequences of these domains differ from one another at several residues and have different interaction specificities [67,145]. For example, the rhesus macaque TRIM5Cyp protein (rhTRIM5Cyp) does not restrict HIV-1 replication and does not bind HIV-1 CA, despite HIV-1 CA binding CypA [61,139,144,146,147]. In contrast, rhTRIM5Cyp does restrict HIV-2 and binds to the HIV-2 CA 4-5 loop [67]. HIV-1 and HIV-2 CA 4-5 loop conformations differ considerably and rhTRIM5Cyp discrimination between the two loops stems from a D66N change from the ancestral CypA sequence [67].

CHAPTER 2: MATERIALS AND METHODS

2.1 Cell Lines

Crandell-Rees Feline Kidney (CRFK; female; ATCC, #CCL-94), Human Embryonic Kidney 293T/17 (HEK293T/17; female; ATCC, #CRL-11268), GP2-293 (presumed to be female based on the sex of the parental HEK293 cells; Clontech, Takara Bio, #631458), and HeLa (female; ATCC, #CCL-2) cells were cultured in Dulbecco's modified Eagle Media (DMEM) supplemented with 10% fetal bovine serum (FBS), 25 mM HEPES, 2 mM L-glutamine (L-glut), and 1% Penicillin-Streptomycin (Pen-Strep). CRFK cell lines engineered to express the HA-tagged TFnull, TF-Nup358, or TF-CypA constructs were maintained in similar media that was also supplemented with 5 μg/ml puromycin. CRFK cell lines engineered to express HA-tagged TRIM5α alleles were also maintained in similar media that was instead supplemented with 0.5 mg/ml G418. THP-1 cells (male) were obtained through the NIH AIDS Reagent Program, Division of AIDS, NIAID, NIH (cat# 9442) from Drs. Li Wu and Vineet N. KewalRamani [148,149] and cultured in Roswell Park Memorial Institute (RPMI)-1640 media supplemented with 10% FBS, 25 mM HEPES, 2 mM L-glut, 1% Pen-Strep, 1 mM sodium pyruvate, and 0.05 mM 2-mercaptoethanol. CEMx174-SEAP (sex unknown; Means et al., 1997), U937 (male; ATCC, #CRL-1593.2), H9 (male; ATCC, #HTB-176), and Jurkat, Clone E6-1 (male; ATCC, #TIB-152) cells were cultured in RPMI-1640 media supplemented with 10% FBS, 25 mM HEPES, 2 mM L-glut, and 1% Pen-Strep. SupT1-CCR5 cells (sex is presumed to be male based on the sex of the parental SupT1 cells; Means et al., 2001) were maintained in similar media that was also supplemented with 300 ng/ml puromycin.

The B-Lymphocyte cell lines listed in Table 2.1 were cultured in RPMI-1640 media supplemented with 10% FBS, 25 mM HEPES, 2 mM L-glut, 1% Pen-Strep, and 4

μM Zidovudine (AZT). The T-Lymphocyte cell lines listed in Table 2.1 were cultured in RPMI-1640 media supplemented with 20% FBS, 25 mM HEPES, 2 mM L-glut, 1% Pen-Strep, and 100 U/ml of interleukin-2 (IL-2). All cell cultures were kept at 37°C in 5% CO_2.

Table 2.1. Sources of RNA/DNA for sooty mangabey, rhesus macaque, and pig-tailed macaque Nup358 fragments sequenced
NEPRC, New England Primate Research Center.

Common name	Species name	Source	ID	Cell type
Sooty mangabey (sm)	*Cercocebus atys*	NEPRC	FIt	B-Lymphocyte
		NEPRC	FJy	B-Lymphocyte
		NEPRC	FMv	B-Lymphocyte
		NEPRC	FPr	B-Lymphocyte
		NEPRC	FWl	B-Lymphocyte
		NEPRC	FWj	B-Lymphocyte
		NEPRC	FYn	B-Lymphocyte
Rhesus macaque (rh)	*Macaca mulatta*	NEPRC	164.02	B-Lymphocyte
		NEPRC	221	T-Lymphocyte
		NEPRC	444	T-Lymphocyte
Pig-tailed macaque (ptm)	*Macaca nemestrina*	NEPRC	5503	B-Lymphocyte
		NEPRC	5403	B-Lymphocyte
		NEPRC	5903	B-Lymphocyte
		NEPRC	6403	B-Lymphocyte
		NEPRC	6603	B-Lymphocyte

2.2 Bacteria

All molecular cloning and plasmid propagation were carried out in One Shot Stbl3 Chemically Competent E. coli (Invitrogen, Thermo Fisher, #C73730). Molecular cloning cultures were grown on Luria-Bertani (LB) agar at 30°C and plasmid propagation cultures were grown in LB media at 30°C while shaking at 250 RPM. Both LB agar and LB media were supplemented with either ampicillin or kanamycin, depending on the plasmid antibiotic resistance.

2.3 Plasmids

2.3.1 Proviral Plasmids

Single-cycle (replication-incompetent), enhanced green fluorescent protein (EGFP) reporter NL4-3 HIV-1 virus was produced from pNL4-3-deltaE-EGFP vector which encodes a NL4-3 HIV-1 provirus where Env has been rendered non-functional due to the in-frame introduction of EGFP, and was obtained through the NIH AIDS Reagent Program, Division of AIDS, NIAID, NIH (Cat# 11100) from Drs. Haili Zhang, Yan Zhou, and Robert Siliciano [152]. Single-cycle, EGFP reporter HIV-2 ROD virus was produced from a plasmid which encodes a HIV-2 ROD provirus where Env has been rendered non-functional due to a deletion at the N-terminus and Nef has been replaced with EGFP. The source of this plasmid is unknown but it has been given the name pHIV-2ROD-Δenv-GFP and the entire plasmid sequence is known (available upon request). Single-cycle, EGFP reporter SIVmac239 virus was produced using pV1EGFP plasmid, which encodes the SIVmac239 provirus that is envelope-deficient due to deletion at N-terminus of *env* and expresses EGFP instead of Nef [153]. Single-cycle, EGFP reporter SIVsmE041 virus was produced using pV1EGFP-E041 plasmid, a pV1EGFP-derived

plasmid where the 5' half of SIVsmE041 provirus has been swapped in [153]. Single-cycle, EGFP reporter SIVpbj1.9 virus was produced using pV1EGFP-pbj1.9 plasmid, which was created by amplifying by PCR the 5' half of SIVsmm PBj14 molecular clone 1.9 provirus from the pPBj1.9 plasmid [which was obtained through the NIH AIDS Reagent Program, Division of AIDS, NIAID, NIH (Cat# 2998) from Dr. James I. Mullins [53]] using the primers pbj1.9-NarI-F and pbj1.9-SphI-R. The NarI and SphI restrictions sites were used to replace the SIVmac239 sequence in the pV1EGFP plasmid with the PCR fragment (SphI restriction site was introduced to the 3' end of PCR product by pbj1.9-SphI-R primer). The 5' half of SIVsmm PBJ14 molecular clone 1.9 comes from SIVpbj non-infectious clone 1.5 (accession number L03295); however, sequencing of both pPBj1.9 and pV1EGFP-pbj1.9 plasmids revealed multiple synonymous and non-synonymous mutations compared to the SIVpbj1.5 reference sequence, including a S171L difference in capsid. The amino acid sequence of the capsid is shown in Figure 2.1 and the sequence of the entire fragment amplified from pPBj1.9 is available upon request. Single-cycle, EGFP reporter SIVstm37.16 virus was produced using pV1EGFP-37.16 plasmid, a pV1EGFP-derived plasmid where the full *gag* and partial *pol* of SIVstm37.16 provirus has been swapped in [153]. Single-cycle, EGFP reporter SIVsmE543 virus was produced using pV1EGFP-E543 plasmid, a pV1EGFP-derived plasmid where the 5' half of SIVsmE543 provirus has been swapped in [153]. Single-cycle, EGFP reporter SIVsmE660-FL14 and SIVsmE660-FL6 viruses were produced using pV1EGFP-E660 FL14 and pV1EGFP-E660 FL6, respectively. These plasmids are pV1EGFP-derived where the 5' half of SIVsmE660-FL14 or SIVsmE660-FL6 has been swapped in [154].

Multi-cycle (replication-competent) HIV-2 ROD virus was produced from pROD10 plasmid which encodes the full-length HIV-2 ROD provirus that contains a mutation in *env* resulting in a premature stop codon at position 720 and expression of a truncated, but functional Env protein. This plasmid was obtained from the Centre for AIDS Reagents, NIBSC, UK (NIH-ARP# 12518; CFAR# 232), supported by EURIPRED (EC FP7 INFRASTRUCTURES-2012 – INFRA-2012-1.1.5.: Grant Number 31266). www.euripred.edu/ [155,156]. Multi-cycle SIVsmE543 virus was produced from pGEM-E543 plasmid, which encodes the full-length SIVsmE543 provirus [157].

The plasmids used to produce single-cycle, EGFP reporter, chimeric SIVmac239 viruses encoding various SIVsm/HIV-2 capsids were created by replacing the entire SIVmac239 CA sequence with the CA from: SIVsmG932 (JX860416); SIVsmD215 (JX860413); HIV-2 GH-1 (M30895); HIV-2 UC1 (L07625); HIV-2 EHO (U27200); SIVsmE041 (HM059825); and HIV-2 ROD (M15390). The SIVsmG932, SIVsmD215, HIV-2 GH-1, HIV-2 UC1, and HIV-2 EHO CA sequences were commercially synthesized as GeneArt Strings DNA fragments (Invitrogen, Thermo Fisher) and were designed to contain silent mutations that created a BsrGI restriction site at nucleotides 3-8 and disrupted any internal BsrGI sites. Additionally, a BbvCI restriction site was added to the C-terminus of each string. The SIVsmE041 CA sequence was amplified by PCR from the pV1EGFP-E041 plasmid using the primers E041-CA-BsrGI-F and E041-CA-BbvCI-R, which add a BsrGI and BbvCI restriction site to the PCR product 5’ and 3’ ends, respectively. For the HIV-2 ROD CA sequence, site-directed mutagenetic PCR was performed first on the pHIV-2ROD-Δenv-GFP plasmid to introduce silent mutations to disrupt an internal BsrGI restriction site, using the 5’ phosphorylated primers ROD-

shuttle-Horn-F and ROD-shuttle-Horn-R. The HIV-2 ROD CA sequence was then amplified by PCR from a properly modified pHIV-2ROD-Δenv-GFP plasmid (confirmed by sequencing and BsrGI restriction digest) using the primers ROD-CA-BsrGI-F and ROD-CA-BbvCI-R, which add a BsrGI and BbvCI restriction site to the PCR product 5' and 3' end, respectively. The BsrGI and BbvCI restriction sites were used to replace the SIVmac239 CA sequence with the SIVsm/HIV-2 CA in an SIVmac239-based *gag-pol* shuttle vector that contains multiple silent mutations within *gag* in order to introduce or remove certain restriction site to facilitate CA chimerization [66]. The chimeric SIVmac239 *gag* from the shuttle vector was then subcloned into pV1EGFP using DraIII and SbfI restriction sites to create the single-cycle, EGFP reporter, chimeric CA SIVmac239 proviral plasmids. These plasmids were given the names pV1EGFP-G932 CA, pV1EGFP-D215 CA, pV1EGFP-GH-1 CA, pV1EGFP-UC1 CA, pV1EGFP-EHO CA, pV1EGFP-E041 CA, and pV1EGFP-ROD CA, in which the SIVmac239 CA has been completely replaced with the CA of SIVsmG932, SIVsmD215, HIV-2 GH-1, HIV-2 UC1, HIV-2 EHO, SIVsmE041, or HIV-2 ROD, respectively. An alignment of the CA sequences of all SIV/HIV viruses used is shown in Figure 2.1. Sequences of primers used are listed in Table 2.2.

Single-cycle, EGFP reporter FIV virus was produced from pGINSIN, an FIV-based transfer vector encoding EGFP [1], and pFP93, an FIV *gag-pol* packaging construct [1]. Single-cycle, EGFP reporter MLV virus was produced from pCIGB, an MLV *gag-pol* packaging plasmid [2], and pLXIN-GFP, a pLXIN-based (Clontech; #631501) transfer vector encoding EGFP. Single-cycle, EGFP reporter EIAV virus was produced from pEV53D, an EIAV *gag-pol* packaging plasmid (a gift from John Olsen;

Addgene plasmid # 44168) [3], and pEIAV-SIN6.1 CGFPW, an EIAV-based transfer vector encoding EGFP (a gift from John Olsen; Addgene plasmid # 44171) [4]. The vesicular stomatitis virus G protein (VSV-G) used to psuedotype all single-cycle, EGFP reporter viruses and recombinant retroviruses used for CRFK cell transduction was produced from pLP-VSVG plasmid (Invitrogen, Thermo Fisher, #K497500).

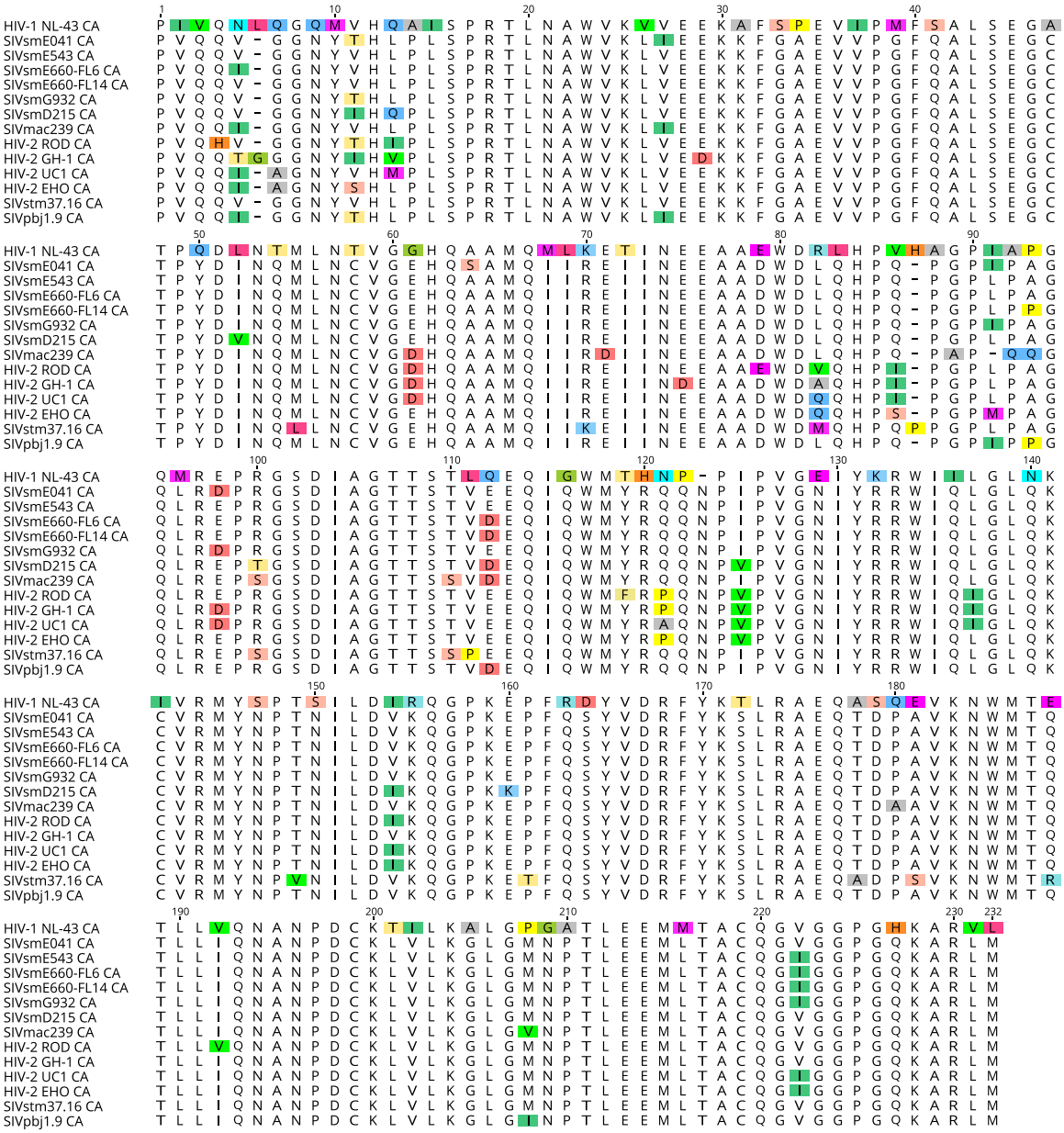

Figure 2.1. Amino acid alignment of primate lentiviral capsid sequences
Amino acid alignment of the HIV/SIV capsids used. Genbank accession numbers: HIV-1 NL4-3 (M19921); SIVsmE041 (HM059825); SIVsmE543 (U72748); SIVsmE660-FL6 (JQ864085); SIVsmE660-FL14 (JQ864087); SIVsmG932 (JX860416); SIVsmD215 (JX860413); SIVmac239 (M33262); HIV-2 ROD (M15390); HIV-2 GH-1 (M30895); HIV-2 UC1 (L07625); HIV-2 EHO (U27200); and SIVstm37.16 (M83293).

Table 2.2. Oligonucleotides for PCR amplification and site-directed mutagenesis of lentiviral proviruses

Primer name	Sequence
pbj1.9-NarI-F	5'-CCGCCTGGTCATCTCGGTACTCGGAC-3'
pbj1.9-SphI-R	5'-CTCTAGAGGGCGGTATAGTTGAG-3'
E041-CA-BsrGI-F	5'-GCAGCATGTACAGCAAGTAGGT-3'
E041-CA-BbvCI-R	5'-ATAATACCTCAGCCATTAGTCTAGCTTTTT-3'
ROD-shuttle-Horn-F	5'Phos-TAACCCGACCAACATCCTAGACATAAAAC-3'
ROD-shuttle-Horn-R	5'Phos-TACATCCTGACACACTTCTGCAATCCTA-3'
ROD-CA-BsrGI-F	5'-ATAATACCTGTACAACATGTAGGCGGCAACTA-3'
ROD-CA-BbvCI-R	5'-ATAAGCCCTCAGCCATTAATCTAGCTTTCTG-3'
E041-CA-Q85I-F	5'Phos-ATACCAGGTCCAATACCAGCAGGAC-3'
E041-CA-Q85I-R	5'Phos-TGGGTGTTGTAAATCCCAATCAGC-3'
E041-CA-QP86QPP-Fv2	5'Phos-CCGCCAGGTCCAATAC-3'
E041-CA-QPP-R	5'Phos-CTGTGGGTGTTGTAAATCCC-3'
E041-CA-G87A-F	5'Phos-GCTCCAATACCAGCAGGACAACTTAG-3'
SIVsmE041_CA-G88V_R	5'Phos-TGGCTGTGGGTGTTGTAAATCC-3'
E041-CA-IPA91QQ-F	5'Phos-CAACAAGGACAACTTAGAGACCCGAG-3'
E041-CA-IPA91QQ-R	5'Phos-TGGACCTGGCTGTGGGTG-3'
E041-G87A+QQ-F	5'Phos-GCTCCACAACAAGGACAACTTAGAGAC-3'
ROD-CA-I85Q-F	5'Phos-CAGCCAGGCCCCTTACCAG-3'
ROD-CA-I85Q-R	5'Phos-TGGATGTTGCACATCCCATTC-3'
pbj1.9-CA-P91A-F	5'Phos-GCAGGACAACTTAGAGAGCCAAGAG-3'
pbj1.9-CA-P91A-R	5'Phos-TGGTATCGGACCTGGCTGC-3'
37.16-CA-ΔP86-F	5'Phos-GGTCCGCTGCCAGCAGG-3'
37.16-CA-ΔP86-R	5'Phos-TGGTTGTGGATGCTGCATGTC-3'
239-CA-A87G-F	5'Phos-GGTCCACAACAAGGACAACTTAGGG-3'
239-CA-A87G-R	5'Phos-TGGTTGTGGGTGCTGCAAGT-3'
239-CA-QQ90LPA-F	5'Phos-CTACCAGCAGGACAACTTAGGGAGC-3'
239_89IPA91_R	5'Phos-TGGAGCTGGTTGTGGGTGC-3'
239-A87G+IPA-F	5'Phos- GGTCCAATACCAGCAGGACAACTTAG-3'

2.3.2 TRIM-Fusion (TF) Assay Plasmids

The TFnull construct – which consists of an N-terminal HA tag, then the first 303 amino acids of rhesus macaque (rh) TRIM5Cyp (rhTRIM5Cyp; Genbank accession number EU359036), followed by an AsiSI restriction site; an adenine; a stop codon; three 'GCC' repeats; and a MluI restriction site (Figure 2.2A) – was commercially synthesized as a GeneArt Strings DNA fragment (Invitrogen, Thermo Fisher) and then amplified by PCR using the primers T5fusion_XhoI_F and T5fusion_EcoRI_R, which add a XhoI and EcoRI restriction site to the PCR product 5' and 3' ends, respectively. The TFnull fragment was inserted into pLPCX vector (Clontech; #631511) using XhoI and EcoRI restriction sites, creating the pLPCX-TFnull plasmid. The pLPCX vector is a retroviral transfer vector that has a puromycin resistance gene for antibiotic selection in eukaryotic cells.

To create the TRIM-Fusion (TF) constructs where the human (hu), sooty mangabey (sm), and rhesus macaque (rh) $Nup358_{Cyp}$ or $Nup358_{R4\text{-}Cyp}$, and human CypA (huCypA) domain is fused to the rhTRIM5Cyp RBCC domains (Figures 2.2B and 2.2C), total RNA was isolated from HEK293T/17 (human), FPr (sooty mangabey), and 444 (rhesus macaque) cells using RNeasy Mini Kit (Qiagen, #74104) according to manufacturer's protocol. From the isolated RNA, human, sooty mangabey, and rhesus macaque $Nup358_{Cyp}$ cDNA was generated by RT-PCR with primers huNup358-Cyp_AsiSI_F and huNup358-Cyp_MluI_R while human, sooty mangabey, and rhesus macaque $Nup358_{R4\text{-}Cyp}$ cDNA was generated by RT-PCR with primers huNup358-RBD4_AsiSI_F and huNup358-Cyp_MluI_R. From the HEK293T/17 isolated RNA, huCypA cDNA was generated by RT-PCR with primers huCypA_AsiSI_F and

huCypA_MluI_R. All three sets of primers add an AsiSI and MluI restriction site to the cDNA product 5' and 3' ends, respectively. RT-PCR was performed using SuperScript III One-Step RT-PCR System with Platinum *Taq* High Fidelity DNA Polymerase (Invitrogen, Thermo Fisher, #12574030). The human, sooty mangabey, and rhesus macaque Nup358-Cyp and $Nup358_{R4\text{-}Cyp}$, and huCypA cDNA products were inserted into the pLPCX-TFnull plasmid using AsiSI and MluI restriction sites, creating the pLPCX-TF-huNup358-Cyp, pLPCX-TF-smNup358-Cyp, pLPCX-TF-rhNup358-Cyp, pLPCX-TF-huNup358-RBD4/Cyp, pLPCX-TF-smNup358-RBD4/Cyp, pLPCX-TF-rhNup358-RBD4/Cyp, and pLPCX-TF-huCypA plasmids, respectively. These plasmids encode the N-terminal HA-tagged rhTRIM5Cyp RBCC domains fused to $huNup358_{Cyp}$ domain, $smNup358_{Cyp}$ domain, $rhNup358_{Cyp}$ domain, $huNup358_{R4\text{-}Cyp}$ domains, $smNup358_{R4\text{-}Cyp}$ domains, $rhNup358_{R4\text{-}Cyp}$ domains, or huCypA domain, respectively. The CypA amino acid sequence is identical for human, sooty mangabey, and rhesus macaque [83,158]. Sequences of primers used are listed in Table 2.3.

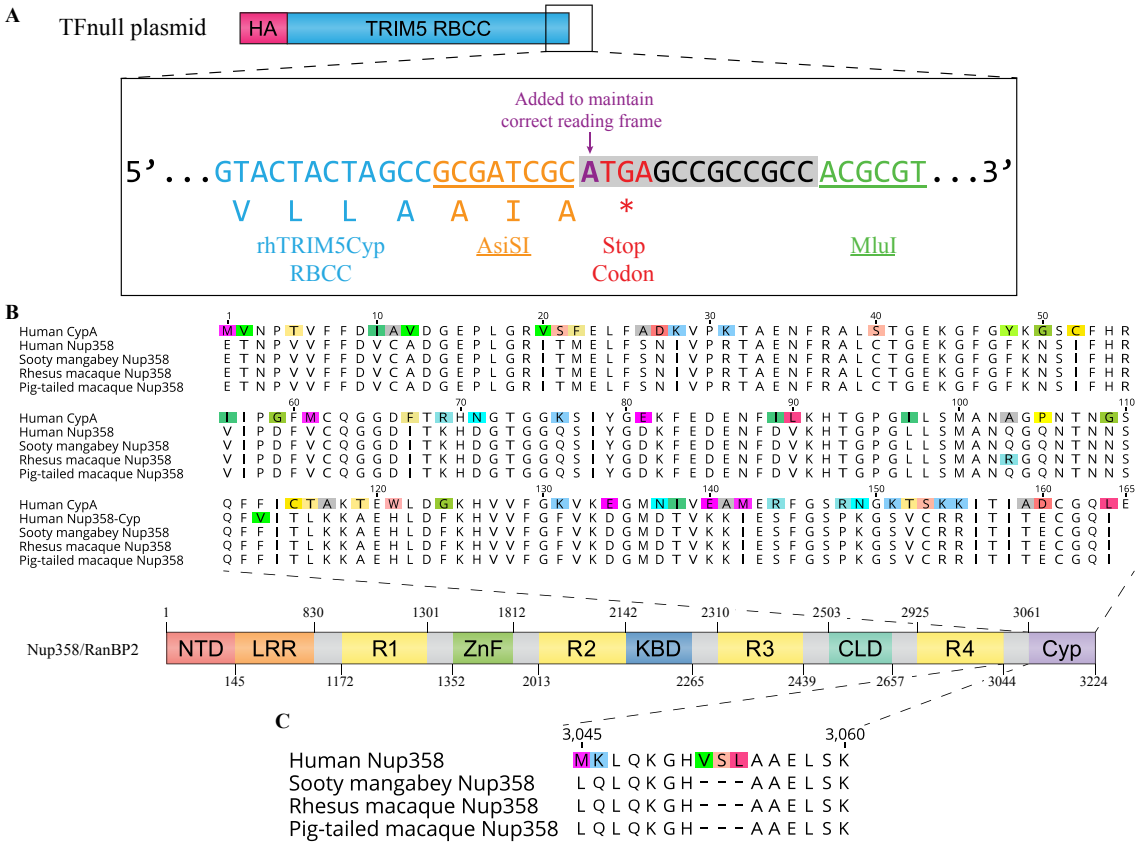

Figure 2.2. Details of TRIM-Fusion (TF) constructs

(A) Schematic of TFnull construct with its C-terminal sequence shown below. The construct has a N-terminal HA tag, followed by the first 303 amino acids of rhTRIM5Cyp (Genbank accession number EU359036) – which contains the RBCC (blue lettering) – then an AsiSI restriction site (orange lettering); an adenine to maintain the correct reading frame (purple lettering); a stop codon (red lettering); three 'GCC' repeats; and a MluI restriction site (green lettering). Thus, the TFnull construct expresses HA-tagged rhTRIM5Cyp RBCC domains plus three additional amino acids. The AsiSI and MluI (green lettering) restriction sites were used to create the TF-Nup358 and TF-CypA constructs (replacing the gray boxed sequence) with the AsiSI restriction site, adenine for correct reading frame, and MluI restriction site introduced to inserts by PCR. Figure not drawn to scale.

(B) Sequence alignment of huCypA and human, sooty mangabey, rhesus macaque, and pig-tailed macaque Nup358$_{Cyp}$ domains. Residues are numbered based on human CypA sequence. Genbank accession numbers for huCypA and huNup358 sequences are NM_021130 and NM_006267, respectively.

(C) Sequence alignment of region between Nup358$_{R4}$ and Nup358$_{Cyp}$ domains for human, sooty mangabey, rhesus macaque, and pig-tailed macaque Nup358 orthologs. Numbering shown based on human Nup358 sequence (Genbank accession number NM_006267). The R4 domain is identical for all four species. Schematic of Nup358 not drawn to scale.

Table 2.3. Oligonucleotides for PCR amplification and site-directed mutagenesis of TF constructs

Primer name	Sequence
T5fusion_XhoI_F	5'-ATAATACTCGAGGCCACCATGTACCCATACGAC-3'
T5fusion_EcoRI_R	5'-ATAATAGAATTCACGCGTGGCGGCGGCTCAT-3'
huNup358-Cyp_AsiSI_F	5'-ATAATAGCGATCGCAGAGACCAATCCTGTG-3'
huNup358-Cyp_MluI_R	5'-ATAATAACGCGTTTATATCTGTCCACATTCTGTGATAGTTATT-3'
huNup358-RBD4_AsiSI_F	5'-ATAATAGCGATCGCATCTGGAGAAGAAGATGAAGAA-3'
huCypA_AsiSI_F	5'-ATAATAGCGATCGCAATGGTCAACCCCACCGTGTT-3'
huCypA_MluI_R	5'-ATAATAACGCGTTTATTCGAGTTGTCCACAGTCAGCAATGGT-3'
huNup358-M3045L-F	5'Phos-TTGAAACTCCAGAAAGGACATGTATCACT-3'
huNup358-M3045L-R	5'Phos-TAAATTCTGCTGACATTCTTCAAATGTTTTCT-3'
huNup358-K3046Q-F	5'Phos-CTCCTCCAGAAAGGACATGTATCACTG-3'
huNup358-K3046Q-R	5'Phos-CATTAAATTCTGCTGACATTCTTCAAATGTTT-3'
Nup358_delta3aa_F	5'Phos-GCAGCAGAATTATCAAAGGAGACCA-3'
Nup358_3aa_R	5'Phos-ATGTCCTTTCTGGAGTTTCATTAAATTCTG-3'
huNup358-V3173F-F	5'Phos-TTTATAACACTGAAGAAAGCAGAACATTTGG-3'
hu358-V3173W_R	5'Phos-AAATTGAGAATTATTGGTATTCTGGCCTTG-3'
smNup358-L3045M-F	5'Phos-ATGCAACTCCAGAAAGGACATGC-3'
smNup358-Q3046K-F	5'Phos-AAACTCCAGAAAGGACATGCAGCA-3'
smNup358-Q3046K-R	5'Phos-CAATAAATTCTGCTGACATTCTTCAAATGTTTT-3'
Nup358_plus3aa_F	5'Phos-GTATCACTGGCAGCAGAATTATCAAAGG-3'
smNup358_3aa_R	5'Phos-ATGTCCTTTCTGGAGTTGCAATAAATTCT-3'
smNup358-F3170V-F	5'Phos-GTTATAACACTGAAAAAAGCAGAACATTTGGAC-3'

2.4 Sequencing of Nup358 C-Terminal Fragment

Genomic DNA was isolated from the sooty mangabey, rhesus macaque, and pig-tailed macaque cell lines listed in Table 2.1 using the Maxwell 16 Cell DNA Purification Kit (Promega, #AS1020) according to manufacturer's protocol. The C-terminal fragment of the *RANBP2* gene (which encodes the Nup358 protein) was amplified by PCR using the primers huNup358-RBD4_AsiSI_F and huNup358-Cyp_MluI_R. PCR was performed with Phusion Flash PCR Master Mix (Thermo Scientific, #F548S). PCR products were sequenced directly by Eton Bio (Boston, MA) and data were analyzed using Geneious (Biomatters Limited, v2020.2.4).

2.5 Site-Directed Mutagenesis

2.5.1 Primer Phosphorylation

The 5' end of primers used for site-directed mutagenesis were phosphorylated by T4 Polynucleotide Kinase (New England Biolabs, cat# M0201S), which was heat inactivated at 65°C for 20 minutes prior to use of primers in PCR.

2.5.2 Lentiviral CA Mutants

The SIVsmE041 Q85I, A91P, ^{85}QP^{86}➔^{85}QPP^{87}, G87A, and ^{89}IPA^{91}➔^{89}QQ^{90} CA mutants were made by site-directed mutagenetic PCR on pV1EGFP-E041 using the following primer pairs: E041-CA-Q85I-F and E041-CA-Q85I-R (for Q85I CA mutation); E041-CA-A91P-F and E041-CA-A91P-R (for A91P CA mutation); E041-CA-QP86QPP-Fv2 and E041-CA-QPP-R (for ^{85}QP^{86}➔^{85}QPP^{87} CA mutation); E041-CA-G87A-F and SIVsmE041_CA-G88V_R (for G87A CA mutation); and E041-CA-IPA91QQ-F and E041-CA-IPA91QQ-R (for ^{89}IPA^{91}➔^{89}QQ^{90} CA mutation). Properly modified clones were identified by sequencing and the mutant CA was subcloned into pV1EGFP-E041

plasmid using DraIII and SbfI restriction sites to create the single-cycle, EGFP reporter, mutant CA SIVsmE041 proviral plasmids. These plasmids were given the names: pV1EGFP-E041 Q85I, pV1EGFP-E041 A91P, pV1EGFP-E041 QP➔QPP, pV1EGFP-E041 G87A, and pV1EGFP-E041 IPA➔QQ, which contain the SIVsmE041 Q85I, A91P, ^{85}QP^{86}➔^{85}QPP^{87}, G87A, or ^{89}IPA^{91}➔^{89}QQ^{90} CA mutation, respectively. The SIVsmE041 G87A + ^{89}IPA^{91}➔^{89}QQ^{90} CA double mutant was created in a similar fashion except site-directed mutagenetic PCR was performed on pV1EGFP-E041 IPA➔QQ using the primers E041-G87A+QQ-F and SIVsmE041_CA-G88V_R, creating the pV1EGFP-E041 G87A+IPA➔QQ plasmid.

The HIV-2 ROD I85Q CA mutant was made by site-directed mutagenetic PCR on pHIV-2ROD-Δenv-GFP using the primers ROD-CA-I85Q-F and ROD-CA-I85Q-R. A properly modified clone was identified by sequencing and the mutant CA was subcloned into pHIV-2ROD-Δenv-GFP and pROD10 plasmids using EcoRV restriction sites to create the single-cycle, EGFP reporter, and multi-cycle HIV-2 ROD I85Q mutant CA viruses, respectively. These plasmids were given the names pHIV-2ROD-Δenv-GFP I85Q and pROD10 I85Q, respectively.

The SIVpbj1.9 P91A CA mutant was made by site-directed mutagenetic PCR on pV1EGFP-pbj1.9 using the primers pbj1.9-CA-P91A-F and pbj1.9-CA-P91A-R. A properly modified clone was identified by sequencing and the mutant CA was subcloned into pV1EGFP-pbj1.9 using NarI and SphI restriction sites, creating the single-cycle, EGFP reporter SIVpbj1.9 P91A CA mutant. This plasmid was given the name pV1EGFP-pbj1.9 P91A.

The SIVstm37.16 ΔP86 CA mutant was made by site-directed mutagenetic PCR on pV1EGFP-37.16 using the primers 37.16-CA-ΔP86-F and 37.16-CA-ΔP86-R. A properly modified clone was identified by sequencing and the mutant CA was subcloned into pV1EGFP-37.16 using DraIII and SbfI restriction sites, creating the single-cycle, EGFP reporter SIVstm37.16 ΔP86 CA mutant. This plasmid was given the name pV1EGFP-37.16 ΔP86.

The SIVmac239 A87G, and ^{89}QQ^{90}➔^{89}IPA^{91} CA mutants were made by site-directed mutagenetic PCR on pV1EGFP using the following primer pairs: 239-CA-A87G-F and 239-CA-A87G-R (for A87G CA mutation); and 239-CA-QQ90LPA-F and 239_89IPA91_R (for ^{89}QQ^{90}➔^{89}IPA^{91} CA mutation). Properly modified clones were identified by sequencing and the mutant CA was subcloned into pV1EGFP plasmid using DraIII and SbfI restriction sites to create the single-cycle, EGFP reporter, mutant CA SIVmac239 proviral plasmids. These plasmids were given the names pV1EGFP-A87G, and pV1EGFP-QQ➔IPA, which contain the SIVmac239 A87G, or ^{89}QQ^{90}➔^{89}IPA^{91} CA mutation, respectively. The SIVmac239 A87G + ^{89}QQ^{90}➔^{89}IPA^{91} CA double mutant was created in a similar fashion except site-directed mutagenetic PCR was performed on pV1EGFP-QQ➔IPA using the primers 239-A87G+IPA-F and 239-CA-A87G-R, creating the pV1EGFP-A87G+QQ➔IPA plasmid.

All site-directed mutagenetic PCR was performed using 5’ phosphorylated primers. Sequences of primers used are listed in Table 2.2.

The creation of SIVmac239 S97R, SIVsmE543 R98S, and SIVsmE543 P37S CA mutants has been previously described [153,159].

2.5.3 TF-Nup358 Mutants

The TF-huNup358$_{R4\text{-}Cyp}$ M3045L, K3046Q, Δ^{3052}VSL^{3054}, and V3173F mutant constructs were made by site-directed mutagenetic PCR on pLPCX-TF-huNup358-RBD4/Cyp using the following primer pairs: huNup358-M3045L-F and huNup358-M3045L-R (for M3045L mutant); huNup358-K3046Q-F and huNup358-K3046Q-R (for K3046Q mutant); Nup358_delta3aa_F and Nup358_3aa_R (for Δ^{3052}VSL^{3054} mutant); and huNup358-V3173F-F and hu358-V3173W_R (for V3173F mutant). The generated TF-huNup358$_{R4\text{-}Cyp}$ mutant plasmids were given the names: pLPCX-TF-huNup358-RBD4/Cyp M3045L, pLPCX-TF-huNup358-RBD4/Cyp K3046Q, pLPCX-TF-huNup358-RBD4/Cyp ΔVSL, and pLPCX-TF-huNup358-RBD4/Cyp V3173F. These plasmids encode the N-terminal HA-tagged rhTRIM5Cyp RBCC domains fused to huNup358$_{R4\text{-}Cyp}$ domains containing a M3045L, K3046Q, Δ^{3052}VSL^{3054} (deletion of "VSL" residue stretch at positions 3052-3054), or V3137F mutation, respectively. The residue numbering of the mutations is in respect to their position within the full-length human Nup358 protein.

The TF-smNup358$_{R4\text{-}Cyp}$ L3045M, Q3046K, $+^{3052}$VSL^{3054}, and F3173V mutants were made by site-directed mutagenetic PCR on pLPCX-TF-smNup358-RBD4/Cyp using the following primer pairs: smNup358-L3045M-F and huNup358-M3045L-R (for L3045M mutant); smNup358-Q3046K-F and smNup358-Q3046K-R (for Q3046K mutant); Nup358_plus3aa_F and smNup358_3aa_R (for $+^{3052}$VSL^{3054} mutant); and smNup358-F3170V-F and hu358-V3173W_R (for F3173V mutant). The generated TF-smNup358$_{R4\text{-}Cyp}$ mutant plasmids were given the names: pLPCX-TF-smNup358-RBD4/Cyp L3045M, pLPCX-TF-smNup358-RBD4/Cyp Q3046K, pLPCX-TF-

smNup358-RBD4/Cyp +VSL, and pLPCX-TF-smNup358-RBD4/Cyp F3170V. These plasmids encode the N-terminal HA-tagged rhTRIM5Cyp RBCC domains fused to sooty mangabey $Nup358_{R4\text{-}Cyp}$ domains containing a L3045M, Q3046K, +3052VSL3054 (insertion of "VSL" residues at positions 3052-3054), or V3137F mutation, respectively. Note: the residue numbering of the mutations is in respect to their position relative to the full-length human Nup358 protein (the F3173V mutation of $smNup358_{R4\text{-}Cyp}$ is at residue 3170 of the full-length sooty mangabey Nup358 protein).

All site-directed mutagenetic PCR was performed using 5' phosphorylated primers. Sequences of primers used are listed in Table 2.3.

2.6 Immunoblotting

Stable CRFK cells expressing the various HA-tagged TF-Nup358/CypA constructs were lysed in NP-40 lysis buffer [55 mM TRIS-HCl, (pH 7.5), 150 mM NaCl, 1% (v/v) IgePal NP-40] and lysate was cleared by centrifugation at 16,100 *x g* for 10 minutes at 4°C. Protein concentration of the cleared lysate was determined using Quick Start Bradford 1X Dye Reagent (Bio-Rad, #5000205) and 40 µg of each sample (mixed with appropriate amount of 2X Laemmli sample buffer and boiled for 5 minutes at 100°C) were separated by SDS-PAGE then transferred onto polyvinylidene fluoride (PVDF) membrane. PVDF membranes were blocked using 5% non-fat milk in PBS. HA was detected using 1:2000 dilution of HRP-conjugated rabbit polyclonal PA1-29751 antibody (Invitrogen, Thermo Fisher, #PA1-29751) in 1% non-fat milk in PBS. B-actin was detected using 1:5000 dilution of HRP-conjugated mouse monoclonal mAbcam 8226 antibody (Abcam, ab20272) in 1% non-fat milk in PBS. Probed membranes were developed using Amersham ECL Prime Western Blotting Detection Reagent (GE

Healthcare Life Sciences, Cytiva, RPN2236). In between incubations with different antibodies, PVDF membranes were stripped using Restore Western Blot Stripping Buffer (Thermo Fisher, #21059). Membrane washings were performed using PBS with 0.05% Tween-20.

2.7 Virus Production

All single-cycle, EGFP reporter HIV/SIV viruses were produced in HEK293T/17 cells by co-transfection of the appropriate proviral plasmid and pVSV-G in a 2:1 ratio. Single-cycle, EGFP reporter FIV virus was produced in HEK293T/17 cells by co-transfection of pGINSIN, pFP93, and pVSV-G in a 3:2:1 ratio. Single-cycle, EGFP reporter EIAV virus was produced in HEK293T/17 cells by co-transfection of pEIAV-SIN6.1 CGFPW, pEV53D, and pVSV-G in a 3:2:1 ratio. Single-cycle, EGFP reporter MLV virus was produced in HEK293T/17 cells by co-transfection of pLXIN-GFP, pCIGB, and pVSV-G in a 3:2:1 ratio. Multi-cycle HIV-2 ROD and SIVsmE543 viruses were produced in HEK293T/17 cells by transfection of pROD10 or pGEM-E543 plasmid, respectively. Recombinant retroviruses used for CRFK cell transduction were produced in GP2-293 cells by co-transfection of pLPCX vector only (empty vector) or pLPCX-TF construct plasmid and pVSV-G in a 1:1 ratio. All transfections were performed using GenJet *In Vitr*o DNA Transfection Reagent (SignaGen Laboratories, #SL100488). Transfection media was left on cells overnight and then replaced with fresh culture media. Supernatant was collected 72 hours post-transfection for single-cycle, EGFP reporter and multi-cycle viruses, and 48 hours post-transfection for recombinant retroviruses packaging either pLPCX vector only or pLPCX-TF construct. Supernatants

were clarified by centrifugation at 500 *x g* for 10 minutes at room temperature, then aliquoted and stored at -80°C.

2.8 Stable Cell Line Creation

CRFK were seeded at a concentration of 1 x 10^5 cells per well in 6-well plates in a total volume of 2 ml of culture media. The following day, media was replaced with 1 ml of VSV-G pseudotyped, recombinant retrovirus packaging either pLPCX vector only or pLPCX-TF construct and plates were centrifuged at 800 *x g* for two hours at 32°C. At 24 hours post-transduction, viral supernatant was removed and replaced with fresh culture media. Starting 48 hours post-transduction, stable CRFK cell lines were selected in culture media supplemented with 10 µg/ml puromycin and subsequently maintained in culture media supplemented with 5 µg/ml puromycin.

2.9 THP-1/U937 Differentiation

THP-1 or U937 cells were seeded at a concentration of 5 x 10^5 cells per well in 12-well plates in a total volume of 1 ml culture media supplemented with 150 nM phorbol 12-myristate 13-acetate (PMA). 72 hours later, PMA-containing media was removed and adhered cells in each well were washed twice with culture media and left in 1 ml fresh culture media overnight prior to infection.

2.10 Infectivity Assays

2.10.1 Single-Cycle Viral Infections

CRFK cells expressing the TF constructs or HA-tagged TRIM5 alleles were seeded at a concentration of 5 x 10^4 cells per well in 24-well plates in a total volume of 500 µl of culture media. The following day, media was replaced with 250 µl of fresh culture media containing the appropriate amount of VSV-G pseudotyped, single-cycle,

EGFP reporter virus. For differentiated U937 or THP-1 cell infections, the day after PMA-containing media was removed and differentiated cells were left in 1 ml culture media, media was replaced with 500 µl of fresh culture media and then 50 µl of VSV-G pseudotyped, single-cycle, EGFP reporter virus was added to each well. For undifferentiated U937 or THP-1 cell infections and H9, CEMx174-SEAP, Jurkat E6-1, or SupT1-CCR5 cell infections, cells were seeded at a concentration of 8 x 10^4 cells per well in 12-well plates in a total volume of 500 µl of culture media. 50 µl of VSV-G pseudotyped, single-cycle, EGFP reporter virus was then added to each well. For 293T or HeLa cell infections, 5 x 10^4 cells were seeded per well in 24-well plate in a total volume of 500 µl of culture media. The following day, media was replaced with 200 µl of fresh culture media and then 50 µl of VSV-G pseudotyped, single-cycle, EGFP reporter virus was added to each well. All infections were performed in triplicate. After three days, samples were fixed in phosphate buffered saline (PBS) with 1% paraformaldehyde and EGFP expression was analyzed by flow cytometry using a FACSCanto flow cytometer (BD Biosciences) and the accompanying FACSDIVA software (v6.1.3).

2.10.2 Multi-Cycle Viral Infections

Jurkat E6-1, H9, CEMx174-SEAP, or SupT1-CCR5 cells were seeded at a concentration of 1 x 10^6 per flask in T25 flasks in a total volume of 1 ml of culture media. 50 µl of multi-cycle HIV-2 ROD or SIVsmE543 virus encoding WT CA or residue 85 mutant CA was then added to each flask. The following day, cells were pelleted at 200 *x g* for three minutes, washed with 1 ml of fresh culture media, and then resuspended in 4 ml of fresh culture media. Starting 48 hours post-infection, timepoints were collected daily by removing 1 ml of culture (media and cells) from each flask and replacing it with

1 ml of fresh culture media. Virus particles were isolated from collected timepoints by centrifuging samples at 250 *x g* for 10 minutes at 4°C, transferring the supernatant into new microcentrifuge tube and centrifuging at 8,000 *x g* for 10 minutes at 4°C, then transferring the supernatant once more into a new microcentrifuge tube and centrifuging at 20,817 *x g* for 2 hours and 15 minutes at 4°C. Finally, supernatant was discarded and viral pellets were stored at -80°C. Once all timepoints were collected, viral RT amounts were quantified using the Reverse Transcriptase Assay, Colorimetric Kit (Roche, Sigma-Aldrich, #11468120910), according to manufacturer's protocols.

CHAPTER 3: RESULTS

3.1 Nup358-CA interaction altered during SIVsm emergence

Detection of capsid-host protein interactions through conventional biochemical means can be difficult since the interaction may only occur in the context of the assembled capsid core, or the host protein has an increased affinity for the capsid core [122,131,160–163]. Therefore, we chose an assay that capitalizes on the capsid binding-dependent restrictive abilities of TRIM5α in order to detect host protein-capsid interactions during infection of cells in culture – informally known as the TRIM-Fusion (TF) assay. In this assay, either the B30.2/PRYSPRY domain of TRIM5α or the Cyp domain of TRIM5Cyp is replaced with the potential CA-interacting host protein of interest (i.e., the potential CA-interacting protein domain is fused to the TRIM5 RBCC domains). Cell lines are then created that stably express this artificial restriction factor and interaction is assessed by infection with the retrovirus of interest (Figure 3.1). Typically, CRFK cells are used for the stable cell line creation as cats naturally encode a truncated TRIM5 protein: eliminating the possibility of endogenous TRIM5 interfering with the expression or function of the engineered restriction factor [164]. Like TRIM5α, viruses whose CA interacts with the fused domain will be restricted in the stable cell line whereas viruses whose CA does not interact will be unrestricted. This assay has been used to detect and characterize other host proteins that interact with HIV-1 CA interactions, including: CypA [62]; Nup153 [165]; CPSF6 [166]; and Nup358Cyp [62,80,82,83]. For Nup153 and CPSF6, the specific residues that mediate interaction with the CA core were identified using the TF assay prior to the solved co-crystal structures [105,165–167].

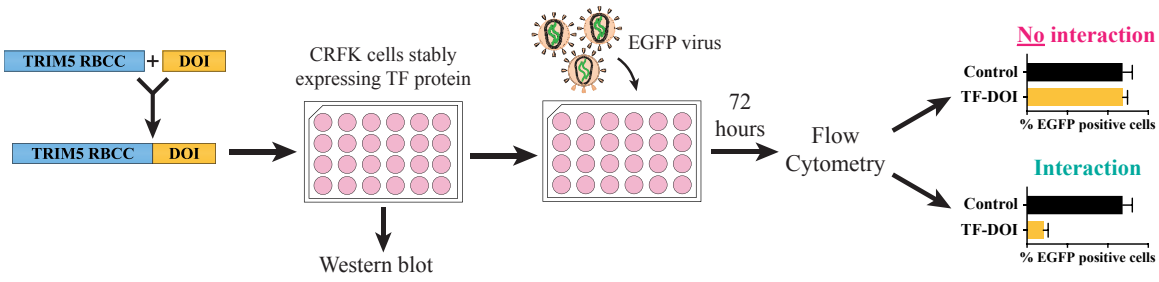

Figure 3.1. Schematic illustrating the TF assay
The potential CA-binding host protein domain of interest (DOI) is fused to the rhTRIM5Cyp RBCC domains and then stably expressed in CRFK cells. Expression of the engineered restriction factor in the stable cell line is confirmed by western blotting. Stable cell lines are infected with EGFP reporter retrovirus containing the CA of interest. Viral infectivity is assessed 72 hours post-infection using flow cytometry by calculating the percentage of EGFP positive cells. A decrease in percentage of EGFP positive cells (or infected cells) compared to the control cells indicates interaction between the viral CA and fused DOI while no change indicates no detectable interaction.

We replaced the C-terminal Cyp domain of rhTRIM5Cyp with the Nup358$_{Cyp}$ or the Nup358$_{R4\text{-}Cyp}$ supradomain from human (*Homo sapiens*; TF-huNup358$_{Cyp}$ and TF-huNup358$_{R4\text{-}Cyp}$, respectively), sooty mangabey (*Cercocebus atys*; TF-smNup358$_{Cyp}$ and TF-smNup358$_{R4\text{-}Cyp}$, respectively), and rhesus macaque (*Macaca mulatta*; TF-rhNup358$_{Cyp}$ and TF-rhNup358$_{R4\text{-}Cyp}$, respectively). We also generated a TRIM5-CypA fusion using the human CypA (huCypA) domain (Figures 3.2A and 3.2B); only the human ortholog was created as the CypA amino acid sequence is identical for human, sooty mangabey, and rhesus macaque [83,158]. The created constructs (referred to here as TF constructs), which have an N-terminal HA tag, were stably introduced into CRFK cells and expression was confirmed by western blotting (Figure 3.2C). For the TF-Nup358$_{R4\text{-}Cyp}$ constructs, two cell lines were independently created that expressed the same construct (Figure 3.2C). The RBCC only construct (TFnull) lacks a C-terminal interaction domain and therefore is incapable of restriction [121,122,125,126,129,130] (Figure 3.2B; see also Figure 2.2A). CRFK cells transduced with empty vector (pLPCX) or TFnull both serve as negative control cell lines. If the fused domain of the TF construct is able to interact with the lentiviral CA, there will be a decrease in infectivity compared to the TFnull cell line.

The ability of these constructs to restrict retroviral replication was confirmed by infecting the stable cell lines with a single-cycle version of HIV-1 isolate NL4-3 (NL4-3 HIV-1) encoding an EGFP reporter. The empty vector pLPCX and TFnull cell lines displayed similar levels of NL4-3 HIV-1 infectivity as expected (Figure 3.3A, compare grey and black bars). Consistent with previous observations, the human TF-Nup358Cyp and TF-CypA constructs restricted NL4-3 HIV-1 infection compared to the control cell

lines (Figure 3.3A, compare blue Cyp and green bars to grey and black bars) [62,80–83]. Similarly, both the rhesus macaque and sooty mangabey TF-Nup358Cyp constructs and all three of the TF-Nup358R4-Cyp constructs restricted NL4-3 HIV-1 infection (Figure 3.3A, compare the purple and pink Cyp bars and the blue, purple, and pink R4-Cyp bars to the grey and black bars). This loss of infectivity indicates that the Nup358Cyp domain from all three species interacts with NL4-3 HIV-1 CA, even in the presence of the R4 domain (Figure 3.3A, compare the Cyp bars to R4-Cyp bars). The observed interaction between NL4-3 HIV-1 CA and smNup358Cyp is in line with a previous observation that the V3173F mutation had little impact on interaction between purified HIV-1 CA N-terminal domain (NTD) and huNup358Cyp, as measured by isothermal titration calorimetry (ITC) [60].

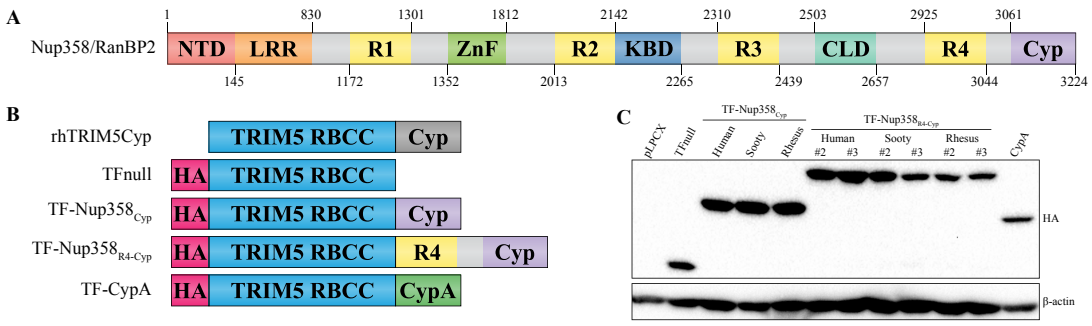

Figure 3.2. TF constructs and stable cell lines created
(A) Schematic of Nup358 protein with its various domains depicted. NTD, N-terminal domain (red); LRR, leucine-rich region (orange); R1-4, Ran-binding domain 1-4 (yellow); ZnF, zinc-finger region (light green); KBD, kinesin-binding domain (blue); CLD, cyclophilin-like domain (teal); Cyp, cyclophilin (purple). In between some of the domains are unstructured regions (depicted in light grey). Domain boundaries are indicated by residue numbers. Residue numbering is based off the human Nup358 ortholog (Genbank accession number NP_006258). Figure not drawn to scale.
(B) Schematic of rhTRIM5Cyp protein, TFnull negative control construct, TF-Nup358$_{Cyp}$, TF-Nup358$_{R4\text{-}Cyp}$, and TF-CypA experimental constructs. rh, rhesus macaque; RBCC, the RING, B-Box, and Coiled-coil domains of rhTRIM5Cyp (blue); Cyp, cyclophilin domain (Cyp domain of rhTRIM5Cyp shown in dark grey; Nup358$_{Cyp}$ shown in purple); R4, Ran-binding domain 4 (yellow); HA, HA-tag (pink); CypA, Cyclophilin A (green). Figure not drawn to scale.
(C) Western blot of CRFK cells transduced to stably express HA-tagged TF constructs or empty vector pLPCX. For each of the TF-Nup358$_{R4\text{-}Cyp}$ constructs, two cell lines were independently created that expressed the same construct.
For additional details regarding construction of the TF constructs, see Methods Section 2.3.2 and Figure 2.2.

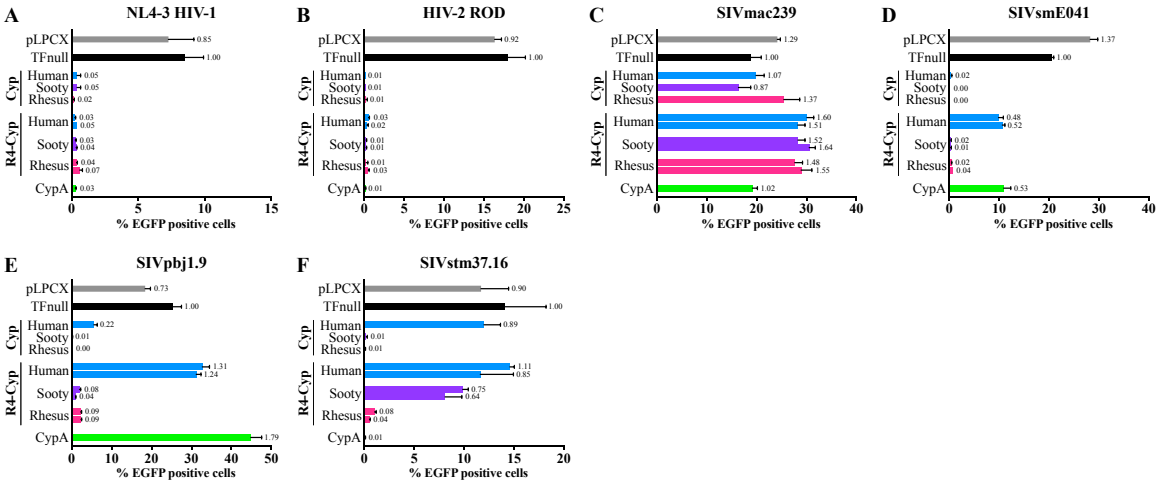

Figure 3.3. Differences in Primate lentiviral CA interaction with Nup358$_{Cyp}$, Nup358$_{R4\text{-}Cyp}$, and CypA

(A-F) Infectivity of VSV-G pseudotyped, single-cycle, EGFP reporter NL4-3 HIV-1 (A), HIV-2 ROD (B), SIVmac239 (C), SIVsmE041 (D), SIVpbj1.9 (E), and SIVstm37.16 (F) on CRFK cells stably expressing TF-CypA (green bar), and human (blue bars), sooty mangabey (purple bars), or rhesus macaque (pink bars) orthologs of TF-Nup358$_{Cyp}$ or TF-Nup358$_{R4\text{-}Cyp}$. Empty vector pLPCX (grey bar) and TFnull (black bar), which contains only the rhTRIM5Cyp RBCC domains, serve as negative controls. Infectivity, or the total percentage of EGFP positive cells, was measured by flow cytometry. The fold-changes in infectivity compared to TFnull are shown next to the bars. Results are representative of at least three independent experiments, with error bars indicating ± standard deviation.

Similar to what we observed for NL4-3 HIV-1, all TF constructs restricted HIV-2 isolate ROD (HIV-2 ROD; Figure 3.3B). Interaction with huNup358$_{Cyp}$ has been previously observed for HIV-2 CA using the TF assay [80,82] and while early CA-CypA research suggested that HIV-2 CA did not interact with CypA [147,168–171], more recent work identified a direct interaction between HIV-2 CA and CypA using ITC [67]. In contrast to NL4-3 HIV-1 and HIV-2 ROD CA, none of the TF constructs restricted SIVmac isolate 239 (SIVmac239; Figure 3.3C), indicating that SIVmac239 CA is unable to interact with the Nup358$_{Cyp}$, Nup358$_{R4\text{-}Cyp}$, or CypA from all three species. The inability to interact with huNup358$_{Cyp}$ and CypA is in line with previous observations [62,80–83,147,170,171]. The ability of the rhesus macaque TF-Nup358$_{Cyp}$ and TF-Nup358$_{R4\text{-}Cyp}$ orthologs to strongly restricted NL4-3 HIV-1 and HIV-2 ROD (Figures 3.3A and 3.3B, compare purple Cyp and R4-Cyp bars to grey and black bars) indicate that the fused domains of these constructs are properly folded and loss of interaction is specific to SIVmac239.

For SIVsm isolate E041 (SIVsmE041), all three of the TF-Nup358$_{Cyp}$ constructs and the rhesus macaque and sooty mangabey TF-Nup358$_{R4\text{-}Cyp}$ constructs strongly restricted replication (Figure 3.3D); however, human TF-Nup358$_{R4\text{-}Cyp}$ and TF-CypA only restricted SIVsmE041 replication by ~2 or 3-fold compared to the TFnull control (Figure 3.3D, compare blue R4-Cyp and green bars to black bar), indicating weak interaction between the fused domains and SIVsmE041 CA. Again, as both of these constructs strongly restricted NL4-3 HIV-1 and HIV-2 ROD (Figures 3.3A and 3.3B, compare blue R4-Cyp and green bars to grey and black bars), this diminished interaction is specific to the SIVsmE041 CA. Thus, SIVsmE041 CA loses the ability to strongly

interact with the huNup358$_{Cyp}$ domain in the huNup358$_{R4\text{-}Cyp}$ supradomain (Figure 3.3D, compare blue Cyp bar to blue R4-Cyp bars). Looking at the results in the context of SIVsm cross-species transmission, emergence of SIVmac coincided with complete loss of CA interaction with CypA/Nup358$_{Cyp}$ (Figures 3.3C and 3.3D, compare blue, purple, and pink Cyp and R4-Cyp and green bars), while emergence of HIV-2 coincided with stronger interaction with huNup358$_{R4\text{-}Cyp}$ domains and CypA (Figures 3.3B and 3.3D, compare blue R4-Cyp and green bars).

SIVsm has jumped into two other macaque species: stump-tailed macaques (stm; *Macaca arctoides*), and pig-tailed macaques (ptm; *Macaca nemestrina*), giving rise to SIV of stump-tailed macaques (SIVstm) and SIV of pig-tailed macaques (SIVpbj), respectively [42,48–53]. Thus, we decided to test the ability of these two viruses to interact with Nup358 and CypA. Sequencing of multiple individuals revealed that the ptmNup358$_{R4\text{-}Cyp}$ and smNup358$_{R4\text{-}Cyp}$ amino acid sequences are identical (see Figures 2.2B and 2.2C). In contrast to SIVmac239, we observed that both SIVpbj isolate 1.9 (SIVpbj1.9) and SIVstm isolate 37.16 (SIVstm37.16) maintained CA interaction with Nup358 (Figures 3.3E and 3.3F). For SIVpbj1.9, both the sooty mangabey and rhesus macaque TF-Nup358$_{Cyp}$ and TF-Nup358$_{R4\text{-}Cyp}$ orthologs restricted replication, indicating interaction between those fused domains and SIVpbj1.9 CA (Figure 3.3E, compare purple and pink Cyp and R4-Cyp bars to grey and black bars); however, the human TF-Nup358$_{Cyp}$ ortholog only weakly restricted SIVpbj1.9 (Figure 3.3E, compare blue Cyp bar to grey and black bars) – indicating weak SIVpbj1.9 CA interaction with huNup358$_{Cyp}$. Additionally, human TF-Nup358$_{R4\text{-}Cyp}$ and TF-CypA orthologs both failed to restrict SIVpbj1.9 replication (Figure 3.3E, compare blue R4-Cyp and green bars to

grey and black bars) – indicating a lack of interaction between SIVpbj1.9 CA and huNup358$_{R4\text{-}Cyp}$, and CypA. These observations, when compared to the ancestral SIVsm CA, suggest a complete loss of huNup358$_{R4\text{-}Cyp}$ and CypA interaction following the emergence of SIVsm as SIVpbj (Figures 3.3D and 3.3E, compare blue R4-Cyp bars and green bars). As far as the authors know, the SIVpbj1.9 CA is the first lentiviral capsid to be able to interact with Nup358$_{Cyp}$ but not CypA.

In contrast to SIVpbj1.9, only the rhesus macaque TF-Nup358$_{R4\text{-}Cyp}$ ortholog was capable of strong SIVstm37.16 restriction as the sooty mangabey ortholog only reduced infectivity by ~1.3 or 1.6-fold, compared to the TFnull control (Figure 3.3F, compare purple and pink R4-Cyp bars to black bar). Thus, of the three Nup358$_{R4\text{-}Cyp}$ constructs, SIVstm37.16 CA only interacts with the rhesus macaque ortholog. Additionally, SIVstm37.16 CA interacts with CypA as the virus was strongly restricted in the TF-CypA cell line (Figure 3.3F, compare green bar to grey and black bars). Compared to the ancestral interaction phenotype, SIVsm CA lost the ability to interact with its original host species' Nup358$_{R4\text{-}Cyp}$ domains during its emergence as SIVstm, but maintained the ability to interact with the rhesus macaque Nup358$_{R4\text{-}Cyp}$ domains (Figures 3.3D and 3.3F, compare purple and pink R4-Cyp bars). The CA-Nup358/CypA interaction phenotypes observed in Figure 3.3 have been summarized in Table 3.1.

Table 3.1. Summary of CA-Nup358/CypA interaction phenotypes from Figure 3.3
'–' = no interaction (a fold-change in infectivity of >0.7 compared to TFnull)
'+' = weak interaction (a fold-change in infectivity of 0.2< and <0.7 compared to TFnull)
'+++' = strong interaction (a fold-change in infectivity of <0.2 compared to TFnull)

Viral CA	$Nup358_{Cyp}$			$Nup358_{R4\text{-}Cyp}$			CypA
	hu	sm	rh	hu	sm	rh	
NL4-3 HIV-1	+++	+++	+++	+++	+++	+++	+++
HIV-2 ROD	+++	+++	+++	+++	+++	+++	+++
SIVmac239	–	–	–	–	–	–	–
SIVsmE041	+++	+++	+++	+	+++	+++	+
SIVpbj1.9	+	+++	+++	–	+++	+++	–
SIVstm37.16	–	+++	+++	–	+	+++	+++

Analytical ultracentrifugation using purified SIVstm37.16 CA NTD and human, sooty mangabey, and rhesus macaque $Nup358_{Cyp}$ domains confirmed that the TF assay results were indicative of direct protein-protein interaction affinity (Table 3.2). The observed Kd values of 380 μM and 160 μM for $smNup358_{Cyp}$ and $rhNup358_{Cyp}$ domains, respectively, are in line with previously observed values for HIV-1 CA NTD and $huNup358_{Cyp}$ [60,84].

Table 3.2. Results of analytical ultracentrifugation using purified SIVstm37.16 CA NTD and Nup358$_{Cyp}$

Nup358$_{Cyp}$ ortholog	Kd (μM)
Human	57000
Sooty mangabey	380
Rhesus macaque	160

Using the TF cell lines, we also examined the ability of the human, sooty mangabey, and rhesus macaque $Nup358_{Cyp}$ domains and $Nup358_{R4\text{-}Cyp}$ supradomains and huCypA, to interact with the CA of several non-primate retroviruses (Figure 3.4). As we observed little difference in viral infectivity levels between the empty vector pLPCX and TFnull negative control lines (Figure 3.3, compare grey and black bars), only the TFnull cell line was used in the rest of the TF assay performed. None of the TF constructs were able to restrict infectivity of murine leukemia virus (MLV; Figure 3.4A), a retrovirus belonging to the Gammaretrovirus genus. The lack of observed interaction is consistent with previous observations that MLV CA does not interact with either CypA or $Nup358_{Cyp}$ [65,81,83,147,171] and the absence of an elongated proline-rich loop between MLV CA α-helix 4 and α-helix 5 [57]. The non-primate lentivirus feline immunodeficiency virus (FIV) CA strongly interacted with all of the TF constructs (Figure 3.4B), similar to NL4-3 HIV-1 and HIV-2 ROD CA (Figures 3.3A and 3.3B). The FIV CA results are in line with previous work showing FIV CA interaction with the $Nup358_{Cyp}$ domain and CypA from multiple species [60,65,69,81,83]. In contrast to FIV, the non-primate lentivirus equine infectious anemia virus (EIAV) CA did not interact with CypA or any of the $Nup358_{Cyp}$ or $Nup358_{R4\text{-}Cyp}$ orthologs (Figure 3.4C). Despite EIAV CA exhibiting the proline-rich 4-5 surface loop characteristic of lentiviral CA [172], the lack of interaction witnessed is in agreement with previous observations that EIAV is unable to bind CypA [65].

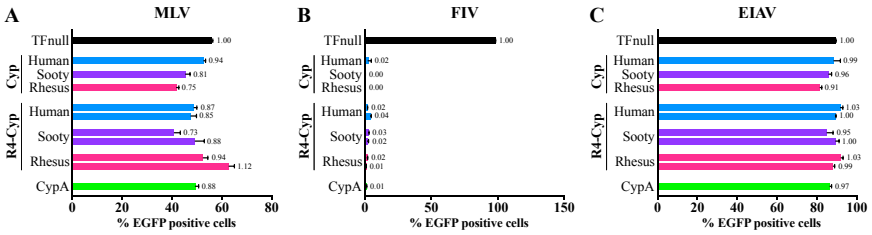

Figure 3.4. Nup358Cyp/CypA interaction is variable in non-primate retroviral CA
(A-C) Infectivity of VSV-G pseudotyped, single-cycle, EGFP reporter MLV (A), FIV (B), and EIAV (C) on CRFK cells stably expressing TF-CypA (green bar), and human (blue bars), sooty mangabey (purple bars), or rhesus macaque (pink bars) orthologs of TF-Nup358$_{Cyp}$ or TF-Nup358$_{R4\text{-}Cyp}$. TFnull, which contains only the rhTRIM5Cyp RBCC domains, serves as a negative control (black bar). Infectivity, or the total percentage of EGFP positive cells, was measured by flow cytometry. The fold-changes in infectivity compared to TFnull are shown next to the bars. Results are representative of at least two independent experiments, with error bars indicating ± standard deviation.

3.2 Nup358$_{R4\text{-}Cyp}$ interaction phenotype is conserved among SIVsm/HIV-2 CA

We decided to test capsids from multiple SIVsm/HIV-2 isolates to confirm that the interaction phenotypes we observed in Figure 3.3 were not specific to those particular isolates. Similar to SIVsmE041, SIVsm isolate E543 (SIVsmE543) interacted strongly with all three Nup358$_{Cyp}$ orthologs and the rhesus macaque and sooty mangabey Nup358$_{R4\text{-}Cyp}$ orthologs and weakly with huNup358$_{R4\text{-}Cyp}$ (Figure 3.5A). We observed similar interaction phenotypes for the CA of SIVsm isolate E660 (SIVsmE660) clone FL6 (SIVsmE660-FL6) and SIVsmE660 clone FL14 (SIVsmE660-FL14) (Figures 3.5B and 3.5C). We then designed SIVmac239-based chimeric viruses that encode the CA of SIVsm isolates G932 and D215 (SIVsmG932 and SIVsmD215, respectively) and several HIV-2 isolates (see Figure 2.1 for CA sequences). Similar to the other SIVsm CA, SIVsmG932 CA interacted with both the sooty mangabey and rhesus macaque Nup358$_{Cyp}$ domains and Nup358$_{R4\text{-}Cyp}$ supradomains (Figure 3.5D, compare purple and pink Cyp bars to purple and pink R4-Cyp bars), and human Nup358$_{Cyp}$ domain but not the Nup358$_{R4\text{-}Cyp}$ supradomain (Figure 3.5D, compare blue Cyp bar to blue R4-Cyp bars). Virions produced by the SIVmac239-based chimeric virus encoding SIVsmD215 CA were non-infectious (data not shown).

Interestingly, we observed that while poor huNup358$_{R4\text{-}Cyp}$ interaction was conserved among SIVsm CAs, the ability to interact with CypA was not; we observed strong, weak, and the complete loss of CypA interaction among the different SIVsm CAs (Figures 3.5A-3.5D, compare green bars). Identical to what we observed for HIV-2 ROD, the CA of HIV-2 isolates GH-1, UC1, and EHO (HIV-2 GH-1, HIV-2 UC1, and HIV-2 EHO, respectively) strongly interacted with CypA, and the Nup358$_{Cyp}$ domains and

$Nup358_{R4\text{-}Cyp}$ supradomains from all three species (Figures 3.5E-3.5G). The observed interaction phenotypes using the CA chimeric viruses are most likely similar to what would be observed in the non-chimeric context as replacing the CA of SIVmac239 with SIVsmE041 or HIV-2 ROD CA recapitulated the interaction phenotype observed for the non-chimeric SIVsmE041 and HIV-2 ROD viruses (Figures 3.6A-3.6C).

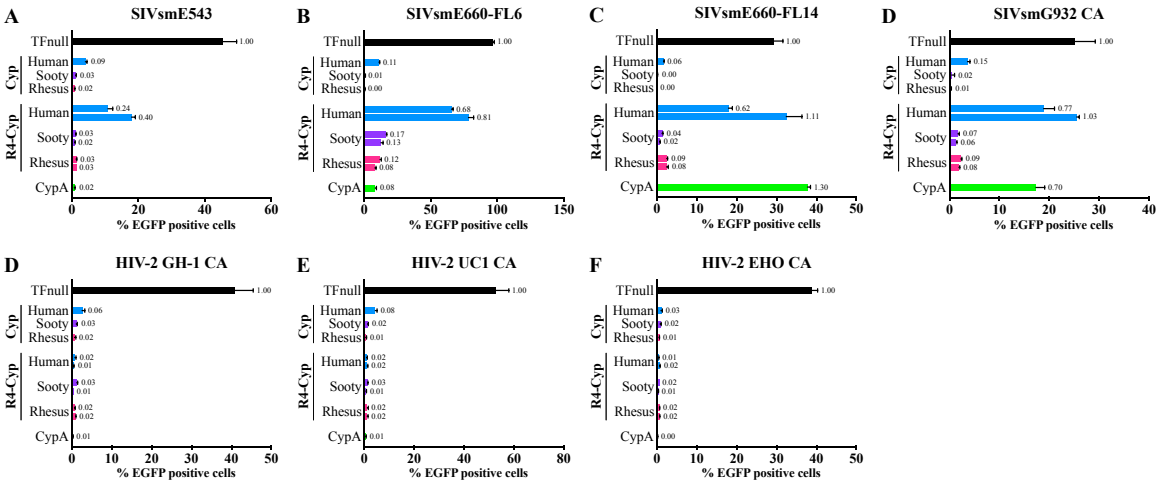

Figure 3.5. Nup358$_{R4\text{-}Cyp}$ interaction phenotypes are consistent among the CA of SIVsm and HIV-2 isolates.

(A-F) Infectivity of VSV-G pseudotyped, single-cycle, EGFP reporter SIVsmE543 (A), SIVsmE660-FL6 (B), SIVsmE660-FL10 (C), and SIVmac239-based chimeric virus encoding the SIVsmG932 CA (D), HIV-2 GH-1 CA (E), HIV-2 UC1 CA (F), or HIV-2 EHO CA (G) on CRFK cells stably expressing TF-CypA (green bar), and human (blue bars), sooty mangabey (purple bars), or rhesus macaque (pink bars) orthologs of TF-Nup358$_{Cyp}$ or TF-Nup358$_{R4\text{-}Cyp}$. TFnull, which contains only the rhTRIM5Cyp RBCC domains, serves as the negative control (black bar). Infectivity, or the total percentage of EGFP positive cells, was measured by flow cytometry. The fold-changes in infectivity compared to TFnull are shown next to the bars. Results are representative of at least three independent experiments, with error bars indicating ± standard deviation.

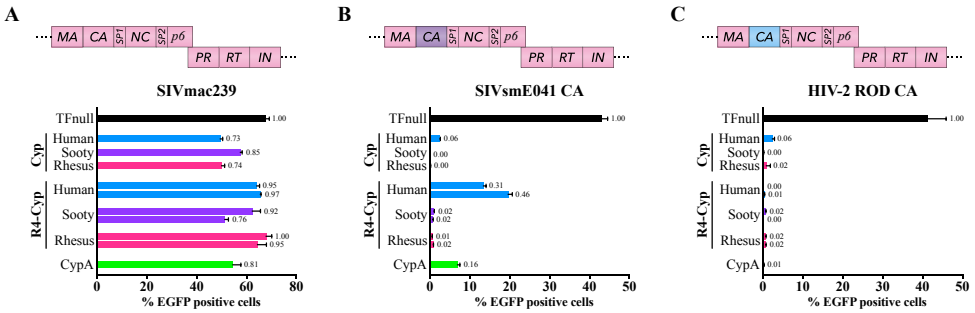

Figure 3.6. Validation of CA chimeric virus interaction phenotypes
(A-C) Infectivity of VSV-G pseudotyped, single-cycle, EGFP reporter SIVmac239 (A) and SIVmac239 where the CA has been replaced with the CA of SIVsmE041 (B) or HIV-2 ROD (C) on CRFK cells stably expressing TF-CypA (green bar) and human (blue bars), sooty mangabey (purple bars), or rhesus macaque (pink bars) orthologs of TF-Nup358$_{Cyp}$ or TF-Nup358$_{R4\text{-}Cyp}$. TFnull, which contains only the rhTRIM5Cyp RBCC domains, serves as the negative control (black bar). Infectivity, or the total percentage of EGFP positive cells, was measured by flow cytometry. The fold-changes in infectivity compared to TFnull are shown next to the bars. Results are representative of at least three independent experiments, with error bars indicating ± standard deviation. Above each graph is a schematic of the *gag-pol* of the virus used below. Pink, purple, and blue coloring correspond to regions deriving from SIVmac239, SIVsmE041, and HIV-2 ROD, respectively.

3.3 SIVsm/HIV-2 CA residue 85 influences human Nup358$_{R4\text{-}Cyp}$ interaction

HIV-1 CA interacts with Nup358$_{Cyp}$ via the 4-5 loop that extends from the surface of the assembled CA core [60,62,83]. Thus, we hypothesized that the genetic difference between SIVsm and HIV-2 CA responsible for their different huNup358$_{R4\text{-}Cyp}$ interaction abilities would be located in that region. An alignment of the CA 4-5 loops from SIVsmE041 and HIV-2 ROD shows that they differ at only three positions (Figure 3.7A; see Figure 2.1 for sequence alignment of full CA protein). Of those differences, position 85 is the only change where the encoded residues differ in polarity and size, with SIVsmE041 CA encoding a glutamine and HIV-2 ROD CA an isoleucine (Figure 3.7A). Furthermore, based on the X-ray crystal structure of HIV-1 CA NTD in complex with huNup358$_{Cyp}$ domain, the residue equivalent to SIVsmE041 and HIV-2 ROD CA position 85 (V86 in NL4-3 HIV-1 CA) is located close to residues on Nup358$_{Cyp}$ that surround the domain's active site (Figure 3.7B). These adjacent residues on Nup358$_{Cyp}$ are known as gate-keeper residues as they have been shown to dictate substrate specificity for the active site of cyclophilin domains [173].

To ask whether the Q85I change in CA was responsible for the enhancement of huNup358$_{R4\text{-}Cyp}$ interaction observed for HIV-2 CA compared to the ancestral SIVsm CA, we engineered this residue change in SIVsmE041 CA and tested its effect on Nup358/CypA interaction using the TF cell lines (Figure 3.7D). Like wild-type (WT) SIVsmE041 CA, the SIVsmE041 Q85I mutant CA strongly interacted with all three species' Nup358$_{Cyp}$ domains and the sooty mangabey and rhesus macaque Nup358$_{R4\text{-}Cyp}$ supradomain (Figures 3.7C and 3.7D, compare Cyp bars and purple and pink R4-Cyp bars to black bar). The Q85I mutant CA also strongly interacted with huNup358$_{R4\text{-}Cyp}$ and

CypA, with its overall Nup358/CypA interaction phenotype matching that of HIV-2 ROD CA (Figures 3.7D and 3.7E). Reverting position 85 to the ancestral glutamine in HIV-2 ROD CA disrupted interaction with huNup358$_{R4\text{-}Cyp}$ (Figure 3.7F), with the HIV-2 ROD I85Q mutant CA capable of only weak interaction like SIVsmE041 CA (Figures 3.7C and 3.7F, compare blue R4-Cyp bars).

Interestingly, despite the observed change in huNup358$_{R4\text{-}Cyp}$ interaction ability, the HIV-2 ROD I85Q mutant CA strongly interacted with CypA like the HIV-2 ROD WT CA (Figures 3.7E and 3.7F, compare green bars). While previous CA mutations identified to disrupt Nup358$_{Cyp}$ interaction also abolished CypA interaction [62,80,81], the I85Q CA mutation shows that these interactions can be genetically distinguished from one another. Alignments of the CA of multiple SIVsm and HIV-2 isolates reveal that the majority of SIVsm CA encode a glutamine at position 85 (Figure 3.7G, right pie chart, and Figure 3.8A) while most HIV-2 CA encode an isoleucine (Figure 3.7G, left pie chart, and Figure 3.8B), further supporting that the observed CA-Nup358 interaction phenotypes of the SIVsm and HIV-2 CAs we tested are representative of most SIVsm and HIV-2 CA proteins.

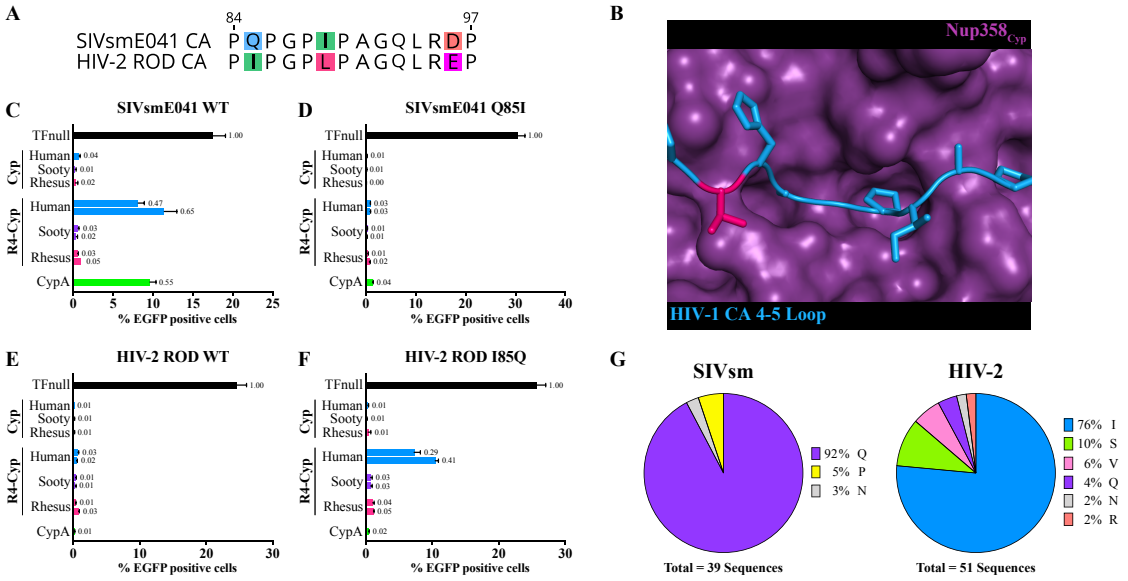

Figure 3.7. Glutamine-to-isoleucine change at SIVsm/HIV-2 CA residue 85 alters human Nup358$_{R4\text{-}Cyp}$ interaction

(A) Alignment of SIVsmE041 and HIV-2 ROD CA 4-5 loop sequences.

(B) Crystal structure of huNup358$_{Cyp}$ (purple) interaction with NL4-3 HIV-1 CA NTD (pdb: 4LQW) with only the 4-5 loop shown (blue). The HIV-1 CA equivalent of SIVsm/HIV-2 CA residue 85 is highlighted in pink (position 86 in HIV-1 NL4-3 CA). Image created in PyMOL.

(C-F) Infectivity of VSV-G pseudotyped, single-cycle, EGFP reporter SIVsmE041 with WT CA (C) or Q85I mutant CA (D), and HIV-2 ROD with WT CA (E) or I85Q mutant CA (F) on CRFK cells stably expressing TF-CypA (green bar), and human (blue bars), sooty mangabey (purple bars), or rhesus macaque (pink bars) orthologs of TF-Nup358$_{Cyp}$ or TF-Nup358$_{R4\text{-}Cyp}$. TFnull, which contains only the rhTRIM5Cyp RBCC domains, serves as the negative control (black bar). Infectivity, or the total percentage of EGFP positive cells, was measured by flow cytometry. The fold-changes in infectivity compared to TFnull are shown next to the bars. Results are representative of at least three independent experiments, with error bars indicating ± standard deviation.

(G) Pie chart showing the distribution of residues encoded at position 85 of SIVsm CA (right) and HIV-2 CA (left) proteins based on sequence alignments obtained from the Los Alamos database.

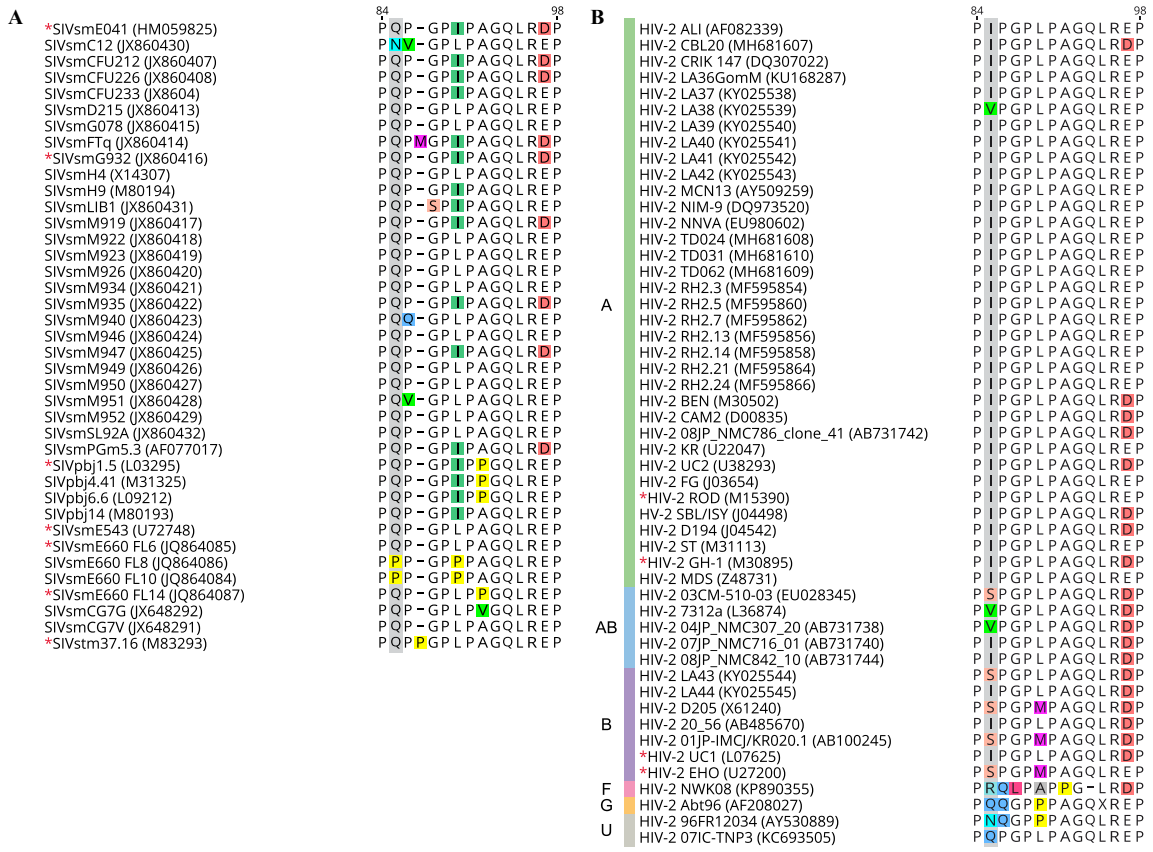

Figure 3.8. Alignment of SIVsm/HIV-2 CA 4-5 loops

(A-B) Amino acid alignment of the 4-5 loop from SIVsm (A) and HIV-2 (B) capsids obtained from the Los Alamos database. The Genbank accession number is written in parenthesis next to each isolate name. Residue 85 of CA is boxed in grey. Residues are numbered based on SIVsmE041 (A) or HIV-2 ROD (B) CA sequences. Red asterisks indicate viral CAs we tested with the TF assay. For HIV-2 sequences, the subtype is indicated on the left.

3.4 Isoleucine at CA residue 85 enhances SIVsm/HIV-2 nuclear import in human cells

To see what impact CA residue 85 has on SIVsm/HIV-2 infectivity in human cells, we infected multiple human cell lines with serially-diluted HIV-2 ROD and SIVsmE041 virus encoding WT CA or the corresponding residue 85 mutant CA. On HEK293T/17 and HeLa cells – two human epithelial cell lines – we observed that the Q85I change in SIVsmE041 CA enhanced infectivity compared to the WT CA (Figures 3.9A and 3.9B), while the I85Q reversion in CA reduced HIV-2 ROD infectivity (Figures 3.9C and 3.9D). We found that these differences in infectivity were observable over the dilution series (Figure 3.9) and the WT CA and mutant CA viral supernatants contained similar amounts of reverse transcriptase (Table 3.3), suggesting that the observed changes in infectivity were not due to differences in the number of viral particles in the supernatants.

Next, we wanted to see what effect changes at CA position 85 had on infectivity in cell types that more relative to HIV/SIV replication *in vivo*, such as macrophages and CD4+ T-cells. THP-1 and U937 cells are two different human (pro-) monocytic cell lines that can be differentiated into macrophages using phorbol-12-myristate-13-acetate (PMA) [174]. We infected these cell lines – both undifferentiated (and thus actively dividing) and differentiated into macrophages (thus non-dividing) – with serially-diluted HIV-2 ROD and SIVsmE041 virus encoding WT CA or residue 85 mutant CA (Figure 3.10). Additionally, for THP-1, we performed identical infections using SIVsmE543 virus instead (Figures 3.10E and 3.10F). Similar to our observations in HEK293T/17 and HeLa cells, the Q85I CA change for the SIVsm viruses increased infectivity (Figures 3.10A-

3.10F), while the I85Q reversion decreased HIV-2 infectivity (Figures 3.10G-3.10J). While overall infectivity was lower in differentiated cells compared to their undifferentiated counterparts, the impact of CA residue 85 on viral replication was the same (compare Figures 3.10A and 3.10B; Figures 3.10C and 3.10D; Figures 3.10E and 3.10F; Figures 3.10G and 3.10H; and Figures 3.10I and 3.10J).

We observed that CA residue 85 had similar effects on HIV-2 ROD, SIVsmE041, and SIVsmE543 infectivity in four different human T-cell lines (Figure 3.11). To confirm that these observed differences were not an artifact of using the VSV-G pseudotyped, single-cycle, EGFP reporter viruses, we infected all four T-cell lines with multi-cycle, full-length HIV-2 ROD or SIVsmE543 encoding WT CA or residue 85 mutant CA and measured viral replication over a period of approximately three weeks (Figure 3.12). Both SIVsmE543 viruses failed to replicate in H9 and Jurkat E6-1 cells (Figures 3.11B and 3.11C) while both HIV-2 ROD viruses failed to replicate in CEMx174-SEAP and H9 cells (Figures 3.11E and 3.11F). This absence of replication is most likely due to differences in co-receptor expression patterns as the single-cycle, EGFP reporter viruses pseudotyped with VSV-G (which has a broad host-cell range [175]) were capable of infecting all of the T-cell lines (Figure 3.11), and that in the case of the CEMx174-SEAP and Jurkat E6-1 cells, replication was observed for the other multi-cycle virus (Figure 3.12, compare panels A and E, and C and D). While SIVsmE543 WT CA and Q85I mutant CA viruses eventually reached similar replication levels in CEMx174-SEAP and SupT1-CCR5 cells, the Q85I mutant appeared to replicate slightly faster initially (Figures 3.12A and 3.12D). For HIV-2 ROD, the impact of CA residue 85 on replication was much more pronounced (Figures 3.13G and 3.13H), as the I85Q CA mutation almost

completely attenuated HIV-2 ROD replication in Jurkat E6-1 and SupT1-CCR5 cells compared to the WT CA.

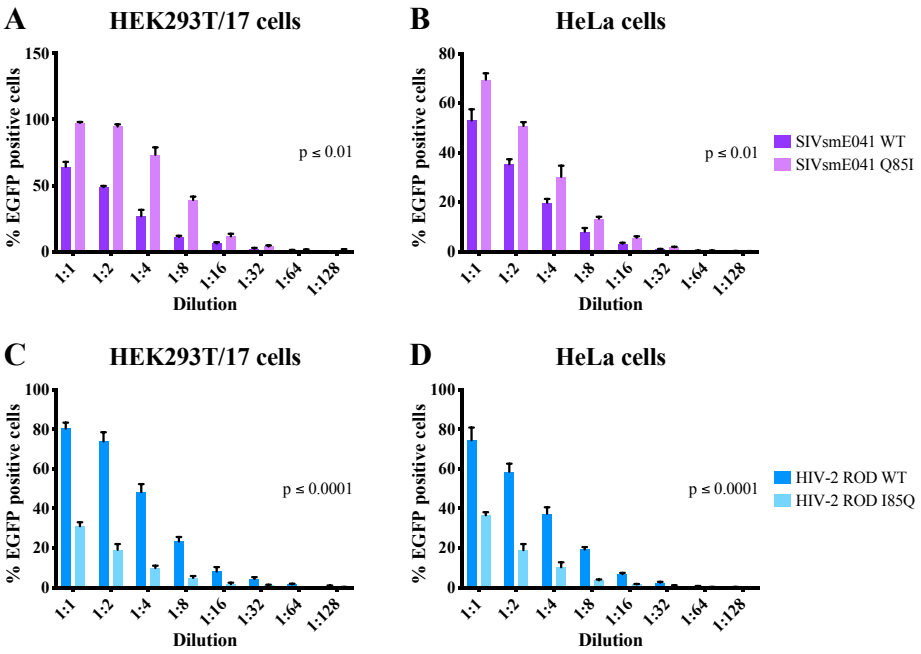

Figure 3.9. Isoleucine at CA residue 85 increases SIVsm/HIV-2 infectivity in human epithelial cell lines

(A-B) Infectivity of serial dilutions of VSV-G pseudotyped, single-cycle, EGFP reporter SIVsmE041 encoding WT CA (darker purple bars) or Q85I mutant CA (lighter purple bars) in HEK293T/17 (A), and HeLa (B) cells.

(C-D) Infectivity of serial dilutions of VSV-G pseudotyped, single-cycle, EGFP reporter HIV-2 ROD encoding WT CA (darker blue bars) or I85Q mutant CA (lighter blue bars) in HEK293T/17 (C), and HeLa (D) cells. Infectivity, or the total percentage of EGFP positive cells, was measured by flow cytometry. Results are representative of at least two independent experiments, with error bars indicating ± standard deviation. Paired two-tailed Student's t-test was used to assess significance.

Table 3.3. Reverse transcriptase (RT) concentrations of SIV/HIV supernatants

Virus		RT concentration (ng/ml)
VSV-G pseudotyped, EGFP reporter viruses	HIV-2 ROD WT	3.514
	HIV-2 ROD I85Q	3.497
	SIVsmE041 WT	3.522
	SIVsmE041 Q85I	3.497
Full-length, replication-competent viruses	HIV-2 ROD WT	3.532
	HIV-2 ROD I85Q	3.473

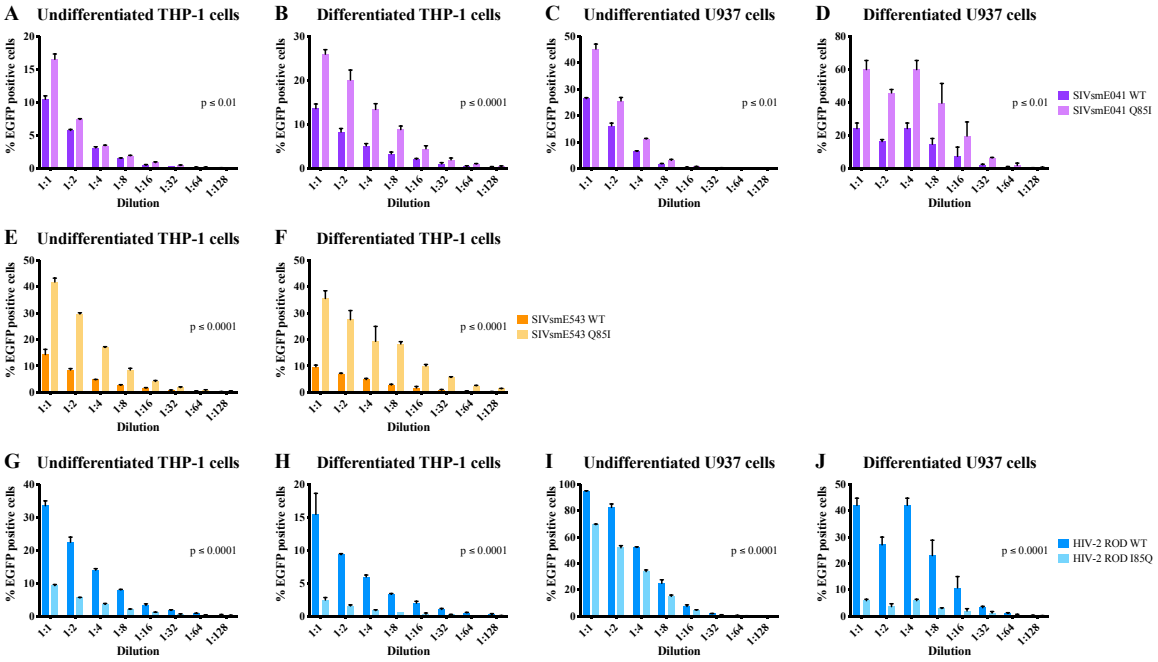

Figure 3.10. Isoleucine at CA residue 85 increases SIVsm/HIV-2 infectivity in dividing and non-dividing human myeloid cell lines

(A-D) Infectivity of serial dilutions of VSV-G pseudotyped, single-cycle, EGFP reporter SIVsmE041 encoding WT CA (darker purple bars) or Q85I mutant CA (lighter purple bars) in undifferentiated (A) and differentiated (B) THP-1 cells and undifferentiated (C) and differentiated (D) U937 cells.

(E-F) Infectivity of serial dilutions of VSV-G pseudotyped, single-cycle, EGFP reporter SIVsmE543 encoding WT CA (darker orange bars) or Q85I mutant CA (lighter orange bars) in undifferentiated (E) and differentiated (F) THP-1 cells.

(G-J) Infectivity of serial dilutions of VSV-G pseudotyped, single-cycle, EGFP reporter HIV-2 ROD encoding WT CA (darker blue bars) or I85Q mutant CA (lighter blue bars) in undifferentiated (G) and differentiated (H) THP-1 cells and undifferentiated (I) and differentiated (J) U937 cells. Infectivity, or the total percentage of EGFP positive cells, was measured by flow cytometry. Results are representative of at least two independent experiments, with error bars indicating ± standard deviation. Paired two-tailed Student's t-test was used to assess significance.

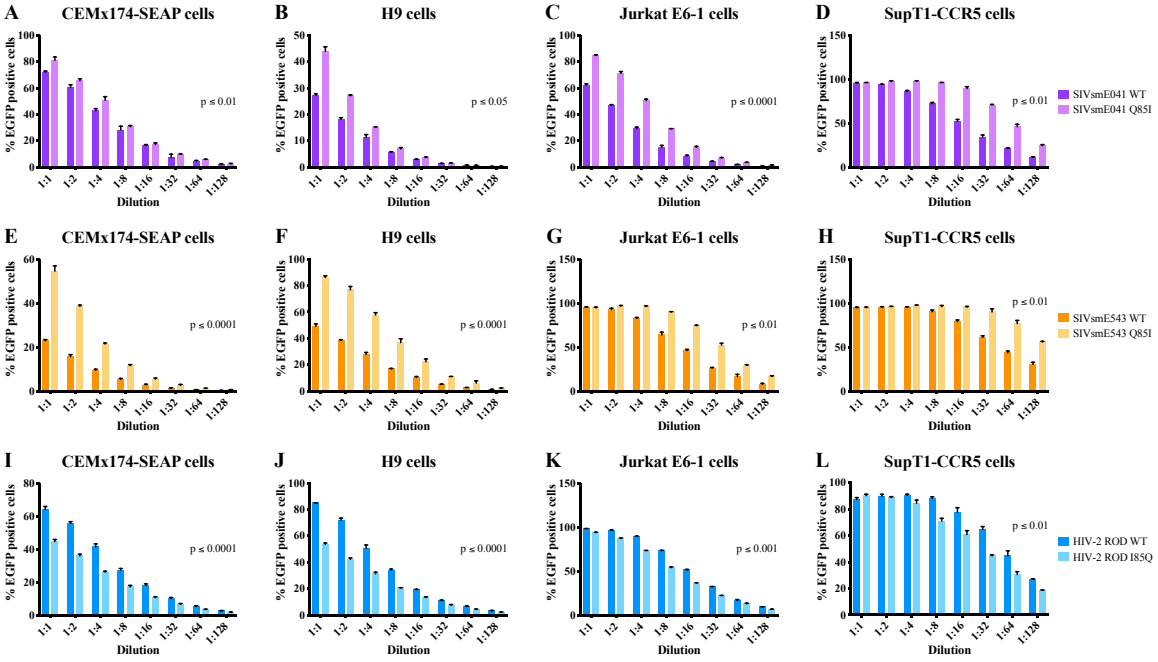

Figure 3.11. Isoleucine at CA residue 85 increases SIVsm/HIV-2 infectivity in human T-cell lines

(A-D) Infectivity of serial dilutions of VSV-G pseudotyped, single-cycle, EGFP reporter SIVsmE041 encoding WT CA (darker purple bars) or Q85I mutant CA (lighter purple bars) in CEMx174-SEAP (A), H9 (B), Jurkat E6-1 (C), and SupT1-CCR5 (D) cells. (E-H) Infectivity of serial dilutions of VSV-G pseudotyped, single-cycle, EGFP reporter SIVsmE543 encoding WT CA (darker orange bars) or Q85I mutant CA (lighter orange bars) in CEMx174-SEAP (E), H9 (F), Jurkat E6-1 (G), and SupT1-CCR5 (H) cells. (I-L) Infectivity of serial dilutions of VSV-G pseudotyped, single-cycle, EGFP reporter HIV-2 ROD encoding WT CA (darker blue bars) or I85Q mutant CA (lighter blue bars) in CEMx174-SEAP (I), H9 (J), Jurkat E6-1 (K), and SupT1-CCR5 (L) cells. Infectivity, or the total percentage of EGFP positive cells, was measured by flow cytometry. Results are representative of at least two independent experiments, with error bars indicating ± standard deviation. Paired two-tailed Student's t-test was used to assess significance.

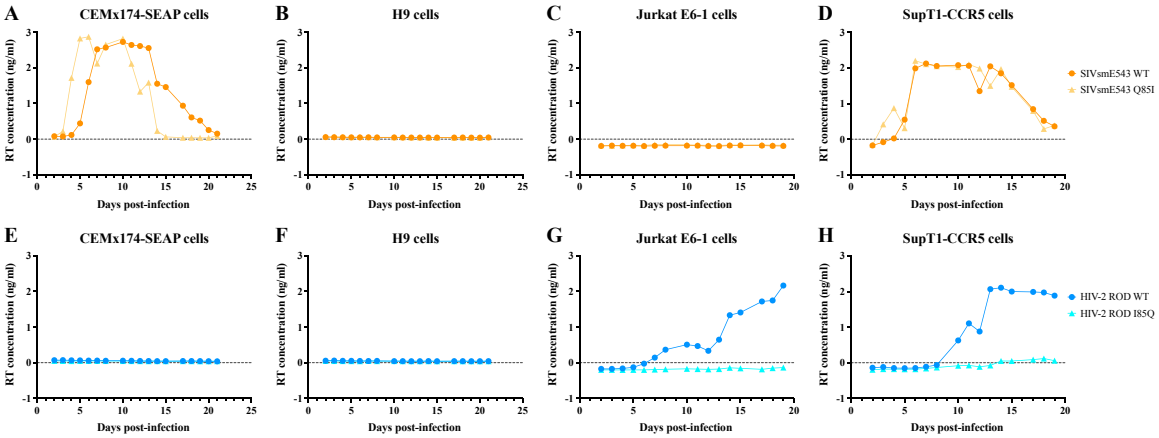

Figure 3.12. SIVsm/HIV-2 replication in human T-cell lines
(A-D) Replication of multi-cycle SIVsmE543 virus encoding WT CA (darker orange circles) or Q85I mutant CA (lighter orange triangles) in CEMx174-SEAP (A), H9 (B), Jurkat E6-1 (C), and SupT1-CCR5 (D) cells.
(E-H) Replication of multi-cycle HIV-2 ROD virus encoding WT CA (darker blue circles) or I85Q mutant CA (lighter blue triangles) in CEMx174-SEAP (E), H9 (F), Jurkat E6-1 (G), and SupT1-CCR5 (H) cells. Replication was measured by measuring RT concentration in cell supernatant at indicated timepoints. Results are representative of at least two independent experiments.

As Nup358 has been implicated in facilitating the nuclear import of HIV-1 [60,62,85,98,99,176], we decided to test the effect of CA residue 85 on SIVsmE041 and HIV-2 ROD nuclear import in human cells. APOBEC3F (A3F) is a DNA cytidine deaminase previously identified as a primate lentivirus host restriction factor [177,178]. In the absence of the lentiviral accessory protein Vif – which counteracts the antiviral activity of A3F by causing its proteosomal degradation [179] – A3F is readily incorporated into assembling virions in the producer cell and remains stably associated with the viral protein complex in the target cell even following nuclear import [180,181]. Expression of yellow fluorescent protein (YFP)-tagged A3F (A3F-YFP) during Vif-deficient SIV/HIV assembly results in YFP-labeled virions whose nuclear import dynamics can be analyzed in infected target cells using live-cell imaging (Figures 3.13A and 3.13B) [180,181]. We observed that the Q85I CA mutation increased nuclear import for SIVsmE041 in HeLa cells (Figure 3.13C, compare light and dark purple bars) whereas the I85Q CA mutation reduced nuclear import for HIV-2 ROD (Figure 3.13C, compare light and dark blue bars). These results suggest that the changes in infectivity observed between SIVsm and HIV-2 viruses encoding WT CA or the respective residue 85 mutant CA (Figures 3.9-3.12) may be due to differences in viral nuclear import kinetics.

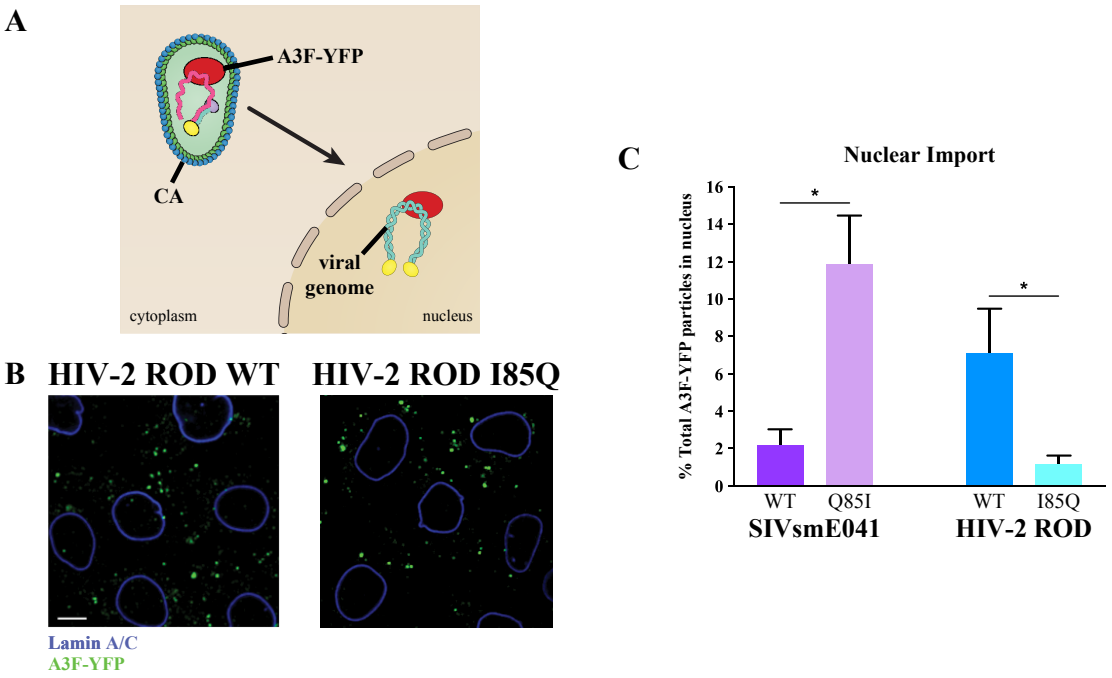

Figure 3.13. Isoleucine at CA residue 85 increases SIVsm/HIV-2 nuclear import levels in HeLa cells

(A) A3F-YFP (which is packaged into the virion within the producer cell) stays associated with the viral protein/genomic complex during infection of the target cell, even after the viral complex is imported into the nucleus.

(B) Representative confocal images of HeLa cells infected with A3F-YFP-labeled HIV-2 ROD particles containing WT CA (top panel) or I85Q CA mutation (bottom panel). The nuclear envelope is stained using an anti-Lamin A/C antibody.

(C) The percentage of total A3F-YFP-labeled particles found in the nucleus following HeLa cell infection with A3F-YFP-labeled SIVsmE041 particles containing WT CA (darker purple bar) or Q85I mutant CA (lighter purple bar) or A3F-YFP-labeled HIV-2 ROD particles containing WT CA (darker blue bar) or I85Q mutant CA (lighter blue bar). Unpaired two-tailed Student's t-test was used to assess significance. *$p \leq 0.05$

3.5 Changes in CA 4-5 loop responsible for alterations in Nup358/CypA interactions of SIVpbj and SIVstm

As we identified CA residue 85 as genetic determinant of SIVsm and HIV-2 CA interaction with the human Nup358$_{R4\text{-}Cyp}$ supradomain, we decided to look at whether amino acids differences in the CA 4-5 loops of SIVstm and SIVpbj were responsible for the observed changes in Nup358/CypA interaction compared to the ancestral SIVsm CA (Figures 3.3D-3.3F). Comparing the SIVsmE041 and SIVpbj.19 CA 4-5 loop sequences, the only significant difference appears at CA position 91, with SIVsmE041 encoding an alanine and SIVpbj1.9 encoding a proline (Figures 3.14A and 3.14B; see Figure 2.1 for sequence alignment of full CA protein). We found that engineering the A91P change in SIVsmE041 CA further disrupted interaction with huNup358$_{R4\text{-}Cyp}$ and CypA (Figures 3.14C and 3.14D, compare the blue R4-Cyp bars and the green bars), resulting in the SIVsmE041 P91A mutant CA possessing a similar Nup358/CypA interaction phenotype as the SIVpbj1.9 WT CA (Figures 3.14D and 3.14E). The reverse P91A mutation in SIVpbj1.9 CA strengthened CypA interaction compared to the WT CA (Figures 3.14E and 3.14F, compare green bars), resulting in a similar ability to interact with CypA as observed for SIVsmE041 WT CA (Figures 3.14C and 3.14F, compare green bars), but had no impact on huNup358$_{R4\text{-}Cyp}$ interaction (Figures 3.14E and 3.14F, compare blue R4-Cyp bars). This observation suggests that additional residue exchanges between SIVsmE041 and SIVpbj1.9 CA are necessary to recapitulate the weak huNup358$_{R4\text{-}Cyp}$ interaction of SIVsmE041 CA in the SIVpbj1.9 P91A mutant CA. Neither CA mutation altered interaction with the sooty mangabey or rhesus macaque Nup358$_{R4\text{-}Cyp}$ orthologs (Figures 3.14C-3.14F, compare purple and pink R4-Cyp bars). Thus, the change at

position 91 of SIVpbj1.9 CA disrupts interaction with the host species' CypA but not Nup358$_{R4\text{-}Cyp}$.

Compared to the SIVsmE041, SIVstm37.16 CA contains a proline insertion within the 4-5 loop at position 86 (Figures 3.15A and 3.15B; see Figure 2.1 for sequence alignment of full CA protein). The SIVsmE041 QP➔QPP mutant CA, where a proline was inserted after CA residue Q85, had almost completely lost the ability to interact with smNup358$_{R4\text{-}Cyp}$ (Figures 3.15C and 3.15D, compare purple R4-Cyp bars), similar to what was observed for the SIVstm37.16 WT CA (Figures 3.15D and 3.15E, compare purple R4-Cyp bars). We also observed that the SIVsmE041 QP➔QPP mutant CA lacked the ability to interact with huNup358$_{Cyp}$ and huNup358$_{R4\text{-}Cyp}$ but strongly interacted with CypA like SIVstm37.16 WT CA (Figures 3.15D and 3.15E, compare green bars). Deletion of residue P86 in SIVstm37.16 CA restored smNup358$_{R4\text{-}Cyp}$ interaction (Figures 3.15E and 3.15F, compare purple R4-Cyp bars) but had no effect on CypA or huNup358$_{R4\text{-}Cyp}$ interaction and only partially restored huNup358$_{Cyp}$ interaction (Figures 3.15E and 3.15F, compare the green bars, the blue Cyp bars, and the blue R4-Cyp bars). Thus, the SIVstm37.16 ΔP86 mutant CA did not completely mimic the Nup358/CypA interaction profile of the SIVsmE041 WT CA. Neither CA mutation appeared to affect rhesus macaque Nup358$_{R4\text{-}Cyp}$ interaction (Figures 3.15C-3.15F, pink R4-Cyp bars).

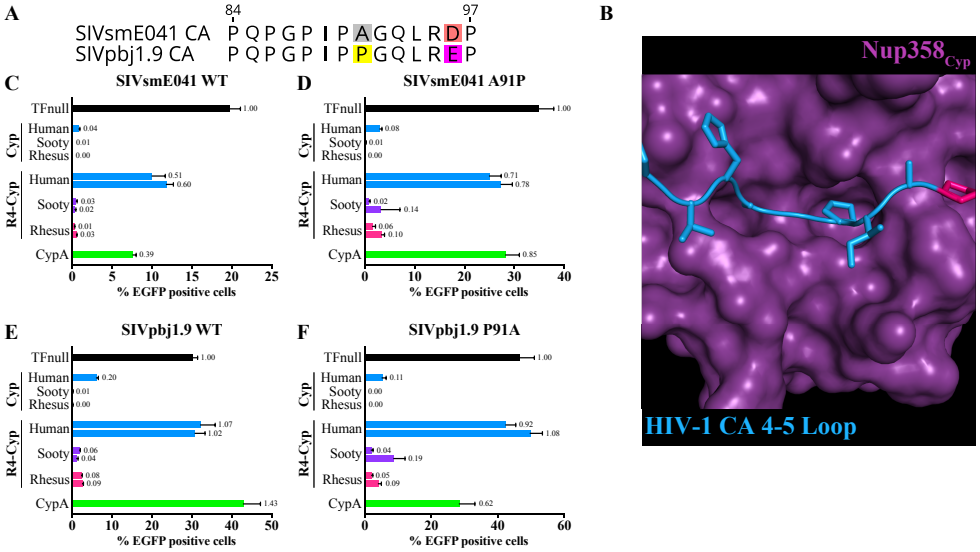

Figure 3.14. Alanine-to-Proline change at SIVpbj CA residue 91 disrupts CypA but not Nup358 interaction

(A) Alignment of SIVsmE041 and SIVpbj1.9 CA 4-5 loop sequences.

(B) Crystal structure of huNup358$_{Cyp}$ (purple) interaction with NL4-3 HIV-1 CA NTD (pdb: 4LQW) with only the 4-5 loop shown (blue). The residue equivalent to position 91 in SIVsmE041 CA is highlighted in pink (position 93 in HIV-1 NL4-3 CA). Image created in PyMOL.

(C-F) Infectivity of VSV-G pseudotyped, single-cycle, EGFP reporter SIVsmE041 with WT CA (C) or A91P mutant CA (D), and SIVpbj1.9 with WT CA (E) or P91A mutant CA (F) on CRFK cells stably expressing TF-CypA (green bar), and human (blue bars), sooty mangabey (purple bars), or rhesus macaque (pink bars) orthologs of TF-Nup358$_{Cyp}$ or TF-Nup358$_{R4\text{-}Cyp}$. TFnull, which contains only the rhTRIM5Cyp RBCC domains, serves as the negative control (black bar). Infectivity, or the total percentage of EGFP positive cells, was measured by flow cytometry. The fold-changes in infectivity compared to TFnull are shown next to the bars. Results are representative of at least three independent experiments, with error bars indicating ± standard deviation.

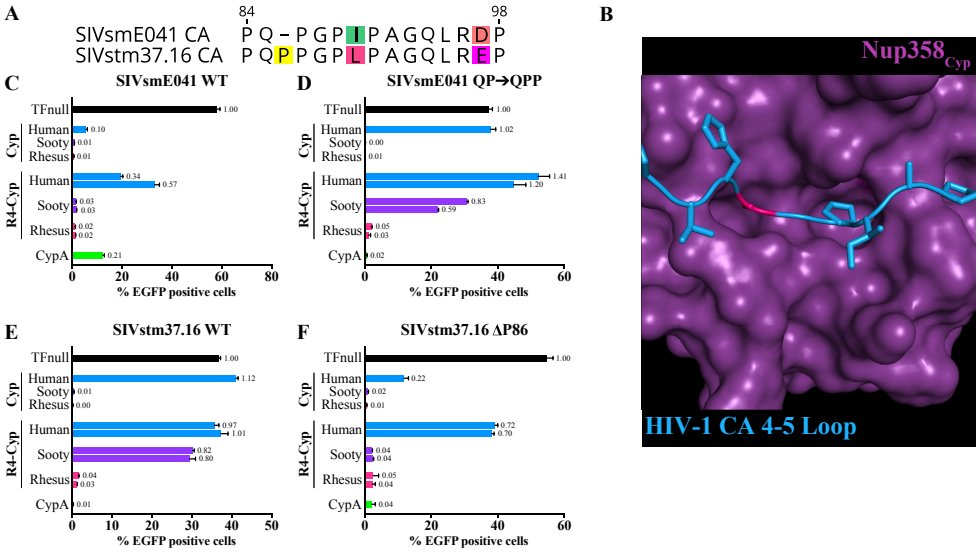

Figure 3.15. Proline-insertion in 4-5 loop of SIVstm CA results in loss of sooty mangabey but not rhesus macaque Nup358

(A) Alignment of SIVsmE041 and SIVstm37.16 CA 4-5 loop sequences. Residues are numbered based on SIVstm37.16 CA sequence.

(B) Crystal structure of huNup358$_{Cyp}$ (purple) interaction with NL4-3 HIV-1 CA NTD (pdb: 4LQW) with only the 4-5 loop shown (blue). The residue equivalent to position 86 in SIVsmE041 CA is highlighted in pink (position 88 in HIV-1 NL4-3 CA). Image created in PyMOL.

(C-F) Infectivity of VSV-G pseudotyped, single-cycle, EGFP reporter SIVsmE041 with WT CA (C) or ^{85}QP^{86}➔^{85}QPP^{87} mutant CA (D), and SIVstm37.16 with WT CA (E) or ΔP86 mutant CA (F) on CRFK cells stably expressing TF-CypA (green bar), and human (blue bars), sooty mangabey (purple bars), or rhesus macaque (pink bars) orthologs of TF-Nup358$_{Cyp}$ or TF-Nup358$_{R4\text{-}Cyp}$. TFnull, which contains only the rhTRIM5Cyp RBCC domains, serves as the negative control (black bar). Infectivity, or the total percentage of EGFP positive cells, was measured by flow cytometry. The fold-changes in infectivity compared to TFnull are shown next to the bars. Results are representative of at least three independent experiments, with error bars indicating ± standard deviation.

3.6 Nup358$_{Cyp}$ residue 3173 modulates SIVsm CA interaction in context of human Nup358$_{R4\text{-}Cyp}$ supradomain

As SIVsm CA strongly interacted with the sooty mangabey but not human Nup358$_{R4\text{-}Cyp}$ supradomains (Figure 3.3D, compare blue and purple R4-Cyp bars), we wanted to map the genetic difference between the two species responsible for this differential interaction ability. Comparing the human and sooty mangabey Nup358$_{R4\text{-}Cyp}$ sequences, there are several differences that lie in the short span of residues between the Nup358$_{R4}$ and Nup358$_{Cyp}$ domains (referred to here as the "linker region"), including a three-residue deletion present in sooty mangabey ortholog (Figure 3.16A, top alignment; see also Figure 2.2C), as well as single residue change in the Nup358$_{Cyp}$ domain (Figure 3.16A, bottom alignment; see also Figure 2.2B). We created a panel of human and sooty mangabey TF-Nup358$_{R4\text{-}Cyp}$ constructs containing reciprocal exchanges of each residue difference and stably expressed them in CRFK cells (Figure 3.16B). None of the residue exchanges impacted HIV-2 ROD CA interaction with either hu- or smNup358$_{R4\text{-}Cyp}$ as infectivity was strongly restricted in all the mutant TF-Nup358$_{R4\text{-}Cyp}$ cell lines (Figure 3.16D). This result was expected as HIV-2 ROD CA interacts strongly both species' Nup358$_{R4\text{-}Cyp}$ and confirms that proper domain folding is occurring in the mutant TF-Nup358$_{R4\text{-}Cyp}$ constructs. As also expected, there was no change in SIVmac239 infectivity in the WT and mutant TF-Nup358$_{R4\text{-}Cyp}$ cell lines compared to TFnull (Figure 3.16E), which indicates SIVmac239 CA does not interact with any of the Nup358$_{R4\text{-}Cyp}$ mutants and further confirms that the domains were correctly folded.

We found that residue 3173 in Nup358$_{Cyp}$ plays a pivotal role in the ability of SIVsm CA to interact with the human and sooty mangabey Nup358$_{R4\text{-}Cyp}$ supradomains

(Figure 3.16F). This residue, which sits within the Nup358$_{Cyp}$ domain active site (Figure 3.16C), is a valine in humans and a phenylalanine in sooty mangabeys (Figure 3.16A; see also Figure 2.2B). Whereas SIVsmE041 CA weakly interacted with the other mutant huNup358$_{R4\text{-}Cyp}$ domains like with WT huNup358$_{R4\text{-}Cyp}$, it strongly interacted with the huNup358$_{R4\text{-}Cyp}$ V3173F mutant to a similar extent as with the WT smNup358$_{R4\text{-}Cyp}$ domains (Figure 3.16F; compare blue V3173F bar with WT purple bars). Conversely, the F3173V mutation in smNup358$_{R4\text{-}Cyp}$ weakened the interaction with SIVsmE041 CA, resulting in an interaction phenotype similar to that of WT huNup358$_{R4\text{-}Cyp}$ (Figure 3.16D, compare purple F3173V bar with WT blue bars). Residue 3173 had a similar impact on Nup358$_{R4\text{-}Cyp}$ interaction for SIVpbj1.9 as well (Figure 3.16G, compare blue V3173F bar to WT blue bars, and purple F3173V bar to purple WT bars), with residue 3173 having a much stronger impact only in the context of the Nup358$_{R4\text{-}Cyp}$ supradomain. We observed a similar impact of residue 3173 on Nup358$_{R4\text{-}Cyp}$ interaction with SIVsm CAs tested (Figures 3.16H-3.16J) as well as the SIVsmE041/SIVpbj1.9 residue 91 CA mutants and the SIVstm37.16 ΔP86 CA mutant (Figures 3.17A-3.17C). Like HIV-2 ROD, all HIV-2 CAs tested interacted strongly with both the WT and mutant human and sooty mangabey Nup358$_{R4\text{-}Cyp}$ constructs (3.17D-3.17G).

These observations are particularly interesting as SIVsm CA is able to interact with both the human and sooty mangabey Nup358$_{Cyp}$ domains, despite residue 3173 forming part of the hydrophobic pocket of this domain into which HIV-1 CA P90 residue binds and mutational studies showing that this residue and the equivalent residue 113 in CypA are important for interaction of HIV-1 CA [60,84,182]. Thus, the valine/phenylalanine difference in human and sooty mangabey Nup358$_{Cyp}$ impacts

SIVsm CA interaction when present alongside the $Nup358_{R4}$ domain. Our previous observations from SIVstm37.16 further support the hypothesis that residue differences in $Nup358_{Cyp}$ may impact CA interaction only in the context of the $Nup358_{R4\text{-}Cyp}$ supradomain (Figure 3.18A). Sooty mangabey and rhesus macaque $Nup358_{R4\text{-}Cyp}$ orthologs differ only at residue 3163, which flanks the $Nup358_{Cyp}$ active site (Figures 3.18B and 3.18C). Yet, while SIVstm37.16 CA strongly interacts with both the sooty mangabey and rhesus macaque $Nup358_{Cyp}$ domains, CA interaction is almost completely abolished with the sooty mangabey but not rhesus macaque $Nup358_{R4/Cyp}$ supradomain – despite identical $Nup358_{R4}$ + linker region sequence added in front of the sooty mangabey and rhesus macaque $Nup358_{Cyp}$ domains to create their $Nup358_{R4\text{-}Cyp}$ counterparts.

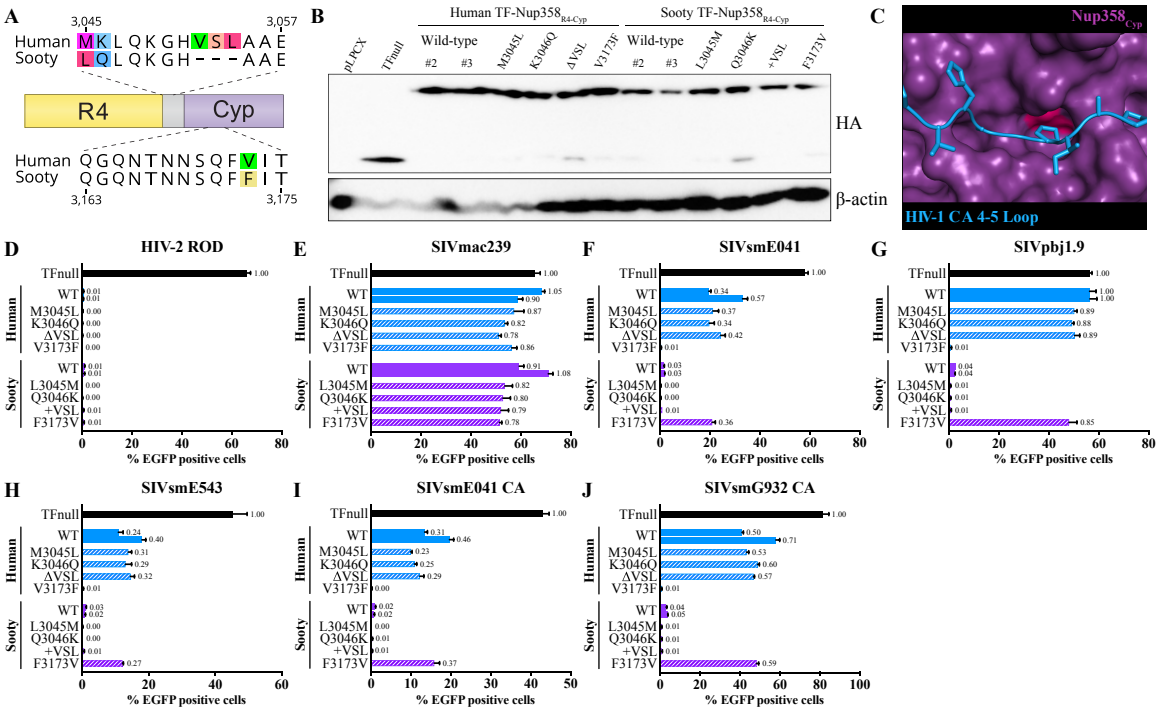

Figure 3.16. Residue 3173 in huNup358$_{Cyp}$ domain modulates SIVsm CA interaction in the context of huNup358$_{R4\text{-}Cyp}$ supradomain

(A) Schematic of Nup358$_{R4\text{-}Cyp}$ domains highlighting residue differences between human and sooty mangabey orthologs. R4, Ran-binding domain 4 (yellow); Cyp, cyclophilin (purple); the "linker region" between the two domains is shown in light grey. Figure not drawn to scale. Residue numbering based on human Nup358 ortholog.

(B) Western blot of CRFK cells transduced to stably express empty vector pLPCX, or HA-tagged TFnull, WT or mutant human and sooty mangabey orthologs of TF-Nup358$_{R4\text{-}Cyp}$. For each of the WT TF-Nup358$_{R4\text{-}Cyp}$ constructs, two independently cell lines were created that expressed the same construct.

(C) Crystal structure of huNup358$_{Cyp}$ (purple) interaction with NL4-3 HIV-1 CA NTD (pdb: 4LQW) with only the 4-5 loop shown (blue). Residue 3173 in Nup358$_{Cyp}$ domain is highlighted in pink. Image created in PyMOL.

(D-J) Infectivity of VSV-G pseudotyped, single-cycle, EGFP reporter HIV-2 ROD (D), SIVmac239 (E), SIVsmE041 (F), SIVpbj1.9 (G), SIVsmE543 (H), and SIVmac239-based chimeric virus encoding the SIVsmE041 CA (I), or SIVsmG932 CA (J) on CRFK cells stably expressing WT (solid bars) or mutant (striped bars) human (blue bars) or sooty mangabey (purple bars) orthologs of TF-Nup358$_{R4\text{-}Cyp}$. TFnull, which contains only the rhTRIM5Cyp RBCC domains, serves as the negative control (black bar). Infectivity, or the total percentage of EGFP positive cells, was measured by flow cytometry. The fold-changes in infectivity compared to TFnull are shown next to the bars. Results are representative of at least three independent experiments, with error bars indicating ± standard deviation.

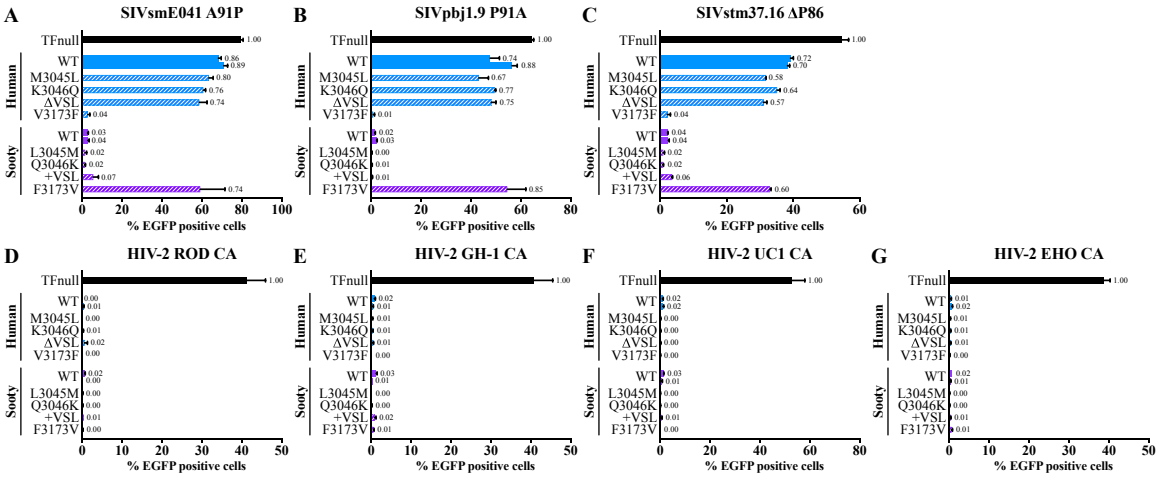

Figure 3.17. Addition of Nup358$_{R4}$ impacts CA interaction with human Nup358$_{Cyp}$
(A-G) Infectivity of VSV-G pseudotyped, single-cycle, EGFP reporter SIVsmE041 with A91P mutant CA (A), SIVpbj1.9 with P91A mutant CA (B), and SIVstm37.16 with ΔP86 mutant CA (C), and SIVmac239-based chimeric virus expressing the HIV-2 ROD CA (D), HIV-2 GH-1 CA (E, HIV-2 UC1 CA (F), or HIV-2 EHO CA (G), on CRFK cells stably expressing WT (solid bars) or mutant (striped bars) human (blue bars) or sooty mangabey (purple bars) orthologs of TF-Nup358$_{R4-Cyp}$. TFnull, which contains only the rhTRIM5Cyp RBCC domains, serves as the negative control (black bar). Infectivity, or the total percentage of EGFP positive cells, was measured by flow cytometry. The fold-changes in infectivity compared to TFnull are shown next to the bars. Results are representative of at least three independent experiments, with error bars indicating ± standard deviation.

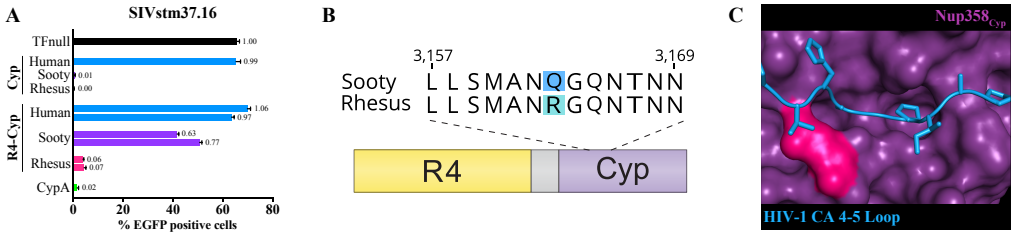

Figure 3.18. Residue 3163 in smNup358$_{Cyp}$ domain modulates SIVstm CA interaction in the context of smNup358$_{R4\text{-}Cyp}$ supradomain

(A) Infectivity of VSV-G pseudotyped, single-cycle, EGFP reporter SIVstm37.16 on CRFK cells stably expressing TF-CypA (green bar), and human (blue bars), sooty mangabey (purple bars), or rhesus macaque (pink bars) orthologs of TF-Nup358$_{Cyp}$ or TF-Nup358$_{R4\text{-}Cyp}$. TFnull, which contains only the rhTRIM5Cyp RBCC domains, serves as the negative control (black bar). Infectivity, or the total percentage of EGFP positive cells, was measured by flow cytometry. The fold-changes in infectivity compared to TFnull are shown next to the bars. Results are representative of at least three independent experiments, with error bars indicating ± standard deviation.

(B) Schematic of Nup358$_{R4\text{-}Cyp}$ domains highlighting the single residue difference between sooty mangabey and rhesus macaque orthologs. Residues are numbered based on human Nup358 sequence. Figure not drawn to scale.

(C) Crystal structure of huNup358$_{Cyp}$ (purple) interaction with NL4-3 HIV-1 CA NTD (pdb: 4LQW) with only the 4-5 loop shown (blue). Residue 3163 in Nup358$_{Cyp}$ domain is highlighted in pink. Image created in PyMOL.

3.7 Escape mutations in SIVmac CA 4-5 loop from rhesus TRIM5Cyp disrupt Nup358 interaction

In contrast to the other viruses tested, SIVmac239 CA does not detectably interact with Nup358Cyp or CypA (Figure. 3.3C) [62,80–83,147,170,171]. An alignment of the SIVsmE041 and SIVmac239 CA 4-5 loops reveal several differences between the two capsids – in particular a glycine to alanine change at residue 87 and the replacement of the isoleucine-proline-alanine stretch of residues at positions 89-91 to a glutamine-glutamine motif (Figures 3.19A and 3.199B). We created a series of SIVsmE041 and SIVmac239 CA mutants that contained these differences individually and together, and tested their effects on Nup358/CypA interaction (Figures 3.19C-3.19J). Neither SIVmac239 single CA mutant recapitulated the ancestral SIVsmE041 CA Nup358/CypA interaction phenotype (Figures 3.19D and 3.19E, compare with Figure 3.19G). We did observe that SIVmac239 QQ➔IPA mutant CA interacted with the sooty mangabey and rhesus macaque Nup358Cyp domains; however, these interactions were not detectable in the Nup358R4-Cyp supradomain orthologs (Figure 3.19E, compare purple and pink Cyp bars with purple and pink R4-Cyp bars). Only reversions at both sites in SIVmac239 CA 4-5 loop to the ancestral SIVsmE041 sequences resulted in restoration of the Nup358/CypA interaction (Figure 3.19F). Interestingly, we observed that either the G87A substitution or the IPA➔QQ substitution is capable of disrupting SIVsmE041 interaction with Nup358R4-Cyp (Figures 3.19H and 3.19I); although – similar to the SIVmac239 QQ➔IPA mutant CA – the SIVsmE041 G87A mutant CA was able to interact with the sooty mangabey and rhesus macaque Nup358Cyp domains (Figures

3.19E and 3.19H). We did observe that the SIVsmE041 G87A + IPA➔QQ double mutant CA weakly interacts with CypA, despite the G87A single CA mutant having lost CypA interaction (Figures 3.19H and 3.19J, compare green bars), suggesting additional residue swaps may be necessary to fully recapitulate the loss of CypA interaction observed for SIVmac239 WT CA. Thus, while introduction of either G87A or IPA➔QQ substitutions is sufficient to disrupt SIVsmE041 CA interaction with Nup358R4-Cyp, both sites must be reverted to the ancestral state in SIVmac239 CA to restore the Nup358R4-Cyp interaction.

Previous work from our lab and others has shown that the SIVsm CA faced selective pressure from rhesus macaque *TRIM5* (*rhTRIM5*) gene during its emergence within the species as SIVmac [153,154,159]. Rhesus macaques encode multiple *TRIM5* alleles that are typically categorized into three functional groups: rhTRIM5α^{TFP} (consisting of the *mamu-1*, *mamu-2*, and *mamu-3* alleles, which all encode residues TFP at positions 339-341 of the B30.2/PRYSPRY domain); rhTRIM5α^{Q} (consisting of the *mamu-4* and *mamu-5* alleles which encode a Q at position 339); and rhTRIM5Cyp (where a CypA-derived domain has completely replaced the TRIM5 C-terminal B30.2/PRYSPRY domain) [139,144,153,154,159,183,184]. SIVsm is sensitive to restriction by rhTRIM5αTFP and rhTRIM5Cyp but not rhTRIM5Q whereas SIVmac is resistant to all three alleles. This resistance is attributed to several amino acid substitutions in SIVmac CA, including the QQ motif at positions 89-90 in 4-5 loop, which imparts resistance to rhTRIM5Cyp [153,154,159]. To assess the impact of the SIVsmE041 and SIVmac239 CA 4-5 loop amino acid differences described above on rhTRIM5 restriction, we infected cells expressing the various sooty mangabey and rhesus

macaque TRIM5 alleles and human TRIM5α with the panel of SIVsmE041/SIVmac239 CA mutants used in Figure 9 (Figures 3.20A-3.20H). As expected, SIVmac239 encoding the WT CA was resistant to all rhTRIM5 alleles (Figure 3.20A). Reverting residue A87 in SIVmac239 CA to the ancestral glycine resulted in gain of sensitivity to the rhTRIM5^{TFP} alleles (Figure 3.20B), in line with previous results from our group [66]. The SIVmac239 QQ➔IPA CA mutant was sensitive to rhTRIM5^{TFP} and rhTRIM5Cyp restriction (Figure 3.20C), with this CA mutant showing stronger sensitivity to rhTRIM5^{TFP} restriction than the A87G mutant (Figures 3.20B and 3.20C, compare pink rhTRIM5^{TFP} bars). The SIVmac239 G87A + QQ➔IPA double mutant CA was also sensitive to rhTRIM5^{TFP} and rhTRIM5Cyp alleles (Figure 3.20D), although sensitivity to rhTRIM5^{TFP} restriction was like that of the A87G CA mutant (Figures 3.20B and 3.20D, compare pink rhTRIM5TFP bars). In accordance with previous observations, SIVsmE041 encoding the WT CA was restricted by all three rhTRIM5^{TFP} alleles and rhTRIM5Cyp (Figure 3.20E) [153,154,159]. While the G87A mutation in SIVsmE041 CA has little impact on sensitivity to either rhTRIM5^{TFP} or rhTRIM5Cyp (Figure 3.20F), both the SIVsmE041 IPA➔QQ CA mutant and SIVsmE041 G87A + IPA➔QQ CA double mutant were resistant to rhTRIM5Cyp restriction (Figures 3.20G and 3.20H).

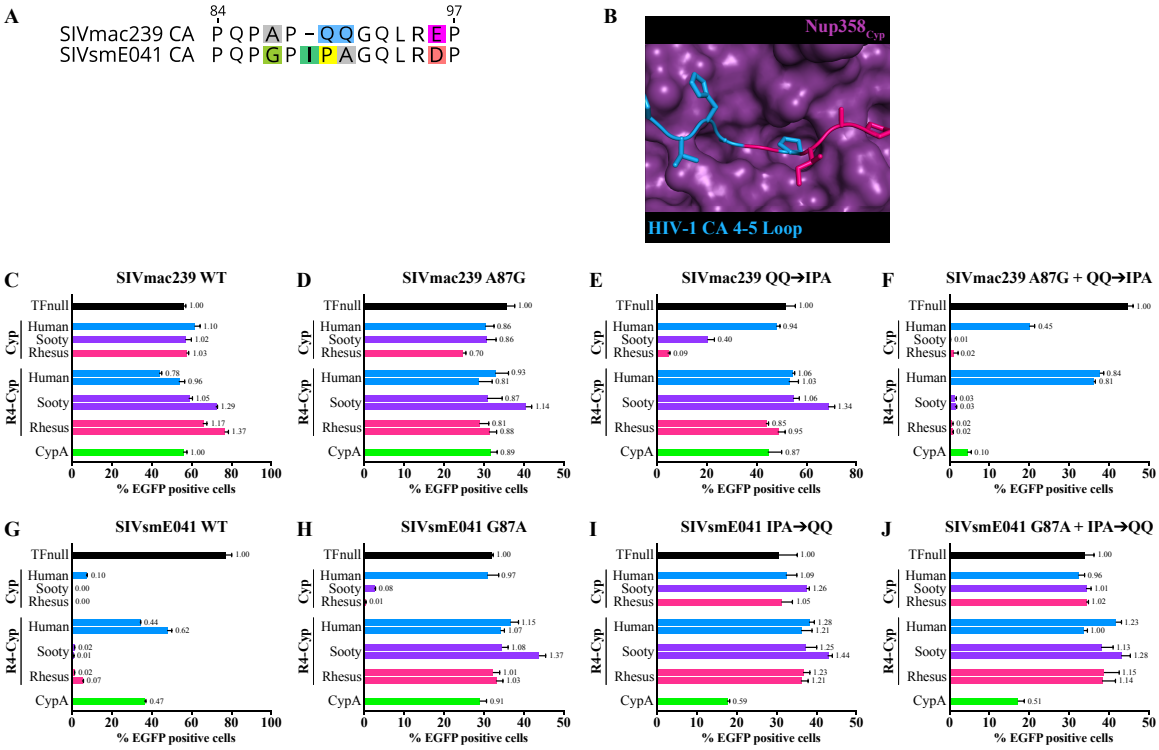

Figure 3.19. Reversion of specific sites in SIVmac CA 4-5 loop to ancestral residues restores interaction with Nup358R4-Cyp

(A) Alignment of SIVmac239 and SIVsmE041 CA 4-5 loop sequences. Residues are numbered based on SIVsmE041 CA sequence.

(B) Crystal structure of huNup358$_{Cyp}$ (purple) interaction with NL4-3 HIV-1 CA NTD (pdb: 4LQW) with only the 4-5 loop shown (blue). The residues equivalent to position 87 and residues 89-91 in SIVsmE041 CA are highlighted in pink (positions 89 and 91-93 in HIV-1 NL4-3 CA). Image created in PyMOL.

(C-J) Infectivity of VSV-G pseudotyped, single-cycle, EGFP reporter SIVmac239 with WT CA (C) or A87G (D), ^{89}QQ^{90}➔^{89}IPA^{91} (E), or A87G + ^{89}QQ^{90}➔^{89}IPA^{91} (F) mutant CA and SIVsmE041 with WT CA (G) or G87A (H), ^{89}IPA^{91}➔^{89}QQ^{90} (I), or G87A + ^{89}IPA^{91}➔^{89}QQ^{90} (J) mutant CA on CRFK cells stably expressing TF-CypA (green bar) and human (blue bars), sooty mangabey (purple bars), or rhesus macaque (pink bars) orthologs of TF-Nup358$_{Cyp}$ or TF-Nup358$_{R4\text{-}Cyp}$. TFnull, which contains only the rhTRIM5Cyp RBCC domains, serves as the negative control (black bar). Infectivity, or the total percentage of EGFP positive cells, was measured by flow cytometry. The fold-changes in infectivity compared to TFnull are shown next to the bars. Results are representative of at least three independent experiments, with error bars indicating ± standard deviation.

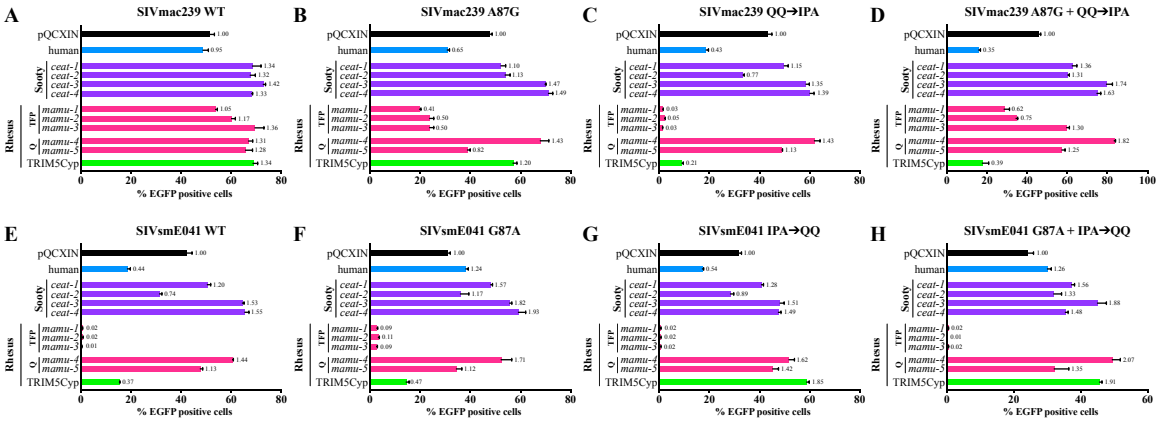

Figure 3.20. Modifications in SIVmac CA 4-5 loop that disrupt Nup358 interaction provide protection against rhTRIM5Cyp restriction

(A-H) Infectivity of VSV-G pseudotyped, single-cycle, EGFP reporter SIVmac239 with WT CA (A) or A87G (B), ^{89}QQ^{90}➔^{89}IPA^{91} (C), or A87G + ^{89}QQ^{90}➔^{89}IPA^{91} (D) mutant CA and SIVsmE041 with WT CA (E) or G87A (F), ^{89}IPA^{91}➔^{89}QQ^{90} (G), or G87A + ^{89}IPA^{91}➔^{89}QQ^{90} (H) mutant CA on CRFK cells stably expressing human (blue bar), sooty mangabey (purple bars), and rhesus macaque (pink bars) TRIM5α alleles or rhTRIM5Cyp (green bar). The pQCXIN cell line, which has been transduced with empty vector pQCXIN, serves as the negative control (black bar). Infectivity, or the total percentage of EGFP positive cells, was measured by flow cytometry. The fold-changes in infectivity compared to pQCXIN are shown next to the bars. Results are representative of at least three independent experiments, with error bars indicating ± SD.

CHAPTER 4: DISCUSSION

During viral replication, lentiviruses gain access to the host chromatin through active transport of the viral genome and associated proteins across the nuclear envelope. Multiple screens identified Nup358 as a possible co-factor for HIV-1 replication and published studies confirm a physical interaction between the HIV-1 CA 4-5 loop and the C-terminal Cyclophilin (Cyp) domain of Nup358; this proline-rich loop that extends from the assembled capsid core surface is the same site that also binds the cytoplasmic protein cyclophilin A (CypA) and the C-terminal Cyp domains of naturally occurring TRIM-Cyp fusion proteins. As Nup358 comprises the main component of the cytoplasmic fibrils extending from the nuclear pore complex (NPC), Nup358 has been hypothesized to potentially play a role in viral docking at the NPC and/or viral active transportation into the nucleus; however; the precise role(s) of the CA-Nup358$_{Cyp}$ interaction during lentiviral replication remain unclear.

Characterizing lentivirus capsid cores interaction with Nup358 is complicated by two considerations: first, the relevant interaction likely involves multimeric assemblies of CA, and not individual CA protein monomers; and second, Nup358 is a massive (358 kDa in size), multi-domain protein that has numerous cellular functions. In order to specifically examine the interaction between lentivirus capsids and Nup358$_{Cyp}$ domain, we capitalized on an assay that allowed us to evaluate the interaction in the relevant context using single-cycle infection. In addition, based on a review of the relevant literature on Nup358, we chose to examine CA interaction with Cyp domain of Nup358 alone (Nup358$_{Cyp}$) and as part of a "supradomain" which is comprised of the adjacent Nup358$_{R4}$ and Nup358$_{Cyp}$ domains (Nup358$_{R4\text{-}Cyp}$). Finally, by examining the interaction in the context of lentiviral cross-species transmission and emergence, we discovered that:

(1) CA interaction with Nup358$_{Cyp}$ is a conserved and possibly ancestral property of primate lentiviruses; and, (2) the CA-Nup358$_{Cyp}$ interaction is selectively advantageous and therefore contributes to viral fitness *in vivo*.

Our data revealed two important considerations when examining lentiviral CA interactions with Nup358$_{Cyp}$: (1) interspecies genetic differences in the Nup358$_{Cyp}$ domain can affect the interaction; and, (2) the Nup358$_{R4}$ domain can have a critical impact on the results of such studies. For the large part, previous work examining the breath of this viral-host interaction have utilized only the human ortholog – despite using non-human lentiviral CA's – and the Nup358$_{Cyp}$ domain in isolation – despite evidence of the upstream Nup358$_{R4}$ domain influencing Nup358$_{Cyp}$ substrate affinity [60,62,80–83]. Our data for SIVpbj and SIVstm shows that interspecies genetic differences in Nup358$_{Cyp}$ can impact interaction even when the Nup358$_{Cyp}$ domain is considered by itself (Figures 3.13E and 3.13F, compare the blue human Cyp bar to purple sooty mangabey and pink rhesus macaque Cyp bars). Meyerson et al. 2018 came to similar conclusions when using CA 4-5 loops from viruses of the SIVrcm/SIVcpz/HIV-1 lineage and the relevant host species Nup358$_{Cyp}$ orthologs [83]. However, we demonstrated for SIVsm, SIVpbj, and SIVstm that the impact of genetic differences present in the Nup358$_{Cyp}$ domain is observable only in the context of the Nup358$_{R4\text{-}Cyp}$ supradomain (Figures 3.16, 3.17 and 3.18). As the virus encounters the full length Nup358 protein during infection (i.e., always encounters Nup358$_{Cyp}$ domain alongside the Nup358$_{R4}$ domain), examining this interaction in the context of Nup358$_{R4\text{-}Cyp}$ is more biologically relevant than just the Nup358$_{Cyp}$ domain alone. It should be noted that the R4 domain appears to only restrict the range of CA's that can interact with Nup358$_{Cyp}$ as we did not observe a case where a

CA could not interact with a specific species' $Nup358_{Cyp}$ domain alone but able to interact with that species' $Nup358_{R4\text{-}Cyp}$.

In the absence of a co-crystal structure of CA interacting with $Nup358_{R4\text{-}Cyp}$, it is impossible to definitively state what effect R4 is having on CA's interaction with $Nup358_{Cyp}$ or if the CA interacts with the R4 domain as well as the Cyp domain within the context of the R4-Cyp supradomain. There are two possibilities as to how $Nup358_{R4}$ is affecting CA-$Nup358_{Cyp}$ interaction: steric hindrance or alterations to the PPIase active site of $Nup358_{Cyp}$. We hypothesize the latter to be true, based on the fact that changing residues in the Cyp domain is enough to restore the interaction with the $Nup358_{R4\text{-}Cyp}$ supradomain (Figures 3.16, 3.17 and 3.18); if $Nup358_{R4}$ was to sterically hinder access to $Nup358_{Cyp}$, we would not expect any change in the Cyp domain to affect the CA-$Nup358_{R4\text{-}Cyp}$ interaction. In further support of this hypothesis, previous work has found that the addition of the R4 domain can affect the PPIase activity of $Nup358_{Cyp}$ toward certain four amino acid-long prolyl substrates [97] and multiple small molecules are able to influence $Nup358_{Cyp}$ PPIase activity despite being predicted to bind sites outside of the active site [185]. In rhTRIM5Cyp, the PPIase active site of the fused Cyp domain fluctuates between several conformations, allowing it to interact with substrates that differ significantly in structure [67]. It is possible that the presence of $Nup358_{R4}$ domain "locks" the $Nup358_{Cyp}$ active site in a particular conformation where residues surrounding the active site then have a greater impact on CA interaction than when the $Nup358_{Cyp}$ domain is alone (i.e., $Nup358_{R4}$ is not present).

Our data also indicates that human $Nup358_{R4\text{-}Cyp}$ domains presented a genetic barrier to the cross-species transmission and emergence of SIVsm into humans as HIV-2.

All of the SIVsm CA's we tested weakly interacted with human Nup358$_{R4\text{-}Cyp}$ (Figures 3.5A-3.5D), whereas all HIV-2 CA's tested strongly interacted with human Nup358$_{R4\text{-}Cyp}$ (Figures 3.5E-3.5G). The HIV-2 CA's tested come from subtypes A and B (Figure 3.8B). As each subtype is thought to have arisen from an independent and separate SIVsm cross-species transmission event [43–45], our data suggests that adaptation to better interact with huNup358$_{R4\text{-}Cyp}$ occurred in both spillover events. Adaptation to huNup358$_{R4\text{-}Cyp}$ appears to be associated with a glutamine to isoleucine change at residue position 85 of SIVsm CA (Figure 3.7). Residue 85 is to be well-conserved among SIVsm/HIV-2 isolates, suggesting that the huNup358$_{R4\text{-}Cyp}$ interaction phenotypes we observed for the isolates in this study are widely conserved (Figure 3.7G and Figure 3.8). It should be noted that the HIV-2 EHO CA encodes a serine at position 85 but shares the same Nup358$_{R4\text{-}Cyp}$ interaction phenotype as the CA's that encode isoleucine at residue 85 (Figures 3.5 and 3.8B), suggesting that HIV-2 CA's with S85 also strongly interact with human Nup358$_{R4\text{-}Cyp}$. We identified genetic differences at Nup358 residue 3173 of sooty mangabeys and humans as responsible for the differential ability of SIVsm to interact with both species' Nup358$_{R4\text{-}Cyp}$ (Figure 3.16). Meyerson et al. 2018 also presented evidence that Nup358 exerted selective pressure upon the emergence of SIVrcm into chimpanzees as SIVcpz and the emergence of SIVcpz into gorillas as SIVgor [83]. Using human Nup358$_{Cyp}$ alone, their data did not suggest that the human ortholog presented a genetic barrier for SIVcpz or SIVgor for emergence into human as HIV-1 group M or HIV-1 group P, respectively. It is possible that re-examining those interactions using the Nup358$_{R4\text{-}Cyp}$ supradomain would show that human Nup358 did present a genetic barrier to those cross-species transmission events.

HIV-1 interacts with human NUP358$_{Cyp}$ and CypA via the CA 4-5 loop with the apical proline at position 90 sitting within the PPIase active site pocket [60,62,83]. Our data suggest that viruses belonging to the SIVsm/HIV-2 lineage interact in a similar fashion as we found that changes to residues in the 4-5 loop affect Nup358$_{Cyp}$/CypA interaction (Figures 3.3, 3.5-3.7). We found that human lentiviral CAs display a broader range of interaction when compared to the simian-specific orthologs. In fact, while SIVsm CA's interact unevenly with CypA but consistently with the Nup358$_{Cyp}$ domain (Figures 3.5A-3.5D) and SIVpbj interacts with Nup358$_{Cyp}$ but not CypA (Figure 3.3E), all HIV-2 isolates strongly interact with Nup358$_{Cyp}$ and CypA (Figures 3.3B and 3.5E-G). This observation intriguingly suggests how, in HIVs, affinity for CypA might itself be the consequence of the interaction with Nup358$_{R4\text{-}Cyp}$, and not the reverse, as it may appear less disingenuous to expect. We also found that HIV-1 and HIV-2 appear to interact with rhesus macaque and sooty mangabey Nup358$_{Cyp}$ orthologs, regardless of the presence of the R4 domain, suggesting that human Nup358$_{R4\text{-}Cyp}$ interaction may result in a more "flexible" 4-5 loop in regards to the ability to tolerate residue changes in the Nup358$_{Cyp}$ domain. Meehan et al. 2014 found that HIV-1 CA was able to interact with the mouse Nup358$_{Cyp}$ ortholog [81]. As Meyerson et al. 2014, found that HIV-1 M group CA 4-5 loop could not interact with gorilla Nup358$_{Cyp}$ or HIV-1 P group CA 4-5 loop could not interact with chimpanzee Nup358$_{Cyp}$, it is possible that the observed "flexibility" of HIV-1 and HIV-2 is limited to Old-World monkey Nup358$_{Cyp}$ orthologs.

Our work is the first to the authors' knowledge to show that lentiviruses that infect old world monkeys are able to interact with Nup358$_{Cyp}$. While Mamede et al., 2013 examined the ability of a panel of SIVs of Old-World monkeys' ability to interact with

Nup358$_{Cyp}$ and drew the conclusion that only HIV-2 was able to interact, they only tested the Nup358$_{Cyp}$ ortholog. Their results lead them to suggest that interaction with Nup358$_{Cyp}$ could be a human lentivirus-specific adaptation; however, both this work and Meyerson's et al. 2018 demonstrate the presence of this interaction for multiple non-human primate lentiviruses indicating the interaction is more widespread than previously expected. It is possible that Mamede et al 2013 would have identified this interaction in their tested panel had they used the relevant host species' orthologs of Nup358$_{Cyp}$.

In contrast to what we observe for SIVstm and SIVpbj, Nup358$_{Cyp}$ interaction appears to have been lost during the emergence of SIVsm into rhesus macaques as SIVmac (Figure 3.3). This loss of interaction appears to be due to changes in the CA 4-5 loop. It is interesting to note that either one of the two observed changes in the 4-5 loop is enough to disrupt interaction with Nup358$_{Cyp}$ (Figure 3.19). We found that one of the changes (IPA➔QQ) that causes loss of Nup358-CypA interaction also results in resistance to restriction by the rhTRIM5Cyp allele. As both the Cyp domain of TRIM5Cyp and the Nup358$_{Cyp}$ domain interact with the capsid 4-5 loop, it is reasonable to hypothesize based on our data that selective pressure from TRIM5Cyp contributed to the loss of Nup358$_{Cyp}$ interaction observed in SIVmac239 CA. However, most likely the presence of additional selective pressures also acting on CA contributed to the loss of Nup358$_{Cyp}$ interaction as the SIVpbj1.9 CA maintained Nup358 interaction following emergence in pig-tailed macaques despite this species only encoding the TRIM5Cyp allele at their *TRIM5* locus [139,144,146,186,187]. It is possible that dual selective pressure from the rhTRIM5α^{TFP} alleles and rhTRIM5Cyp drove the loss of this interaction. Previous work from our group has shown that rhTRIM5α^{TFP} targets multiple

CA residues that have been associated with HIV-1 cofactor interaction/dependency, including Nup358 [66]. It is also possible that other CA-targeting restriction factors may have placed selective pressure resulting in loss of the $Nup358_{Cyp}$ interaction, such as Mx2, although this could easily be experimentally validated by testing whether SIVsm is restricted by the rhesus macaque Mx2 ortholog. The conservation of the $Nup358_{Cyp}$ interaction among primate lentiviruses and the observation of genetic differences in $Nup358_{Cyp}$ exerting selective pressure during cross-species transmission together argues that this interaction is important to viral replication. Thus, in the case of SIVmac, the loss of said interaction was most likely an evolutionary trade-off to escape from rhesus macaque TRIM5 restriction.

REFERENCES

1. Goff SP (2013) Retroviridae. *Fields Virology*, eds Knipe DM, Howley PM (University of California Press, Philadelphia), pp 1424–1473. Sixth Edit.
2. Khan AS, Bodem J, Buseyne F, Gessain A, Johnson W, Kuhn JH, Kuzmak J, Lindemann D, Linial ML, Löchelt M, Materniak-Kornas M, Soares MA, Switzer WM (2018) Spumaretroviruses: Updated taxonomy and nomenclature. *Virology* 516(December 2017):158–164.
3. Gifford RJ (2012) Viral evolution in deep time: Lentiviruses and mammals. *Trends Genet* 28(2):89–100.
4. Gifford RJ, Katzourakis A, Tristem M, Pybus OG, Winters M, Shafer RW (2008) A transitional endogenous lentivirus from the genome of a basal primate and implications for lentivirus evolution. *Proc Natl Acad Sci* 105(51):20362–20367.
5. Brown M, Munkhtsog B, Troyer J, Ross S, Sellers R, Fine A, Swanson W, Roelke M, SJ O (2010) Feline Immunodeficiency Virus (FIV) in Wild Pallas' Cats. *Vet Immunol Immunopathol* 134(1–2). doi:10.1016/j.vetimm.2009.10.014.FELINE.
6. Reina R, Bertolotti L, Dei Giudici S, Puggioni G, Ponti N, Profiti M, Patta C, Rosati S (2010) Small ruminant lentivirus genotype E is widespread in Sarda goat. *Vet Microbiol* 144(1–2):24–31.
7. Hron T, Fábryová H, Pačes J, Elleder D (2014) Endogenous lentivirus in Malayan colugo (Galeopterus variegatus), a close relative of primates. *Retrovirology* 11(1):84.
8. Sharp PM, Hahn BH (2011) Origins of HIV and the AIDS pandemic. *Cold Spring Harb Perspect Med* 1:1–22.
9. Sharp P, Shaw G, Hahn B (2005) Simian Immunodeficiency Virus Infection of Chimpanzees. *J Virol* 79(7):3891–3902.
10. Han GZ, Worobey M (2012) Endogenous lentiviral elements in the weasel family (mustelidae). *Mol Biol Evol* 29(520):2905–2908.
11. Freed EO (2015) HIV-1 assembly, release and maturation. *Nat Rev Microbiol* 13(8):484–496.
12. Collins DR, Collins KL (2014) HIV-1 Accessory Proteins Adapt Cellular Adaptors to Facilitate Immune Evasion. *PLoS Pathog* 10(1):2–5.
13. Alkhatib G, Berger EA (2007) HIV coreceptors: from discovery and designation to new paradigms and promise. *Eur J Med Res* 12(9):375–84.
14. Dalgleish AG, Clapham PR, Crawford DH, Greaves MF, Weiss RA, Beverley PC, Clapham PR, Crawford DH, Greaves MF, Weiss RA (1984) The CD4 (T4) antigen is an essential component of the receptor for the AIDS retrovirus. *Nature* 321:763–767.
15. Klatzmann D, Champagne E, Chamaret S, Gruest J, Guetard D, Hercend T, Gluckman JC, Montagnier L (1984) T-lymphocyte T4 molecule behaves as the receptor for human retrovirus LAV. *Nature* 312(5996):767–768.
16. Choe H, Farzan M, Sun Y, Sullivan N, Rollins B, Ponath PD, Wu L, Mackay CR, LaRosa G, Newman W, Gerard N, Gerard C, Sodroski J (1996) The β-chemokine receptors CCR3 and CCR5 facilitate infection by primary HIV-1 isolates. *Cell* 85(7):1135–1148.
17. Deng HK, Liu R, Ellmeier W, Choe S, Unutmaz D, Burkhart M, Di Marzio P, Marmon S, Sutton RE, Mark Hill C, Davis CB, Peiper SC, Schall TJ, Littman DR,

Landau NR (1996) Identification of a major co-receptor for primary isolates of HIV-1. *Nature* 381(6584):661–666.
18. Doranz BJ, Rucker J, Yi Y, Smyth RJ, Samson M, Peiper SC, Parmentier M, Collman RG, Doms RW (1996) A dual-tropic primary HIV-1 isolate that uses fusin and the β-chemokine receptors CKR-5, CKR-3, and CKR-2b as fusion cofactors. *Cell* 85(7):1149–1158.
19. Dragic T, Litwin V, Allaway GP, Martin SR, Huang Y, Nagashima KA, Cayanan C, Maddon PJ, Koup RA, Moore JP, Paxton WA (1996) HIV-1 entry into CD4+ cells is mediated by the chemokine receptor CC-CKR-5. *Nature* 381(6584):667–673.
20. Chen Z, Zhou P, Ho DD, Landau NR, Marx PA (1997) Genetically divergent strains of simian immunodeficiency virus use CCR5 as a coreceptor for entry. *J Virol* 71(4):2705–2714.
21. Campbell EM, Hope TJ (2015) HIV-1 capsid: the multifaceted key player in HIV-1 infection. *Nat Rev Microbiol* 13(8):471–483.
22. Accola MA, Ohagen Å, Göttlinger HG (2000) Isolation of human immunodeficiency virus type 1 cores: retention of Vpr in the absence of p6(gag). *J Virol* 74(13):6198–202.
23. Welker R, Hohenberg H, Tessmer U, Huckhagel C, Kräusslich H-G (2000) Biochemical and structural analysis of isolated mature cores of human immunodeficiency virus type 1. *J Virol* 74(3):1168–77.
24. Kotov A, Zhou J, Flicker P, Aiken C (1999) Association of Nef with the Human Immunodeficiency Virus Type 1 Core. *J Virol* 73(10):8824–8830.
25. Baltimore D (1970) RNA-dependent DNA polymerase in Virions of RNA Tumour Viruses. *Nature* 226(5252):1209–11.
26. Miller MD, Farnet CM, Bushman FD (1997) Human immunodeficiency virus type 1 preintegration complexes: studies of organization and composition. *J Virol* 71(7):5382 LP – 5390.
27. Farnet CM, Haseltine WA (1991) Determination of viral proteins present in the human immunodeficiency virus type 1 preintegration complex. *J Virol* 65(4):1910–1915.
28. Francis AC, Marin M, Prellberg MJ, Palermino-Rowland K, Melikyan GB (2020) HIV-1 Uncoating and Nuclear Import Precede the Completion of Reverse Transcription in Cell Lines and in Primary Macrophages. *Viruses* 12(11):1234.
29. Dharan A, Bachmann N, Talley S, Zwikelmaier V, Campbell EM (2020) Nuclear pore blockade reveals that HIV-1 completes reverse transcription and uncoating in the nucleus. *Nat Microbiol*. doi:10.1038/s41564-020-0735-8.
30. Geeraert L, Kraus G, Pomerantz RJ (2008) Hide-and-Seek: The Challenge of Viral Persistence in HIV-1 Infection. *Annu Rev Med* 59(1):487–501.
31. Lewis P, Hensel M, Emerman M (1992) Human immunodeficiency virus infection of cells arrested in the cell cycle. *EMBO J* 11(8):3053–3058.
32. Lewis PF, Emerman M (1994) Passage through mitosis is required for oncoretroviruses but not for the human immunodeficiency virus. *J Virol* 68(1):510–516.
33. Hemelaar J (2012) The origin and diversity of the HIV-1 pandemic. *Trends Mol*

Med 18(3):182–192.
34. Tebit DM, Arts EJ (2011) Tracking a century of global expansion and evolution of HIV to drive understanding and to combat disease. *Lancet Infect Dis* 11(1):45–56.
35. Hahn BH (2000) AIDS as a Zoonosis: Scientific and Public Health Implications. *Science (80-)* 287(5453):607–614.
36. Peeters M, D'Arc M, Delaporte E (2014) Origin and diversity of human retroviruses. *AIDS Rev* 16:23–34.
37. Bailes E (2003) Hybrid Origin of SIV in Chimpanzees. *Science (80-)* 300(5626):1713–1713.
38. Keele BF, Van Heuverswyn F, Li Y, Bailes E, Takehisa J, Santiago ML, Bibollet-Ruche F, Chen Y, Wain L V., Liegeois F, Loul S, Ngole EM, Bienvenue Y, Delaporte E, Brookfield JFY, Sharp PM, Shaw GM, Peeters M, Hahn BH (2006) Chimpanzee reservoirs of pandemic and nonpandemic HIV-1. *Science* 313(5786):523–6.
39. Takehisa J, Kraus MH, Ayouba A, Bailes E, Van Heuverswyn F, Decker JM, Li Y, Rudicell RS, Learn GH, Neel C, Ngole EM, Shaw GM, Peeters M, Sharp PM, Hahn BH (2009) Origin and biology of simian immunodeficiency virus in wild-living western gorillas. *J Virol* 83(4):1635–1648.
40. Neel C, Etienne L, Li Y, Takehisa J, Rudicell RS, Ndong Bass I, Moudindo J, Mebenga A, Esteban A, Van Heuverswyn F, Liegeois F, Kranzusch PJ, Walsh PD, Sanz CM, Morgan DB, Ndjango J-BN, Plantier J-C, Locatelli S, Gonder MK, Leendertz FH, Boesch C, Todd A, Delaporte E, Mpoudi-Ngole E, Hahn BH, Peeters M (2010) Molecular Epidemiology of Simian Immunodeficiency Virus Infection in Wild-Living Gorillas. *J Virol* 84(3):1464–1476.
41. D'arc M, Ayouba A, Esteban A, Learn GH, Boué V, Liegeois F, Etienne L, Tagg N, Leendertz FH, Boesch C, Madinda NF, Robbins MM, Gray M, Cournil A, Ooms M, Letko M, Simon VA, Sharp PM, Hahn BH, Delaporte E, Mpoudi Ngole E, Peeters M (2015) Origin of the HIV-1 group O epidemic in western lowland gorillas. *Proc Natl Acad Sci* 112(11):E1343-52.
42. Apetrei C, Robertson DL, Marx PA (2004) The history of SIVs and AIDS: Epidemiology, phylogeny and biology of isolates from naturally SIV infected non-human primates (NHP) in Africa. *Front Biosci* 9(May 2014):225–254.
43. Chen Z, Luckay A, Sodora DL, Telfer P, Reed P, Gettie A, Kanu JM, Sadek RF, Yee J, Ho DD, Zhang L, Marx PA (1997) Human immunodeficiency virus type 2 (HIV-2) seroprevalence and characterization of a distinct HIV-2 genetic subtype from the natural range of simian immunodeficiency virus-infected sooty mangabeys. *J Virol* 71(5):3953–3960.
44. Lemey P, Pybus OG, Wang B, Saksena NK, Salemi M, Vandamme A-M (2003) Tracing the origin and history of the HIV-2 epidemic. *Proc Natl Acad Sci* 100(11):6588–6592.
45. Eberle J, Gürtler L (2012) HIV types, groups, subtypes and recombinant forms: Errors in replication, selection pressure and quasispecies. *Intervirology* 55(2):79–83.
46. Gardner MB (2003) Simian AIDS: an historical perspective. *J Med Primatol* 32(4–5):180–186.

47. Mansfield KG, Lerche NW, Gardner MB, Lackner AA (1995) Origins of simian immunodeficiency virus infection in macaques at The New England Regional Primate Research Center. *J Med Primatol* 24(3):116–122.
48. Apetrei C, Lerche NW, Pandrea I, Gormus B, Silvestri G, Kaur A, Robertson DL, Hardcastle J, Lackner AA, Marx PA (2006) Kuru experiments triggered the emergence of pathogenic SIVmac. *AIDS* 20(3):317–21.
49. Khan AS, Galvin TA, Lowenstine LJ, Jennings MB, Gardner MB, Buckler CE (1991) A highly divergent simian immunodeficiency virus (SIVstm) recovered from stored stump-tailed macaque tissues. *J Virol* 65(12):7061–7065.
50. Novembre FJ, Hirsch VM, McClure HM, Fultz PN, Johnson PR (1992) SIV from stump-tailed macaques: molecular characterization of a highly transmissible primate lentivirus. *Virology* 186(2):783–7.
51. Fultz PN, McClure HM, Anderson DC, Switzer WM (1989) Identification and biologic characterization of an acutely lethal variant of simian immunodeficiency virus from sooty mangabeys (SIV/SMM). *AIDS Res Hum Retroviruses* 5(4):397–409.
52. Novembre FJ, Johnson PR, Lewis MG, Anderson DC, Klumpp S, McClure HM, Hirsch VM (1993) Multiple viral determinants contribute to pathogenicity of the acutely lethal simian immunodeficiency virus SIVsmmPBj variant. *J Virol* 67(5):2466–74.
53. Dewhurst S, Embretson JE, Anderson DC, Mullins JI, Fultz PN (1990) Sequence analysis and acute pathogenicity of molecularly cloned SIVSMM-PBj14. *Nature* 345(6276):636–640.
54. Benveniste RE, Arthur LO, Tsai CC, Sowder R, Copeland TD, Henderson LE, Oroszlan S (1986) Isolation of a lentivirus from a macaque with lymphoma: comparison with HTLV-III/LAV and other lentiviruses. *J Virol* 60(2):483–490.
55. VandeWoude S, Apetrei C (2006) Going Wild: Lessons from Naturally Occurring T-Lymphotropic Lentiviruses. *Clin Microbiol Rev* 19(4):728–762.
56. McCarthy KR, Johnson WE, Kirmaier A (2016) Phylogeny and History of the Lost SIV from Crab-Eating Macaques: SIVmfa. *PLoS One* 11(7):1–14.
57. Mortuza GB, Haire LF, Stevens A, Smerdon SJ, Stoye JP, Taylor I a (2004) High-resolution structure of a retroviral capsid hexameric amino-terminal domain. *Nature* 431(2000):481–485.
58. Gamble TR, Yoo S, Vajdos FF, Von Schwedler UK, Worthylake DK, Wang H, McCutcheon JP, Sundquist WI, Hill CP (1997) Structure of the carboxyl-terminal dimerization domain of the HIV-1 capsid protein. *Science (80-)* 278(5339):849–853.
59. Berthet-Colominas C, Monaco S, Novelli A, Sibaï G, Mallet F, Cusack S (1999) Head-to-tail dimers and interdomain flexibility revealed by the crystal structure of HIV-1 capsid protein (p24) complexed with a monoclonal antibody Fab. *EMBO J* 18(5):1124–1136.
60. Bichel K, Price AJ, Schaller T, Towers GJ, Freund SM V, James LC (2013) HIV-1 capsid undergoes coupled binding and isomerization by the nuclear pore protein NUP358. *Retrovirology* 10(1):81.
61. Gamble TR, Vajdos FF, Yoo S, Worthylake DK, Houseweart M, Sundquist WI,

Hill CP (1996) Crystal structure of human cyclophilin A bound to the amino-terminal domain of HIV-1 capsid. *Cell* 87:1285–1294.
62. Schaller T, Ocwieja KE, Rasaiyaah J, Price AJ, Brady TL, Roth SL, Hué S, Fletcher AJ, Lee K, KewalRamani VN, Noursadeghi M, Jenner RG, James LC, Bushman FD, Towers GJ (2011) HIV-1 capsid-cyclophilin interactions determine nuclear import pathway, integration targeting and replication efficiency. *PLoS Pathog* 7(12). doi:10.1371/journal.ppat.1002439.
63. Goff SP (2007) Retroviridae: The Retroviruses and Their Replication. *Fields' Virology.*, eds Knipe DM, Howley PM (Wolters Kluwer Health/Lippincott Williams & Wilkins, Philadelphia), pp 1999–2070. 5th Ed.
64. Fassati A (2006) HIV infection of non-dividing cells: a divisive problem. *Retrovirology* 3(1):74.
65. Goldstone DC, Yap MW, Robertson LE, Haire LF, Taylor WR, Katzourakis A, Stoye JP, Taylor I a. (2010) Structural and functional analysis of prehistoric lentiviruses uncovers an ancient molecular interface. *Cell Host Microbe* 8(3):248–59.
66. McCarthy KR, Schmidt AG, Kirmaier A, Wyand AL, Newman RM, Johnson WE (2013) Gain-of-Sensitivity Mutations in a Trim5-Resistant Primary Isolate of Pathogenic SIV Identify Two Independent Conserved Determinants of Trim5α Specificity. *PLoS Pathog* 9(5):e1003352.
67. Price AJ, Marzetta F, Lammers M, Ylinen LMJ, Schaller T, Wilson SJ, Towers GJ, James LC (2009) Active site remodeling switches HIV specificity of antiretroviral TRIMCyp. *Nat Struct Mol Biol* 16(10):1036–1042.
68. Tipper CH, Sodroski JG (2014) Contribution of Glutamine Residues in the Helix 4-5 Loop to Capsid-Capsid Interactions in Simian Immunodeficiency Virus of Macaques. *J Virol* 88(18):10289–10302.
69. Lin T-Y, Emerman M (2006) Cyclophilin A interacts with diverse lentiviral capsids. *Retrovirology* 3:70.
70. McEwan W (2010) Factors affecting replication and cross-species transmission of feline immunodeficiency virus. Dissertation (University of Glasgow). Available at: http://theses.gla.ac.uk/1388/.
71. Bollman B (2013) Role of the Capsid Helix 4-5 Loop in Equine Infectious Anemia Virus Infection. Dissertation (Harvard University).
72. Forshey BM, von Schwedler UK, Sundquist WI, Aiken C (2002) Formation of a Human Immunodeficiency Virus Type 1 Core of Optimal Stability Is Crucial for Viral Replication. *J Virol* 76(11):5667–5677.
73. Braaten D, Franke EK, Luban J (1996) Cyclophilin A is required for an early step in the life cycle of human immunodeficiency virus type 1 before the initiation of reverse transcription. *J Virol* 70(6):3551–3560.
74. Ptak RG, Gallay P a., Jochmans D, Halestrap AP, Ruegg UT, Pallansch L a., Bobardt MD, De Béthune MP, Neyts J, De Clercq E, Dumont JM, Scalfaro P, Besseghir K, Wenger RM, Rosenwirth B (2008) Inhibition of human immunodeficiency virus type 1 replication in human cells by Debio-025, a novel cyclophilin binding agent. *Antimicrob Agents Chemother* 52(4):1302–1317.
75. Ambrose Z, Aiken C (2014) HIV-1 uncoating: connection to nuclear entry and

regulation by host proteins. *Virology* 454–455(1):371–9.
76. Hilditch L, Towers GJ (2014) A model for cofactor use during HIV-1 reverse transcription and nuclear entry. *Curr Opin Virol* 4:32–36.
77. Rasaiyaah J, Tan CP, Fletcher AJ, Price AJ, Blondeau C, Hilditch L, Jacques D a, Selwood DL, James LC, Noursadeghi M, Towers GJ (2013) HIV-1 evades innate immune recognition through specific cofactor recruitment. *Nature* 503(7476):402–405.
78. Rihn SJ, Wilson SJ, Loman NJ, Alim M, Bakker SE, Bhella D, Gifford RJ, Rixon FJ, Bieniasz PD (2013) Extreme Genetic Fragility of the HIV-1 Capsid. *PLoS Pathog* 9(6). doi:10.1371/journal.ppat.1003461.
79. von Schwedler UK, Stray KM, Garrus JE, Sundquist WI (2003) Functional Surfaces of the Human Immunodeficiency Virus Type 1 Capsid Protein. *J Virol* 77(9):5439–5450.
80. Mamede JI, Sitbon M, Battini J-L, Courgnaud V (2013) Heterogeneous susceptibility of circulating SIV isolate capsids to HIV-interacting factors. *Retrovirology* 10:77.
81. Meehan AM, Saenz DT, Guevera R, Morrison JH, Peretz M, Fadel HJ, Hamada M, van Deursen J, Poeschla EM (2014) A Cyclophilin Homology Domain-Independent Role for Nup358 in HIV-1 Infection. *PLoS Pathog* 10(2):1–17.
82. Mamede JI, Damond F, Bernardo A de, Matheron S, Descamps D, Battini J-L, Sitbon M, Courgnaud V (2017) Cyclophilins and nucleoporins are required for infection mediated by capsids from circulating HIV-2 primary isolates. *Sci Rep* 7(November 2016):45214.
83. Meyerson NR, Warren CJ, Vieira DASA, Diaz-Griffero F, Sawyer SL, Diaz-Griferro F, Sawyer SL, Diaz-Griffero F, Warren CJ, Vieira DASA, Diaz-Griferro F, Sawyer SL, Diaz-Griferro F, Sawyer SL, Diaz-Griffero F, Warren CJ, Vieira DASA, Diaz-Griferro F, Sawyer SL (2018) Correction: Species-specific vulnerability of RanBP2 shaped the evolution of SIV as it transmitted in African apes. *PLOS Pathog* 14(4):e1006983.
84. Lin DH, Zimmermann S, Stuwe T, Stuwe E, Hoelz A (2013) Structural and functional analysis of the C-terminal domain of Nup358/RanBP2. *J Mol Biol* 425(8):1318–1329.
85. Di Nunzio F, Danckaert A, Fricke T, Perez P, Fernandez J, Perret E, Roux P, Shorte S, Charneau P, Diaz-Griffero F, Arhel NJ (2012) Human Nucleoporins Promote HIV-1 Docking at the Nuclear Pore, Nuclear Import and Integration. *PLoS One* 7(9). doi:10.1371/journal.pone.0046037.
86. Wu J, Matunis MJ, Kraemer D, Blobel G, Coutavas E (1995) Nup358, a cytoplasmically exposed nucleoporin with peptide repeats, Ran-GTP binding sites, zinc fingers, a cyclophilin A homologous domain, and a leucine-rich region. *J Biol Chem* 270(23):14209–14213.
87. Yokoyama N, Hayashi N, Seki T, Panté N, Ohba T, Nishii K, Kuma K, Hayashida T, Miyata T, Aebi U, Fukui M, Nishimoto T (1995) A giant nucleopore protein that binds Ran/TC4. *Nature* 376(6536):184–188.
88. Lounsbury KM, Richards S a., Perlungher RR, Macara IG (1996) Ran binding domains promote the interaction of Ran with p97/beta-karyopherin, linking the

docking and translocation steps of nuclear import. *J Biol Chem* 271(5):2357–2360.
89. Yaseen NR, Blobel G (1999) Two distinct classes of Ran-binding sites on the nucleoporin Nup-358. *Proc Natl Acad Sci* 96(10):5516–5521.
90. Yaseen NR, Blobel G (1999) GTP Hydrolysis Links Initiation and Termination of Nuclear Import on the Nucleoporin Nup358. *J Biol Chem* 274(37):26493–26502.
91. Wälde S, Thakar K, Hutten S, Spillner C, Nath A, Rothbauer U, Wiemann S, Kehlenbach RH (2012) The Nucleoporin Nup358/RanBP2 Promotes Nuclear Import in a Cargo- and Transport Receptor-Specific Manner. *Traffic* 13(2):218–233.
92. Nigro P, Pompilio G, Capogrossi MC (2013) Cyclophilin A: a key player for human disease. *Cell Death Dis* 4(10):e888–e888.
93. Ferreira P a., Orry A (2012) From Drosophila to Humans: Reflections on the Roles of the Prolyl Isomerases and Chaperones, Cyclophilins, in Cell Function and Disease. *J Neurogenet* 26(2):132–143.
94. Lu KP, Finn G, Lee TH, Nicholson LK (2007) Prolyl cis-trans isomerization as a molecular timer. *Nat Chem Biol* 3(10):619–629.
95. Ferreira PA, Nakayama TA, Travis GH (1997) Interconversion of red opsin isoforms by the cyclophilin-related chaperone protein Ran-binding protein 2. *Proc Natl Acad Sci* 94(4):1556–1561.
96. Ferreira PA, Nakayama TA, Pak WL, Travis GH (1996) Cyclophilin-related protein RanBP2 acts as chaperone for red/green opsin. *Nature* 383(6601):637–40.
97. Cho K-I, Patil H, Senda E, Wang J, Yi H, Qiu S, Yoon D, Yu M, Orry A, Peachey NS, Ferreira PA (2014) Differential loss of prolyl isomerase or chaperone activity of ran-binding protein 2 (Ranbp2) unveils distinct physiological roles of its cyclophilin domain in proteostasis. *J Biol Chem* 289(8):4600–4625.
98. Zhang R, Mehla R, Chauhan A (2010) Perturbation of host nuclear membrane component RanBP2 impairs the nuclear import of human immunodeficiency virus -1 preintegration complex (DNA). *PLoS One* 5(12). doi:10.1371/journal.pone.0015620.
99. Lee K, Ambrose Z, Martin TD, Oztop I, Mulky A, Julias JG, Vandegraaff N, Baumann JG, Wang R, Yuen W, Takemura T, Shelton K, Taniuchi I, Li Y, Sodroski J, Littman DR, Coffin JM, Hughes SH, Unutmaz D, Engelman A, KewalRamani VN (2010) Flexible Use of Nuclear Import Pathways by HIV-1. *Cell Host Microbe* 7(3):221–233.
100. Aslanukov A, Bhowmick R, Guruju M, Oswald J, Raz D, Bush RA, Sieving PA, Lu X, Bock CB, Ferreira PA (2006) RanBP2 modulates Cox11 and hexokinase I activities and haploinsufficiency of RanBP2 causes deficits in glucose metabolism. *PLoS Genet* 2(10):1653–1665.
101. Hamada M, Haeger A, Jeganathan KB, van Ree JH, Malureanu L, Wälde S, Joseph J, Kehlenbach RH, van Deursen JM (2011) Ran-dependent docking of importin-β to RanBP2/Nup358 filaments is essential for protein import and cell viability. *J Cell Biol* 194(4):597–612.
102. Ribbeck K, Görlich D (2001) Kinetic analysis of translocation through nuclear pore complexes. *EMBO J* 20(6):1320–30.
103. Dawlaty MM, Malureanu L, Jeganathan KB, Kao E, Sustmann C, Tahk S, Shuai

K, Grosschedl R, van Deursen JM (2008) Resolution of Sister Centromeres Requires RanBP2-Mediated SUMOylation of Topoisomerase IIα. *Cell* 133(1):103–115.
104. Ocwieja KE, Brady TL, Ronen K, Huegel A, Roth SL, Schaller T, James LC, Towers GJ, Young JAT, Chanda SK, König R, Malani N, Berry CC, Bushman FD (2011) HIV integration targeting: A pathway involving transportin-3 and the nuclear pore protein RanBP2. *PLoS Pathog* 7(3):19–21.
105. Price AJ, Fletcher AJ, Schaller T, Elliott T, Lee K, KewalRamani VN, Chin JW, Towers GJ, James LC (2012) CPSF6 Defines a Conserved Capsid Interface that Modulates HIV-1 Replication. *PLoS Pathog* 8(8):e1002896.
106. Hori T, Takeuchi H, Saito H, Sakuma R, Inagaki Y, Yamaoka S (2013) A carboxy-terminally truncated human CPSF6 lacking residues encoded by exon 6 inhibits HIV-1 cDNA synthesis and promotes capsid disassembly. *J Virol* 87(13):7726–36.
107. Di Nunzio F, Fricke T, Miccio A, Valle-Casuso JC, Perez P, Souque P, Rizzi E, Severgnini M, Mavilio F, Charneau P, Diaz-Griffero F (2013) Nup153 and Nup98 bind the HIV-1 core and contribute to the early steps of HIV-1 replication. *Virology* 440(1):8–18.
108. Di Nunzio F (2013) New insights in the role of nucleoporins: A bridge leading to concerted steps from HIV-1 nuclear entry until integration. *Virus Res* 178(2):187–196.
109. Koh Y, Wu X, Ferris AL, Matreyek KA, Smith SJ, Lee K, KewalRamani VN, Hughes SH, Engelman AN (2013) Differential Effects of Human Immunodeficiency Virus Type 1 Capsid and Cellular Factors Nucleoporin 153 and LEDGF/p75 on the Efficiency and Specificity of Viral DNA Integration. *J Virol* 87(1):648–658.
110. Hall MN, Corbett AH, Pavlath GK (2011) Regulation of nucleocytoplasmic transport in skeletal muscle. *Curr Top Dev Biol* 96(2):273–302.
111. Hetzer MW, Wente SR (2009) Border Control at the Nucleus: Biogenesis and Organization of the Nuclear Membrane and Pore Complexes. *Dev Cell* 17(5):606–616.
112. D'Angelo M a., Raices M, Panowski SH, Hetzer MW (2009) Age-Dependent Deterioration of Nuclear Pore Complexes Causes a Loss of Nuclear Integrity in Postmitotic Cells. *Cell* 136(2):284–295.
113. Puckelwartz MJ, Kessler EJ, Kim G, DeWitt MM, Zhang Y, Earley JU, Depreux FFS, Holaska J, Mewborn SK, Pytel P, McNally EM (2010) Nesprin-1 mutations in human and murine cardiomyopathy. *J Mol Cell Cardiol* 48(4):600–608.
114. Smitherman M, Lee K, Swanger J, Kapur R, Clurman BE (2000) Characterization and targeted disruption of murine Nup50, a p27(Kip1)-interacting component of the nuclear pore complex. *Mol Cell Biol* 20(15):5631–5642.
115. Raices M, D'Angelo M a. (2012) Nuclear pore complex composition: a new regulator of tissue-specific and developmental functions. *Nat Rev Mol Cell Biol* 13(11):687–699.
116. Stremlau M, Owens CM, Perron MJ, Kiessling M, Autissier P, Sodroski J (2004) The cytoplasmic body component TRIM5alpha restricts HIV-1 infection in Old

World monkeys. *Nature* 427(February):848–853.
117. Mascarenhas AP, Musier-Forsyth K (2009) The capsid protein of human immunodeficiency virus: Interactions of HIV-1 capsid with host protein factors. *FEBS J* 276:6118–6127.
118. Johnson WE, Sawyer SL (2009) Molecular evolution of the antiretroviral TRIM5 gene. *Immunogenetics* 61(3):163–176.
119. Nisole S, Stoye JP, Saïb A (2005) TRIM family proteins: retroviral restriction and antiviral defence. *Nat Rev Microbiol* 3(10):799–808.
120. Battivelli E, Migraine J, Lecossier D, Matsuoka S, Perez-Bercoff D, Saragosti S, Clavel F, Hance AJ (2011) Modulation of TRIM5alpha activity in human cells by alternatively spliced TRIM5 isoforms. *J Virol* 85(15):7828–35.
121. Sebastian S, Luban J (2005) TRIM5alpha selectively binds a restriction-sensitive retroviral capsid. *Retrovirology* 2(2):40.
122. Stremlau M, Perron M, Lee M, Li Y, Song B, Javanbakht H, Diaz-Griffero F, Anderson DJ, Sundquist WI, Sodroski J (2006) Specific recognition and accelerated uncoating of retroviral capsids by the TRIM5 restriction factor. *Proc Natl Acad Sci* 103(14):5514–5519.
123. Malim MH, Bieniasz PD (2012) HIV restriction factors and mechanisms of evasion. *Cold Spring Harb Perspect Med* 2(5):1–16.
124. Luban J (2012) TRIM5 and the Regulation of HIV-1 Infectivity. *Mol Biol Int* 2012:426840.
125. Li Y, Li X, Stremlau M, Lee M, Sodroski J (2006) Removal of Arginine 332 Allows Human TRIM5α To Bind Human Immunodeficiency Virus Capsids and To Restrict Infection. *J Virol* 80(14):6738–6744.
126. Stremlau M, Perron M, Welikala S, Sodroski J (2005) Species-Specific Variation in the B30.2(SPRY) Domain of TRIM5 Determines the Potency of Human Immunodeficiency Virus Restriction. *J Virol* 79(5):3139–3145.
127. Yap MW, Nisole S, Stoye JP (2005) A Single Amino Acid Change in the SPRY Domain of Human Trim5alpha Leads to HIV-1 Restriction. *Curr Biol* 15(1):73–78.
128. Sawyer SL, Wu LI, Emerman M, Malik HS (2005) Positive selection of primate TRIM5alpha identifies a critical species-specific retroviral restriction domain. *Proc Natl Acad Sci* 102(8):2832–2837.
129. Ohkura S, Yap MW, Sheldon T, Stoye JP (2006) All Three Variable Regions of the TRIM5 B30.2 Domain Can Contribute to the Specificity of Retrovirus Restriction. *J Virol* 80(17):8554–8565.
130. Song B, Gold B, O'Huigin C, Javanbakht H, Li X, Stremlau M, Winkler C, Dean M, Sodroski J (2005) The B30.2(SPRY) domain of the retroviral restriction factor TRIM5alpha exhibits lineage-specific length and sequence variation in primates. *J Virol* 79(10):6111–6121.
131. Yang H, Ji X, Zhao G, Ning J, Zhao Q, Aiken C, Gronenborn AM, Zhang P, Xiong Y (2012) Structural insight into HIV-1 capsid recognition by rhesus TRIM5α. *Proc Natl Acad Sci* 109(45):18372–7.
132. Perez-Caballero D, Hatziioannou T, Yang A, Cowan S, Bieniasz PD (2005) Human Tripartite Motif 5α Domains Responsible for Retrovirus Restriction

Activity and Specificity. *J Virol* 79(14):8969–8978.
133. James LC, Keeble AH, Khan Z, Rhodes DA, Trowsdale J (2007) Structural basis for PRYSPRY-mediated tripartite motif (TRIM) protein function. *Proc Natl Acad Sci U S A* 104(15):6200–6205.
134. Ganser-Pornillos BK, Pornillos O (2019) Restriction of HIV-1 and other retroviruses by TRIM5. *Nat Rev Microbiol* 17(9):546–556.
135. Ganser-Pornillos BK, Chandrasekaran V, Pornillos O, Sodroski JG, Sundquist WI, Yeager M (2011) Hexagonal assembly of a restricting TRIM5α protein. *Proc Natl Acad Sci U S A* 108(2):546–550.
136. Biris N, Yang Y, Taylor AB, Tomashevski A, Guo M, Hart PJ, Diaz-Griffero F, Ivanov DN (2012) Structure of the rhesus monkey TRIM5α PRYSPRY domain, the HIV capsid recognition module. *Proc Natl Acad Sci U S A* 109(33):13278–13283.
137. Biris N, Tomashevski A, Bhattacharya A, Diaz-Griffero F, Ivanov DN (2013) Rhesus monkey TRIM5α SPRY domain recognizes multiple epitopes that span several capsid monomers on the surface of the HIV-1 mature viral core. *J Mol Biol* 425(24):5032–5044.
138. Sayah DM, Sokolskaja E, Berthoux L, Luban J (2004) Cyclophilin A retrotransposition into TRIM5 explains owl monkey resistance to HIV-1. *Nature* 430(6999):569–573.
139. Wilson SJ, Webb BLJ, Ylinen LMJ, Verschoor E, Heeney JL, Towers GJ (2008) Independent evolution of an antiviral TRIMCyp in rhesus macaques. *Proc Natl Acad Sci* 105(9):3557–3562.
140. Malfavon-Borja R, Wu LI, Emerman M, Malik HS (2013) Birth, decay, and reconstruction of an ancient TRIMCyp gene fusion in primate genomes. *Proc Natl Acad Sci* 110(7):E583-92.
141. Mu D, Yang H, Zhu J-W, Liu F-L, Tian R-R, Zheng H-Y, Han J-B, Shi P, Zheng Y-T (2014) Independent Birth of a Novel TRIMCyp in Tupaia belangeri with a Divergent Function from Its Paralog TRIM5. *Mol Biol Evol* 31(11):2985–2997.
142. Boso G, Shaffer E, Liu Q, Cavanna K, Buckler-White A, Kozak CA (2019) Evolution of the rodent Trim5 cluster is marked by divergent paralogous expansions and independent acquisitions of TrimCyp fusions. *Sci Rep* 9(1):1–14.
143. Boudinot P, van der Aa LM, Jouneau L, Pasquier L, Pontarotti P, Briolat V, Benmansour A, Levraud JP (2011) Origin and evolution of TRIM proteins: New insights from the complete TRIM repertoire of zebrafish and pufferfish. *PLoS One* 6(7). doi:10.1371/journal.pone.0022022.
144. Newman RM, Hall L, Kirmaier A, Pozzi LA, Pery E, Farzan M, O'Neil SP, Johnson WE (2008) Evolution of a TRIM5-CypA splice isoform in old world monkeys. *PLoS Pathog* 4(2):1–8.
145. Ylinen LMJ, Price AJ, Rasaiyaah J, Hué S, Rose NJ, Marzetta F, James LC, Towers GJ (2010) Conformational Adaptation of Asian Macaque TRIMCyp Directs Lineage Specific Antiviral Activity. *PLoS Pathog* 6(8):67–68.
146. Virgen CA, Kratovac Z, Bieniasz PD, Hatziioannou T (2008) Independent genesis of chimeric TRIM5-cyclophilin proteins in two primate species. *Proc Natl Acad Sci* 105(9):3563–3568.

147. Luban J, Bossolt KL, Franke EK, Kalpana G V., Goff SP (1993) Human immunodeficiency virus type 1 Gag protein binds to cyclophilins A and B. *Cell* 73(6):1067–1078.
148. Wu L, Martin TD, Carrington M, KewalRamani VN (2004) Raji B cells, misidentified as THP-1 cells, stimulate DC-SIGN-mediated HIV transmission. *Virology* 318(1):17–23.
149. Tsuchiya S, Yamabe M, Yamaguchi Y, Kobayashi Y, Konno T, Tada K (1980) Establishment and characterization of a human acute monocytic leukemia cell line (THP-1). *Int J Cancer* 26(2):171–176.
150. Means RE, Greenough T, Desrosiers RC (1997) Neutralization sensitivity of cell culture-passaged simian immunodeficiency virus. *J Virol* 71(10):7895–7902.
151. Means RE, Matthews T, Hoxie JA, Malim MH, Kodama T, Desrosiers RC (2001) Ability of the V3 Loop of Simian Immunodeficiency Virus To Serve as a Target for Antibody-Mediated Neutralization: Correlation of Neutralization Sensitivity, Growth in Macrophages, and Decreased Dependence on CD4. *J Virol* 75(8):3903–3915.
152. Zhang H, Zhou Y, Alcock C, Kiefer T, Monie D, Siliciano J, Li Q, Pham P, Cofrancesco J, Persaud D, Siliciano RF (2004) Novel Single-Cell-Level Phenotypic Assay for Residual Drug Susceptibility and Reduced Replication Capacity of Drug-Resistant Human Immunodeficiency Virus Type 1. *J Virol* 78(4):1718–1729.
153. Kirmaier A, Wu F, Newman RM, Hall LR, Morgan JS, O'Connor S, Marx PA, Meythaler M, Goldstein S, Buckler-White A, Kaur A, Hirsch VM, Johnson WE (2010) TRIM5 suppresses cross-species transmission of a primate immunodeficiency virus and selects for emergence of resistant variants in the new species. *PLoS Biol* 8(8):e1000462.
154. Wu F, Kirmaier A, White E, Ourmanov I, Whitted S, Matsuda K, Riddick N, Hall LR, Morgan JS, Plishka RJ, Buckler-White A, Johnson WE, Hirsch VM (2016) TRIM5α Resistance Escape Mutations in the Capsid Are Transferable between Simian Immunodeficiency Virus Strains. *J Virol* 90(24):11087–11095.
155. Clavel F, Guetard D, Brun-Vezinet F, Chamaret S, Rey M, Santos-Ferreira M, Laurent A, Dauguet C, Katlama C, Rouzioux C, Al. E (1986) Isolation of a new human retrovirus from West African patients with AIDS. *Science (80-)* 233(4761):343–346.
156. Guyader M, Emerman M, Sonigo P, Clavel F, Montagnier L, Alizon M (1987) Genome organization and transactivation of the human immunodeficiency virus type 2. *Nature* 326(6114):662–669.
157. Hirsch V, Adger-Johnson D, Campbell B, Goldstein S, Brown C, Elkins WR, Montefiori DC (1997) A molecularly cloned, pathogenic, neutralization-resistant simian immunodeficiency virus, SIVsmE543-3. *J Virol* 71(2):1608–1620.
158. Ortiz M, Bleiber G, Martinez R, Kaessmann H, Telenti A (2006) Patterns of evolution of host proteins involved in retroviral pathogenesis. *Retrovirology* 3:11.
159. Wu F, Kirmaier A, Goeken R, Ourmanov I, Hall L, Morgan JS, Matsuda K, Buckler-White A, Tomioka K, Plishka R, Whitted S, Johnson WE, Hirsch VM (2013) TRIM5 alpha drives SIVsmm evolution in rhesus macaques. *PLoS Pathog*

9(8):e1003577.
160. Fricke T, White TE, Schulte B, de Souza Aranha Vieira DA, Dharan A, Campbell EM, Brandariz-Nunez A, Diaz-Griffero F (2014) MxB binds to the HIV-1 core and prevents the uncoating process of HIV-1. *Retrovirology* 11(1):68.
161. Kong J, Xu B, Wei W, Wang X, Xie W, Yu X-F (2014) Characterization of the amino-terminal domain of Mx2/MxB-dependent interaction with the HIV-1 capsid. *Protein Cell* 5(12):954–957.
162. Duran-Troise G, Bassin RH, Rein A, Gerwin BI (1977) Loss of Fv-1 restriction in Balb/3T3 cells following infection with a single N tropic murine leukemia virus particle. *Cell* 10(3):479–488.
163. Dodding MP, Bock M, Yap MW, Stoye JP (2005) Capsid processing requirements for abrogation of Fv1 and Ref1 restriction. *J Virol* 79(16):10571–7.
164. McEwan WA, Schaller T, Ylinen LMJ, Hosie MJ, Towers GJ, Willett BJ (2009) Truncation of TRIM5 in the Feliformia explains the absence of retroviral restriction in cells of the domestic cat. *J Virol* 83(16):8270–8275.
165. Matreyek KA, Yucel SS, Li X, Engelman AN (2013) Nucleoporin NUP153 Phenylalanine-Glycine Motifs Engage a Common Binding Pocket within the HIV-1 Capsid Protein to Mediate Lentiviral Infectivity. *PLoS Pathog* 9(10):e1003693.
166. Lee K, Mulky A, Yuen W, Martin TD, Meyerson NR, Choi L, Yu H, Sawyer SL, KewalRamani VN (2012) HIV-1 capsid-targeting domain of cleavage and polyadenylation specificity factor 6. *J Virol* 86(7):3851–60.
167. Price AJ, Jacques D a., McEwan W a., Fletcher AJ, Essig S, Chin JW, Halambage UD, Aiken C, James LC (2014) Host Cofactors and Pharmacologic Ligands Share an Essential Interface in HIV-1 Capsid That Is Lost upon Disassembly. *PLoS Pathog* 10(10):e1004459.
168. Braaten D, Luban J (2001) Cyclophilin A regulates HIV-1 infectivity, as demonstrated by gene targeting in human T cells. *EMBO J* 20(6):1300–1309.
169. Braaten D, Franke EK, Luban J (1996) Cyclophilin A is required for the replication of group M human immunodeficiency virus type 1 (HIV-1) and simian immunodeficiency virus SIV(CPZ)GAB but not group O HIV-1 or other primate immunodeficiency viruses. *J Virol* 70(7):4220–4227.
170. Franke EK, Yuan HEH, Luban J (1994) Specific incorporation of cyclophilin A into HIV-1 virions. *Nature* 372:359–362.
171. Thali M, Bukovsky A, Kondo E, Rosenwirth B, Walsh CT, Sodroski JG, Gottlinger HG (1994) Functional association of cyclophilin A with HIV-1 virions. *Nature* 372(6504):363–5.
172. Jin Z, Jin L, Peterson DL, Lawson CL (1999) Model for lentivirus capsid core assembly based on crystal dimers of EIAV p26. *J Mol Biol* 286(1):83–93.
173. Davis TL, Walker JR, Campagna-Slater V, Finerty PJ, Paramanathan R, Bernstein G, MacKenzie F, Tempel W, Ouyang H, Lee WH, Eisenmesser EZ, Dhe-Paganon S (2010) Structural and Biochemical Characterization of the Human Cyclophilin Family of Peptidyl-Prolyl Isomerases. *PLoS Biol* 8(7):e1000439.
174. Chanput W, Peters V, Wichers H (2015) THP-1 and U937 Cells. *The Impact of Food Bioactives on Health: In Vitro and Ex Vivo Models*, eds Verhoeckx K, et al. (Springer International Publishing, Cham), pp 147–159.

175. Cronin J, Zhang X-Y, Reiser J (2005) Altering the Tropism of Lentiviral Vectors through Pseudotyping. *Curr Gene Ther* 5(4):387–398.
176. Konig R, Zhou Y, Elleder D, Diamond TL, Bonamy GMC, Irelan JT, Chiang CY, Tu BP, De Jesus PD, Lilley CE, Seidel S, Opaluch AM, Caldwell JS, Weitzman MD, Kuhen KL, Bandyopadhyay S, Ideker T, Orth AP, Miraglia LJ, Bushman FD, Young JA, Chanda SK (2008) Global Analysis of Host-Pathogen Interactions that Regulate Early-Stage HIV-1 Replication. *Cell* 135(1):49–60.
177. Sheehy AM, Gaddis NC, Choi JD, Malim MH (2002) Isolation of a human gene that inhibits HIV-1 infection and is suppressed by the viral Vif protein. *Nature* 418(6898):646–650.
178. Zheng Y-H, Irwin D, Kurosu T, Tokunaga K, Sata T, Peterlin BM (2004) Human APOBEC3F Is Another Host Factor That Blocks Human Immunodeficiency Virus Type 1 Replication. *J Virol* 78(11):6073–6076.
179. Simon V, Bloch N, Landau NR (2015) Intrinsic host restrictions to HIV-1 and mechanisms of viral escape. *Nat Immunol* 16(6):546–553.
180. Burdick RC, Hu W-S, Pathak VK (2013) Nuclear import of APOBEC3F-labeled HIV-1 preintegration complexes. *Proc Natl Acad Sci* 110(49):E4780–E4789.
181. Burdick RC, Delviks-Frankenberry KA, Chen J, Janaka SK, Sastri J, Hu W, Pathak VK (2017) Dynamics and regulation of nuclear import and nuclear movements of HIV-1 complexes. *PLoS Pathog* 13(8):e1006570.
182. Bosco DA, Eisenmesser EZ, Clarkson MW, Wolf-Watz M, Labeikovsky W, Millet O, Kern D (2010) Dissecting the microscopic steps of the cyclophilin A enzymatic cycle on the biological HIV-1 capsid substrate by NMR. *J Mol Biol* 403(5):723–738.
183. Newman RM, Hall L, Connole M, Chen G-L, Sato S, Yuste E, Diehl W, Hunter E, Kaur A, Miller GM, Johnson WE (2006) Balancing selection and the evolution of functional polymorphism in Old World monkey TRIM5. *Proc Natl Acad Sci* 103(50):19134–19139.
184. Wilson SJ, Webb BLJ, Maplanka C, Newman RM, Verschoor EJ, Heeney JL, Towers GJ (2008) Rhesus macaque TRIM5 alleles have divergent antiretroviral specificities. *J Virol* 82(14):7243–7247.
185. Cho K, Orry A, Park SE, Ferreira P a. (2015) Targeting the Cyclophilin Domain of Ran-binding Protein 2 (Ranbp2) with Novel Small Molecules to Control the Proteostasis of STAT3, hnRNPA2B1 and M-Opsin. *ACS Chem Neurosci* 6(8):1476–1485.
186. Brennan G, Kozyrev Y, Hu SL (2008) TRIMCyp expression in Old World primates Macaca nemestrina and Macaca fascicularis. *Proc Natl Acad Sci U S A* 105(9):3569–3574.
187. Liao C-H, Kuang Y-Q, Liu H-L, Zheng Y-T, Su B (2007) A novel fusion gene, TRIM5-Cyclophilin A in the pig-tailed macaque determines its susceptibility to HIV-1 infection. *AIDS* 21(Suppl 8):S19–S26.